Fermi surface instabilities with and without magnetic transitions

Adrien Gourgout

Communauté
UNIVERSITÉ Grenoble Alpes

THÈSE

Pour obtenir le grade de

DOCTEUR de la Communauté UNIVERSITÉ GRENOBLE ALPES

Spécialité : **Physique de la matière condensée et du rayonnement**

Arrêté ministériel : 7 Août 2006

Présentée par

Adrien Gourgout

Thèse dirigée par **Daniel Braithwaite**
et codirigée par **Alexandre Pourret**

préparée au sein de **PHotonique, ELectronique et Ingénierie QuantiqueS (PHELIQS)**
et de l'**École Doctorale de Physique, Grenoble**

Instabilités de surface de Fermi avec et sans transitions magnétiques

Étude de URhGe, UPd_2Al_3, UCoGe et $CeIrIn_5$

Thèse soutenue publiquement le **6 Janvier 2017**,
devant le jury composé de :

Dr. Rafik BALLOU
Institut Néel, Grenoble, Président
Prof. Gertrud ZWICKNAGL
Technische Universität Braunschweig, Braunschweig, Rapporteur
Dr. Manuel BRANDO
Max Planck Institute for Chemical Physics of Solids, Dresden, Rapporteur
Dr. Sylvie HEBERT
Laboratoire de Cristallographie et Science des Matériaux, Caen, Examinatrice
Dr. Daniel BRAITHWAITE
Commissariat à l'énergie atomique et aux énergies alternatives, Grenoble, Directeur de thèse
Dr. Alexandre POURRET
Université Grenoble Alpes, Grenoble, Co-Directeur de thèse

Fermi surface instabilities with and without magnetic transitions

Study of URhGe, UPd_2Al_3, UCoGe and $CeIrIn_5$.

Abstract

In this thesis, we have studied the evolution of the Fermi surface under the influence of a magnetic field in bulk materials that can be easily polarized at low temperature. The first part was devoted to the cases of the ferromagnetic superconductor UCoGe with a magnetic field applied along the easy magnetization c-axis and the paramagnetic superconductor $CeIrIn_5$ with the field along the c-axis. In UCoGe, several successive anomalies were detected in resistivity, Hall effect and thermoelectric power, without any thermodynamic transition being detected in magnetization. The direct observation of quantum oscillations showed that these anomalies are related to topological change of the Fermi surface, also known as Lifshitz transition. In $CeIrIn_5$, the thermoelectric power detected an anomaly at $H_M = 28$ T and the quantum oscillations observed in torque magnetometry showed that a Lifshitz transition occurs at this field.

In the second part of this thesis, we studied evolution of the Fermi surface through first order magnetic transitions induced by magnetic field. In the ferromagnetic superconductor URhGe with the field applied along the hard magnetization b-axis and the antiferromagnetic superconductor UPd_2Al_3 with the field in the basal plane. In URhGe, the thermoelectric power allowed to observe a change in the Fermi surface at the spin reorientation transition at $H_R = 11.75$ T defining the ferromagnetic state and along with resistivity confirmed the first order character of the transition as well as give a location of the tricritical point. In UPd_2Al_3, a new branch was observed in de Haas-van Alphen experiment in the antiferromagnetic phase and the thermoelectric power showed that the Fermi surface is reconstructed at the metamagnetic transition at $H_M = 18$ T where the antiferromagnetic state is suppressed and could suggest that the Fermi surface changes before this transition. Additionally, four new branches were observed in the polarized paramagnetic phase, above H_M that cannot be associated with calculated branches in the paramagnetic or antiferromagnetic states.

Key words

Heavy fermions
Thermoelectricity, Nernst effect
Superconductivity, Magnetism
Electronic Correlations

Remerciements
Aknowledgements

I first want to thank Gertrud Zwicknagl and Manuel Brando for accepting to be the referees of my PhD thesis, et également Rafik Ballou ainsi que Sylvie Hébert pour avoir bien voulu être examinateurs de ma thèse.

Je remercie Alex, pour m'avoir initié à la physisque expérimentale alors que je rentrais tout juste à l'ESPCI (encore désolé pour ton porte échantillon!) et Kamran Behnia, qui m'a encouragé dans cette voie et m'a dÃ©niché cette thèse Ã Grenoble.

Alex encore, puisqu'il a réussi à encadrer cette thèse malgrès toutes ses responsabilités d'enseignement, j'ai énormément appris avec toi et j'ai beaucoup apprécié notre collaboration. Georg, je t'aurais bien mis un mot en Allemand, mais mon niveau n'est pas suffisant. Cependant, je te remercie pour ton aide, ta relecture du manuscrit ainsi que tes désormais célèbres pfffff. Je remercie également Daniel et Jean-Pascal pour les discussions, ainsi que nos collègues du D5 Christophe, Gérard et Karine, pour les cafés et l'aide apportée tout au long de cette thèse. Jacques, ton aide m'a été très précieuse, de part tes connaissances mais aussi parce-que tu as su me pousser pour maximiser la qualité de mon travail.

Dai, for all the discussions, the time I spent in your laboratory in Oarai and the excellent samples without which all this work would not have been possible, arigat$\bar{o}$gozaimasu! Mes collègues thésards, Gaël et Beilun, avec qui j'ai eu beaucoup de plaisir à partager ces trois années. Les discussions que l'on a pu avoir, tant scientifiques que sur d'autres sujets, ont été pour moi très enrichissantes.

Nos collaborateurs du LNCMI Grenoble, Gabriel et Ilya, où l'on a passé des nuits de mesures excellentes.

De manière générale, je souhaite remercier toutes les personnes avec qui j'ai pu collaborer et/ou discuter durant ces trois années.

Un petit mot également pour l'Étrier du Dauphiné, qui m'a fourni un endroit pour travailler loin de toute distraction pendant la période de rédaction.

Je dédie cette thèse à mes parents, sans qui il est évident que rien n'aurait été possible, le reste de ma famille et bien sûr Éloïse, sur qui j'ai toujours pu compter et qui m'a toujours soutenu.

Introduction

More than one hundred years ago, Kamerlingh Onnes was measuring a resistance equal to zero in mercury, this was the first discovery of superconductivity. A theoretical explanation to this phenomenon was proposed decades later, with the Bardeen-Cooper-Schrieffer theory. During all the years up to now, a large number of superconductors have been discovered, such as high-T_C Cuprates or iron pnictides, which cannot be described by this theory and were therefore classified as "unconventional".

Among unconventional superconductors, some are also part of the heavy fermion family, which are intermetallic compounds and where the electronic correlations give rise to effective masses that can be several orders of magnitude above the bare electron mass and which often exhibit magnetic ordering. Looking closer, one can even find some which present at low temperature a coexistence of a long range magnetic order and superconductivity. Since superconductivity and magnetism were considered antagonist effects, the discovery, in UGe_2, of the coexistence of ferromagnetism and superconductivity was a surprise as well as a new interest in the scientific community [32, Saxena 2000]. URhGe belongs to this family of ferromagnetic superconductors and while it was discovered 15 years ago [33, Aoki 2001], a lot of questions have yet to be answered. The interplay between itinerant ferromagnetism and superconductivity, the differences between the phase diagrams of the ferromagnetic superconductors, the link between the re-entrant superconducting phase far above the upper critical field H_{C2} of the low field superconductivity [85, Lévy 2005] and the first order spin-reorientation transition induced by a magnetic field along a hard magnetization axis, are among them.

The answers to these points may lie in the study of the Fermi surface. Even in simple cases, the exact link between the Fermi surface and the very low temperature properties of a metal is still unclear. However, the study of the different bands participating to the transport or thermodynamic properties as well as the topology of the Fermi surface can give valuable informations about the ground state properties of the studied system. The Fermi surface, especially in heavy fermion compounds, is challenging to determine experimentally due to the high effective masses and the extreme conditions required (low temperature, high magnetic field). From a theoretical point of view, the presence of the f-electrons and their hybridization with the conduction electrons make the band calculations difficult.

The band structure and the Fermi energy of a material can be modified through the application of an external parameter, such as pressure, chemical composition or magnetic field and therefore the Fermi surface. A change of the Fermi surface can occur suddenly, with a reconstruction at a transition that modifies the ground state, or continuously, in what is called a Lifshitz transition, where the topology of the Fermi surface changes

with no clear modification of the ground state. The possibility of a topological change of the Fermi surface under the influence of an external parameter was theoretically studied more than 50 years ago by I. M. Lifshitz [25, Lifshitz 1960]. Recently, experimental and theoretical work showing the presence of these Lifshitz transitions in heavy fermion compounds such as $YbRh_2Si_2$ [72, Pfau 2013] or $CeRu_2Si_2$ [55, 56, Daou 2006, Boukahil 2014], induced by magnetic field. Additionally, the interplay between the phase transitions and the modification of the Fermi surface in itinerant systems, for instance which one drives the other, is not clear.

In this thesis, the primary objective was to study the evolution of the Fermi surface close to the reentrant superconductivity in URhGe and through the magnetic transition at H_R. The focus was given on the study of the magnetic field dependence of the thermoelectric power, which is a very sensitive probe to any change of the Fermi surface, in order to understand the interplay between magnetism, Fermi surface and surperconductivity. The presence of anomalies in the magnetoresistivity in the parent compound UCoGe and the absence of associated magnetic transitions lead us to study these anomalies with the thermoelectric power in order to understand how the magnetic field can modify the Fermi surface in this compound. $CeIrIn_5$, which is a paramagnetic superconductor, shows the same kind of anomaly observed in UCoGe, and UPd_2Al_3, an antiferromagnetic superconductor which exhibits a metamagnetic transition where the Fermi surface may be reconstructed.

This thesis is therefore divided into four main parts. The first one gives an overview of the theoretical and experimental approach in condensed matter of the magnetic orders, the Fermi surface and its observation and the Lifshitz transitions. The second part details the experimental apparatus used to grow the studied single crystals, measure the thermoelectric power, resistivity and de Haas-van Alphen oscillations. The third part presents the experimental results on field induced transitions that gives no signature in the magnetization and study these with thermoelectric power. In the ferromagnetic superconductor UCoGe, we completed a Hall effect and resistivity study, where we investigated the effect of magnetic polarization on the Fermi surface, revealing successive Lifshitz type transitions by thermoelectric power and quantum oscillations in Seebeck and resistivity. In the paramagnetic superconductor $CeIrIn_5$, the thermoelectric power along with quantum oscillations detected in torque magnetometry also showed the presence of a Lifshitz transition. In the fourth part, we studied the suppression of magnetic orders with magnetic field with the objective to understand the role of the Fermi surface in these transitions. The spin reorientation transition in the ferromagnetic superconductor URhGe at H_R when the field is applied along the hard magnetization b-axis was probed with thermoelectric power and resistivity measurements and was shown to host a reconstruction of the Fermi surface, as well as being confirmed to be of first order at low temperature. The position of the tricritical point was extracted as well as a non-Fermi liquid regime extending from this point. In UPd_2Al_3, we studied the Fermi surface across the metamagnetic transition with a magnetic field in the basal plane by thermoelectric power and de Haas-van Alphen oscillations. It allowed us uncover a Fermi surface reconstruction as the metamagnetic transition in this system.

Contents

List of Figures

Chapter 1

Theoretical Background

1.1 Landau's Fermi Liquid Theory.

In this thesis, we are dealing with the physical properties of solids at low temperature. The most simple treatment of fermions in solids is by considering them as free. This means that all interactions between one fermion and its environment (for example the other fermions or the lattice) are neglected. That way the system can be described by calculating the eigenfunctions of the single-particle Schrödinger equation and even taking into account the high fermion density of a solid, it is governed by a simple quadratic hamiltonian given by the kinetic energy, where the eigenstates are easily found:

$$H = \sum_{k,\sigma} \frac{\hbar^2 k^2}{2m} c^\dagger_{k\sigma} c_{k\sigma} \tag{1.1}$$

Taking into account the electron-electron interaction is an entirely different and much more complex problem. The electron-electron interaction requires to add a new term in the hamiltonian of the form:

$$H_{int} \propto \sum c^\dagger_\alpha c^\dagger_\beta c_\gamma c_\delta \tag{1.2}$$

which is a quartic term and much more complicated to deal with. A way to circumvent this problem is given by the Fermi liquid theory. The theory of Landau describing Fermi liquids was first developed to take into account interactions in ^{3}He [1, 2, Landau 1957, Leggett 1975] and was later applied to electrons in metals. It starts from a non-interacting Fermi gas and the interaction is slowly turned on in order to have an adiabatic transformation from the Fermi gas to the Fermi liquid. This allows the description of interacting fermions without changing their fundamental properties. In Fermi liquids, the spin, charge and momentum of the electrons remains unchanged. The effect of the interactions are visible only on the dynamical properties of the fermions such as their mass, which is renormalized. The renormalized fermions are then called quasiparticles.

This renormalization of the mass gives rise to changes in some properties of the system. For instance, the electronic specific heat divided by temperature is enhanced and when $T \to 0$ is given by:

$$\gamma = \left.\frac{C}{T}\right|_{T\to 0} = \gamma_0 \frac{m^*}{m_0} \tag{1.3}$$

where γ_0 is the Sommerfeld coefficient in the case of a non-interacting Fermi gas and m^* and m_0 are the renormalized and free electron masses, respectively. Thus, larger effective mass will give rise to a larger γ value.

In the frame of a Fermi liquid state, resistivity behaves as:

$$\rho = \rho_0 + AT^2 \tag{1.4}$$

where ρ_0 represents the scattering of quasiparticles with impurities and the other term is the electron-electron interaction with $A \propto m^{*^2}$. Similarly, larger effective mass will give a larger A coefficient. The term correlations is a generic term commonly used to describe the interaction of one electron with the other electrons including fluctuations.

1.1.1 Thermoelectricity

In this section, we will describe in more details the thermoelectric coefficient because this is the main probe we used in this thesis. Additionally, contrary to resistivity and specific heat, thermoelectricity is not a common probe to study the electronic properties of a system.

In this work, we have been interested in two thermoelectric coefficients : the Seebeck and Nernst effect. Under the influence of a thermal current, the quasiparticles moves from the hot part of the sample toward the cold one, where their energy is lower. This movement creates a longitudinal electrical field, characterized by the Seebeck coefficient, given by:

$$S = -\frac{E_x}{\nabla_x T} \tag{1.5}$$

When a transverse magnetic field is applied, then a transverse electric field is created. This is the Nernst effect, given by:

$$N = -\frac{E_y}{\nabla_x T} \tag{1.6}$$

These two effects are schematically represented in Fig. 1.1. The interest of thermoelectric power lies in its relation to the density of states. While other probes, such as conductivity or specific heat are proportional to it, Seebeck effect is not. In a semi-classical approach, the Seebeck coefficient is linked to the electrical conductivity by the Mott formula [3, Mott and Jones 1936]:

$$S = -\frac{\pi^2 {k_B}^2 T}{3e} \left(\frac{\partial \ln \sigma(\epsilon)}{\partial \epsilon} \right)_{\epsilon=\epsilon_F} \tag{1.7}$$

So the Seebeck coefficient appears as the logarithmic derivative of the electrical conductivity with respect to the energy, taken at the Fermi energy. In the simple case of a spherical Fermi surface with an isotropic scattering time, one can write the conductivity as:

$$\sigma(\epsilon) \propto \tau(\epsilon) g(\epsilon) \tag{1.8}$$

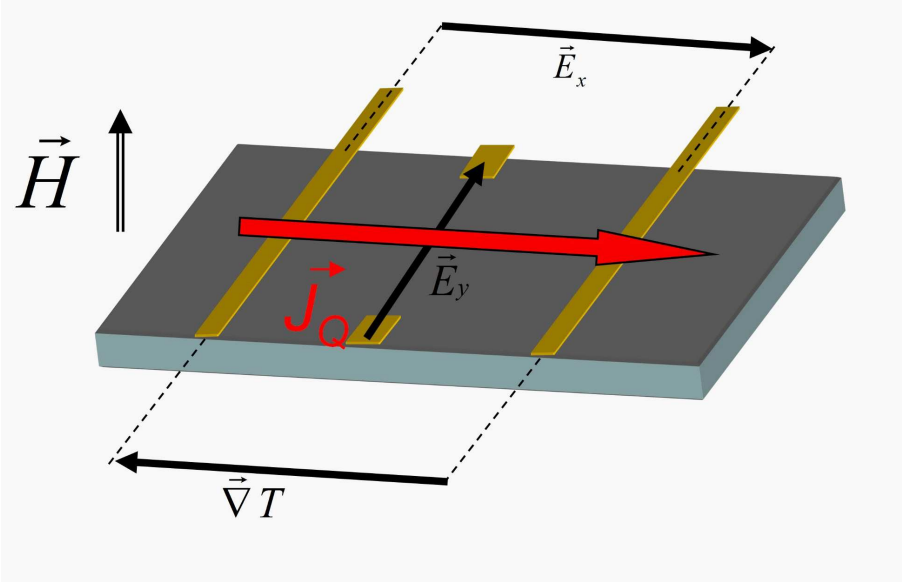

Figure 1.1: Schematic view of a sample with a thermal gradient applied along x and magnetic field along z.

where τ is the life-time of the quasiparticles between two scattering events and $g(\epsilon)$ is the density of states. This then gives, in a semi-classical approach of the electronic scattering, for the thermoelectric power:

$$S = -\frac{\pi^2 {k_B}^2 T}{3e}\left(\frac{\partial \ln\, \tau(\epsilon)}{\partial \epsilon} + \frac{\partial \ln\, g(\epsilon)}{\partial \epsilon}\right)_{\epsilon=\epsilon_F} \tag{1.9}$$

We can see that Seebeck effect has a contribution in logarithmic derivative of the density of states with respect to energy. It is then natural to expect that any anomaly in the density of states will give a small effect in the conductivity but a large one in the thermoelectric power. At low temperature, in a Fermi liquid regime, S/T is expected to be independent of temperature. It was proposed by Behnia and coworkers [57, Behnia 2004] that, in the zero temperature limit, the Seebeck coefficient is directly linked to the Sommerfeld coefficient γ of the specific heat by the dimensionless coefficient q, through the density of states.

Starting from Eq. 1.9, one can show that in the zero temperature limit and in a free electron gas, we can get:

$$S = -\frac{\pi^2 {k_B}^2 T}{3\, e\, \epsilon_F}\left(\frac{3}{2} - \zeta\right) \tag{1.10}$$

where ζ represents the energy dependence of the relaxation time: $\tau = \epsilon^{\zeta}$. For free electrons, the density of states at the Fermi level is given by $g(\epsilon_F) = 3n/2\epsilon_F$ where n is the number of electrons. Substitution in Eq. 1.10 gives:

$$S = -\frac{\pi^2 {k_B}^2 T g(\epsilon_F)}{3\, e\, n}\left(1 - \frac{2\zeta}{3}\right) \tag{1.11}$$

The expression of the electronic specific heat for free electrons is given by:

$$C_{el} = \frac{\pi^2}{3} k_B^2 T g(\epsilon_F) \tag{1.12}$$

These two expressions are close to each other and it is possible to define a ratio q given by:

$$q = \frac{S}{T} \frac{N_{Av} e}{\gamma} \tag{1.13}$$

where N_{Av} is the Avogadro number, e = - 1.6 10^{-19} C is the electron charge and $\gamma = \left(\frac{C_{el}}{T}\right)_{T \to 0}$ is the Sommerfeld coefficient. For a free electron gas and for an energy independent relaxation time, we get q = -1 for a single electron per formula unit. This ratio grows larger (smaller) as the number of electrons per formula unit decreases (increases). If the charge carriers considered are holes instead of electrons, the charge taken into account will be e = + 1.6 10^{-19} C and the q ratio will be positive. So comparing γ and S/T at low temperature allows us to have an idea of the number of carriers in the system.

In the different systems we have studied, the Fermi surface is composed of multiple bands, so the Seebeck coefficient is not as simple as Eq. 1.10. Indeed, for a multiband system, one can show that contributions from each sheet of the Fermi surface add up [4, Miyake and Kohno 2005] and give:

$$S = \sum_i \frac{\sigma_i}{\sigma} S_i \tag{1.14}$$

Since with a heat current, both hole and electron-like quasiparticles move in the same direction, thermoelectric power behaves like Hall effect in regards to its sign. Holes will give positive contribution and electrons will give negative contribution. So the thermoelectric power comes from the asymmetry between electrons and holes in the system:

$$S \propto -m_e \tau_e + m_h \tau_h \tag{1.15}$$

depending on the scattering time and effective mass of the quasiparticles for each band, the total signal will be either negative or positive. This is especially important at low temperature, because usually one band will dominate the others and give the final sign of the thermoelectric power.

In the Fermi liquid picture, the Nernst signal can be expressed as :

$$N = \frac{\pi^2}{3} \frac{k_B}{e} \frac{k_B T}{\epsilon_F} \mu B \tag{1.16}$$

where $\mu = \frac{e\tau}{m^*}$ is the electronic mobility and B is the magnetic field. The magnitude of the Nernst effect is therefore large if the mobility is high and the Fermi energy is small. Similar to the Hall effect, the Nernst coefficient is supposed to be linear with magnetic field. However, contrary to the Seebeck and Hall effect, the Nernst signal cannot be compensated: the signal given by electrons and holes will both be of the same sign.

1.1.2 Heavy fermion systems

Heavy fermion systems are intermetallic compounds based on lanthanides, such as cerium or ytterbium with a partially filled $4f$ shell or actinides, such as uranium with a partially filled $5f$ shell. In the bare atoms, the f shells are localized, meaning that in the real space, the electrons on these shells are very close to the nucleus and even in solids, the f electrons keep a strong localized character. In energy, the f-electrons density of states is usually close to the Fermi energy, allowing these electrons to hybridize with the conduction ones, leading to a high density of states close to the Fermi level.

The high temperature behavior of $4f$ heavy fermion systems is usually described by the Kondo effect [5, Kondo 1964]. In this model, a single magnetic impurity in a non-magnetic metal is considered. Below a characteristic temperature T_K, there is a spin-flip scattering of the conduction electrons on the magnetic impurity, leading to an increase of the electrical resistivity. There is therefore a screening of the impurity spin by the conduction electrons. In $4f$ heavy fermion systems, the f levels are close enough to the nucleus that there is almost no overlap between their spatial wave functions and each site plays the role of an independent magnetic impurity at high temperature. However, the main difference from the single impurity model is the hybridization with the conduction electrons. At a temperature $T_{coh} < T_K$, these electrons will start to form bands and be the mediator of an indirect interaction between the lanthanide sites, forming the so-called Kondo lattice. The main consequence is that the scattering of the conduction electrons becomes coherent, and the resistivity shows a sharp drop when decreasing the temperature. This is well known for $4f$ systems (cerium or ytterbium based) which have very localized f orbitals. For uranium compounds, the $5f$ orbitals are less localized and some of the f electrons are itinerants, due to the overlap of their wave functions. This makes the description with the Kondo model more complicated, as the uranium sites will not behave as perfectly independent impurities at high temperature.

Astonishingly, at low temperature and far from any magnetic instability, despite the large electronic correlations, heavy fermion systems follow the Fermi liquid predictions with, for example, a quadratic temperature dependence of the resistivity. Since the Fermi liquid theory was developed to treat weakly interacting fermions, this observation was unexpected. This leads to a large renormalization of the effective masses of the quasi-particles, which can be several hundred times the free electron mass. Thus, it is usually seen in heavy fermion systems that the Sommerfeld coefficient extrapolated at zero temperature is quite high. For example, in UBe_{13}, $\gamma = 1$ J.mol^{-1}.K^{-2} or in $CeCu_2Si_2$, $\gamma = 0.7$ J.mol^{-1}.K^{-2} compared to copper, where $\gamma = 0.7$ mJ.mol^{-1}.K^{-2}. The main consequence to the high renormalization of the quasiparticle effective mass is that the energy dispersion in momentum space is very flat and the Fermi energy is small. The relatively small Fermi energy as well as the high density of states at the Fermi level makes these materials very sensitive to the tuning of external parameters, such as pressure, magnetic field or doping. With doping, the addition or removal of quasiparticles in the system will shift the Fermi energy, therefore changing the Fermi surface and the ground state properties of the system. The application of pressure can change the volume of the unit cell, thus changing the distance between the atoms and the strength of their interaction (the magnetic exchange interaction, for example) which can also modify the ground state. Compared to d-electrons systems, the ground state of heavy fermion systems will be much

easier to modify as the characteristic energy scales are far lower.

In heavy fermion systems, due to the high effective masses of the different bands of the Fermi surface, the thermoelectric power generated by each band is expected to be large. Due to the multiband character of these systems, it is obviously difficult to have general expectations of the absolute value at low temperature, the electrons and holes contributions canceling each other, possibly leading to a small measured value of the thermoelectric power. Nevertheless, the value at $T = 4$ K is generally of the order of 10 μV.K^{-1} or lower and can go down to very low values at lower temperature. At room temperature, the incoherent Kondo scattering along with the crystal field effect can lead to large values of the termoelectric power of the order of 0.1 mV.K^{-1}. The Fermi liquid regime where the thermoelectric power is linear in temperature is, in many cases, observed below $T \approx \frac{1}{3}T_{coh}$ [57, Behnia 2004]. The linear temperature dependence of the thermoelectric power is usually observed far below the T^2 dependence of the resistivity.

1.2 Magnetic orders

The interaction of the f-electrons with the conduction electrons gives rise to an indirect magnetic exchange between the sites mediated by the d electrons called the Rudermann-Kittel-Kasuya-Yosida [6, Rudermann and Kittel 1954] interaction that will tend to form a magnetic ground state in the system. On the other hand, the Kondo effect will tend to form a non-magnetic ground state. In heavy fermion systems, the ground state at zero temperature is determined by the competition of these two effects, which are of the same order of magnitude in energy and was studied by Doniach [7, Doniach 1977]. This explains the observation that these systems are almost always either magnetic or close to a magnetic instability. This picture of Doniach works quite well with lanthanides based systems and describes the competition between RKKY interaction and the Kondo effect that gives rise to the localized magnetism in $4f$ materials. For uranium based compounds, the magnetism coming from the $5f$-electrons will have a more itinerant character, making the study in the Doniach model difficult.

In this thesis, the systems with a magnetic ground state we studied were uranium based: URhGe and UCoGe, both ferromagnetic with uniaxial anisotropy and UPd_2Al_3 which is antiferromagnetic with a simple wave vector. Additionally, a cerium based compound was studied, $CeIrIn_5$, which is paramagnetic.

The ferromagnetic order is the most simple magnetic ground state. The magnetic moments are oriented in the same direction, giving a spontaneous macroscopic magnetization even with no applied magnetic field. Common examples are transition metals such as Iron, Cobalt or rare earths such as Dysprosium or Gadolinium. The antiferromagnetic order has magnetic moments oriented antiparallel to each other, cancelling the spontaneous magnetization. In simple antiferromagnets, there is only one wave vector, called k, with gives the direction and the periodicity of the magnetic order. Examples are given in oxides such as NiO and heavy fermion compounds, such as $CeIn_3$. However, much more complicated magnetic structures exist, such as ferrimagnets, helical orders, spin density waves or antiferromagnets with more than one wave vector.

The magnetism is called itinerant if the spins are carried by the conduction electrons at the Fermi surface. It can be described, in the most simple approach, by the Stoner model.

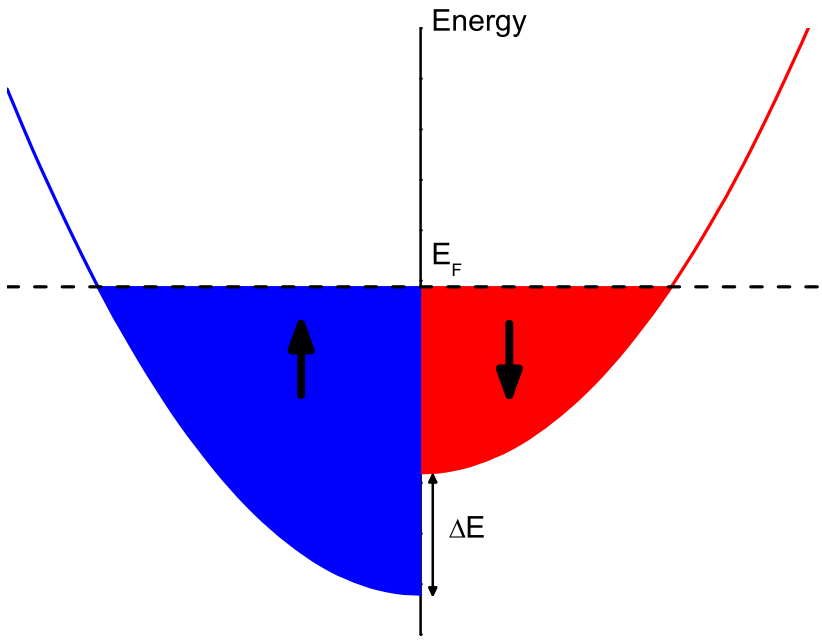

Figure 1.2: Schematic band dispersion for an itinerant ferromagnet. The "up-spin" band contains more electrons than the "down-spin" one, and the system is ferromagnetic.

A simple schematic picture of the itinerant ferromagnetism is shown on Fig. 1.2. The bands are spin-split and separated into an "up-spin" band and a "down-spin" band. This is due to the exchange interaction that will lower the energy of the "up-spin" band and increase the energy of the "down-spin" one. Therefore, with a constant Fermi energy, it is clear that an imbalance is created and there are more electrons which have an "up-spin" and less with a "down-spin" and the total magnetic moment is non-zero : the system is ferromagnetic. The properties of itinerant magnetic systems are closely related to their Fermi surface topology, which can favor crystallographic directions for the magnetization and a modification of the Fermi surface may induce a change in the ground state of such systems. In many uranium based heavy fermion systems, however, the f-electrons have a localized/itinerant duality, making the use of such models difficult as the magnetism will most often be partially localized, but also partially itinerant. So the crystal field effect is usually not the dominant parameter in the magnetic properties at low temperature in uranium compounds.

As we have seen before, in heavy fermion systems, the ground state can be modified rather easily with the application of an external parameter, such as pressure, doping or magnetic field. The next section will give an overview of the ferro- and antiferromagnetic ground states and what can be expected when these orders are suppressed by an external parameter.

1.2.1 Antiferromagnetism

Among heavy fermion materials, the antiferromagnetic ground state is the most often observed. It is characterized by the Néel temperature, T_N, which marks the transition

from the high temperature, disordered paramagnetic state to the low temperature, ordered antiferromagnetic state and by a wave vector k which corresponds to the periodicity of the alternated magnetic moments orientation. In simple cases, one can define two sub-lattices in which the magnetic moments are ordered ferromagnetically and the antiferromagnetic coupling is between these two sub-lattices. The preferred direction of the ferromagnetically ordered moments gives the easy magnetization axis.

The application of an external parameter, such as hydrostatic pressure, doping or magnetic field can suppress the order in various ways. In cerium based antiferromagnets, the Néel temperature is often continuously decreased down to zero temperature under pressure, thus the magnetic transition stays of second order even a $T = 0$ K. This gives rise to a quantum critical point, close to which quantum fluctuations are strong and are the driving force of the transition. These fluctuations are also responsible for the emergence of exotic orders, such as superconductivity. Above the critical pressure, the influence of the quantum fluctuations can be seen in thermodynamic and transport properties even at rather high temperature, notably in resistivity, where the observed temperature dependence is not the one expected in a Fermi liquid. The predictions close to a quantum critical point will be discussed in chapter 1.3.3. This was observed for example in $CeIn_3$ [9, Knebel 2001] or $CePd_2Si_2$ [10, Mathur 1998].

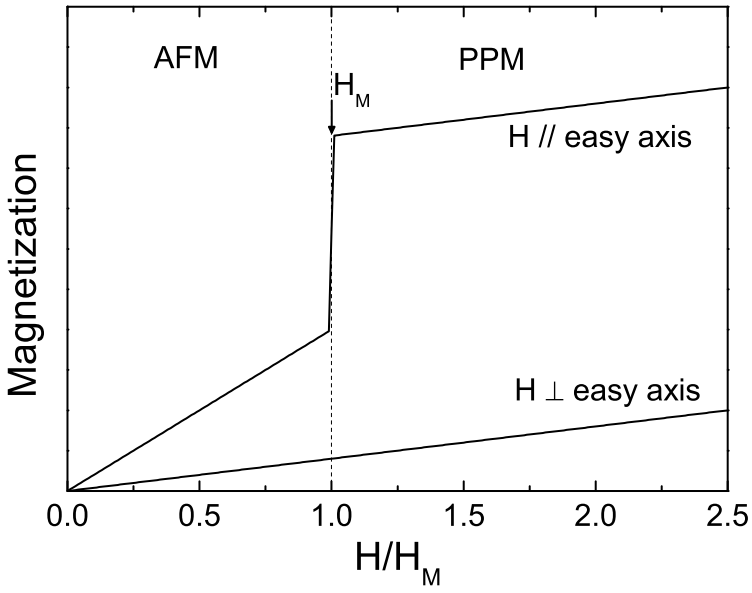

Figure 1.3: Schematic field dependence of magnetization for a magnetic field applied parallel and orthogonal to the easy magnetization axis.

When a magnetic field is applied in an antiferromagnet, the situation is different from pressure and depends on which direction the field is applied with regards to the easy magnetization axis. If the field is applied orthogonal to the easy magnetization axis, then the susceptibility is in general very low and in most cases no phase transitions occurs up to high magnetic field. Along the easy magnetization axis, the susceptibility is generally much higher and the magnetic polarization induced by magnetic field can be enough to reach some critical value at which point, in simple cases, the system will undergo a spin-flip transition called a metamagnetic transition (see Fig. 1.3). This transition corresponds to

the alignment of the magnetic moments parallel to the applied field. At low temperature, this metamagnetic transition is of first order, which means that with the application of an external magnetic field, the antiferromagnetic order is not continuously suppressed down to zero temperature. This prevents the apparition of a quantum critical point and the associated fluctuations. This was observed for example in $CeRh_2Si_2$ [15, Abe 1998] and UPd_2Al_3 [115, Oda 1994].

1.2.2 Ferromagnetism

The ferromagnetic order is characterized by the appearance of a spontaneous macroscopic magnetization, in absence of any applied magnetic field, below the Curie temperature, T_C. The easy magnetization axis is given by the direction in which the magnetic moments align themselves.

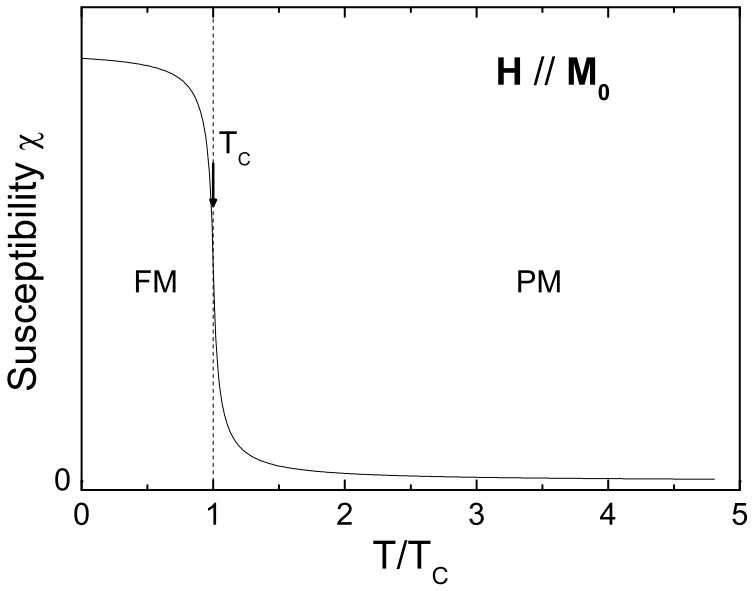

Figure 1.4: Schematic temperature dependence of the susceptibility in a ferromagnet that orders at $T = T_C$, for a magnetic field applied along the easy magnetization axis (the spontaneous magnetization, M_0, direction).

The temperature dependence of the susceptibility in a ferromagnetic compound is shown on Fig. 1.4. It shows the Curie-Weiss behavior in the paramagnetic state with a temperature dependence $\chi \propto \frac{1}{T-T_C}$. Around the Curie temperature, the susceptibility increases strongly and finally saturates when $T \to 0$.

The application of hydrostatic pressure usually suppresses the ferromagnetic order, such as in UCoGe [41, Bastien 2016] or UGe_2 [16, Taufour 2010], for example. However, in some cases such as URhGe, the Curie temperature is instead increased by pressure. A theoretical study of the evolution of the ferromagnetic order with pressure has been done in the case of itinerant ferromagnets [26, Belitz 2005]. The schematic phase diagram expected is shown on Fig. 1.5. It shows that it is not possible to continuously tune the Curie temperature down to $T = 0$ K. At some point, called tricritical, the transition switches from second order to first order. From this point, two second order lines on top of

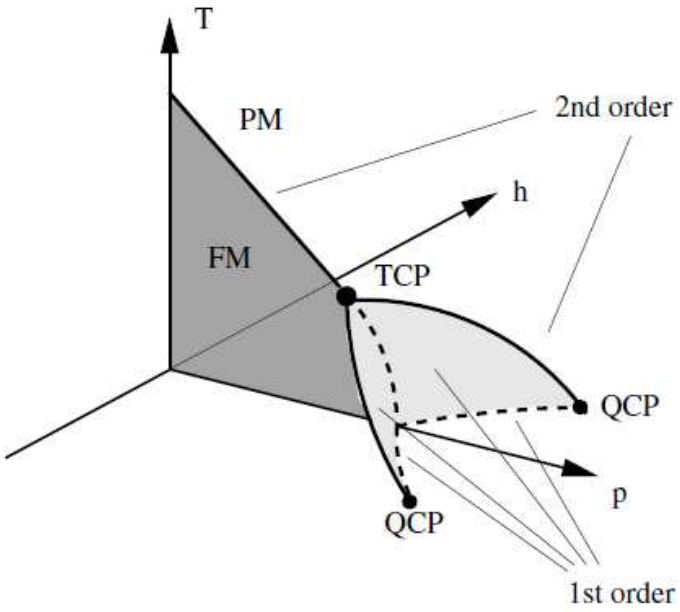

Figure 1.5: Schematic P-T-H phase diagram expected for quantum itinerant ferromagnets, taken from Ref. [26, Belitz 2005].

first order planes spread from the tricritical point and can be driven to zero temperature in the temperature-pressure-magnetic field space at a quantum critical end point. The direction of the magnetic field is the one of the easy magnetization axis. This theoretical phase diagram is in good agreement with what was measured in UGe_2 [16, Taufour 2010].

The effect of a magnetic field depends mostly on the direction, but also on the magnetic anisotropy of the considered material. For a field applied along the easy magnetization axis, the magnetic field breaks the time reversal symmetry, therefore the phase transition becomes a crossover. In this thesis we have studied only itinerant ferromagnets, where the spontaneous magnetization is much smaller than the free ion value. In the case of the uranium ions, both the U^{3+} and U^{4+} have a free ion magnetization value around 3.2 μ_B. The saturation value can be reduced by crystal field effect, therefore it is difficult to know if a system is close or not to this value. In most cases, above the coercitive magnetic field required to align the magnetic domains, the magnetization is linear and increases slowly. There is however some cases, such as UCoGe, where the field induced magnetization becomes higher than the spontaneous one with a low field of a few Tesla applied along the easy magnetization c-axis..

What is supposed to happen when the magnetic field is applied along a hard magnetization axis depends strongly on the magnetic anisotropy of the system. If the anisotropy is strong, then the susceptibility along the hard magnetization axis is low, and the magnetic field required to induce a high enough polarization in the system will be high, probably higher than what is currently available. If, on the other hand, the anisotropy between two axes is low, as in the case of $NdCo_5$ [17, Bartashevich 1993], URhGe [85, Lévy 2005] or YbNiSn [18, Bonville 1992], then it is possible to suppress the ferromagnetism. In these rare cases, the magnetization behave in low magnetic field as would a paramagnet, increasing linearly but usually with a rather high slope. At higher field, the magnetization suddenly

jumps in a metamagneticlike transition very similar to the antiferromagnetic case (see Fig. 1.3). In the few reported cases, this transition is first order at low temperature however no general behavior is known. This transition corresponds to the reorientation of the magnetic moments along the magnetic field direction.

1.2.3 Quantum criticality and magnetic fluctuations

The emergence of superconductivity close to quantum critical points has attracted a lot of interest in the past few decades. As stated before, quantum fluctuations arise from the point where a phase transition is continuously tuned to zero temperature. Indeed, at $T = 0$ K, thermal fluctuations are not present anymore, and the transition has to be driven by another kind of fluctuations. The quantum fluctuations have an influence on the thermodynamic and transport properties of the system. This influence changes the temperature dependence of such quantities, which do not follow the predictions of the Fermi liquid state in the vicinity of the quantum critical point and this region is usually called "Non-Fermi liquid".

As we have seen before, quantum criticality only arises when the ordered phase is suppressed through a second order transition. A few different kind of quantum criticality have been experimentally reported. For example:
- The pressure induced antiferromagnetic quantum critical point in $CeIn_3$ [9, Knebel 2001].
- The field induced Kondo breakdown in $YbRh_2Si_2$ [11, Steglich 2014]

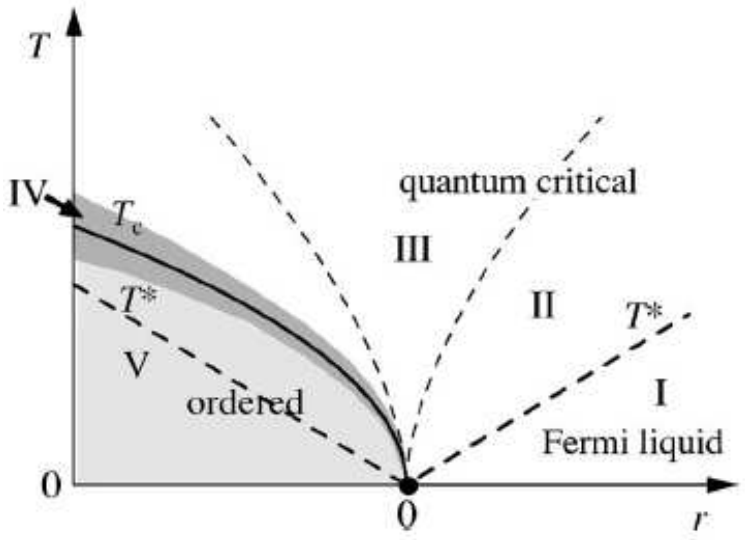

Figure 1.6: Phase diagram in the Hertz-Millis-Moriya model. Different regions are shown : the Fermi liquid (I), quantum critical (II and III), classical critical (IV) and the magnetically ordered phase (V). Here r is the tuning parameter. Taken from Ref.[12, Löhneysen 2007]

The vicinity of a quantum critical point and the consequences of the strong associated quantum fluctuations were studied by Hertz [13, Hertz 1976], Millis [14, Millis 1993] and

Moriya [8, Moriya 1985] and is well summarized in Ref. [12, Löhneysen 2007] . This is shown on Fig. 1.6. The continuous suppression of the magnetically ordered phase (V) gives rise to a quantum critical point and quantum fluctuations in the regions II and III. Below the temperature T^* (I), the Fermi liquid state is recovered. The expected temperature dependences of inverse susceptibility, specific heat and resistivity in a Fermi liquid regime and for ferromagnetic and antiferromagnetic fluctuations in 2 and 3 dimensions in the quantum critical region are given in table 1.1.

Table 1.1: Temperature dependence of several quantities in a Fermi liquid regime and in the presence of magnetic quantum fluctuations, in the cases of a ferromagnetic and antiferromagnetic quantum critical point in two or three dimensions. Adapted from Ref. [8, Moriya 1985].

	Fermi liquid	Ferromagnetic (Q=0)		Antiferromagnetic (Q≠0)	
		3D	2D	3D	2D
$1/\chi$	T	$T^{4/3}$	-T lnT	$T^{3/2}$	-T ln(|lnT|)/lnT
C/T	cst	-lnT	$T^{-1/3}$	cst-$T^{1/2}$	-lnT
ρ	T^2	$T^{5/3}$	$T^{4/3}$	$T^{3/2}$	T

Comparing the temperature dependences of the inverse susceptibility, specific heat and resistivity in the Fermi liquid state and in the quantum critical regions, one can observe crossovers between the two regimes. In this thesis, we have only studied three dimensional systems and we chose to look for quantum fluctuations by studying the resistivity, as it is the most simple to measure and compare. In the Fermi liquid state, the resistivity is quadratic and in the quantum critical region the exponent should be less than 2. By plotting the resistivity as a function of T^2, one can see if the system is in a Fermi liquid regime or not and, by fitting with $\rho = \rho_0 + A\,T^n$, one can know the exponent and associate the system with a given kind of quantum critical point. This method has been used in this thesis.

1.3 Fermi Surface

1.3.1 From band structure to Fermi surfaces

In an atom there are several discrete energy levels. If two atoms form a molecule those energy levels will split into a bonding and an anti-bonding level. In a solid with about 10^{23} atoms the discrete energy levels will broaden into bands with energy $\epsilon(k)$, where k denotes the crystal momentum. As the atoms composing a crystalline solid arrange to form a periodic structure, it is convenient to represent the band dispersion $\epsilon(k)$ in the reciprocal k-space inside the first Brillouin zone (equivalent to the primitive cell in the k-space). The gradient of an energy band $\epsilon_n(k)$ with respect to k is proportional to the velocity of the corresponding electron.

$$\nu_n(k) = \frac{1}{\hbar}\nabla_k \epsilon_n(k) = \frac{1}{\hbar}\frac{\partial \epsilon_n(k)}{\partial k} \tag{1.17}$$

At $T = 0$ K, all states with energies $\epsilon_n(k) \leq \epsilon_F$ will be occupied and all states with energies $\epsilon_n(k) > \epsilon_F$ will be unoccupied. This defines the Fermi energy also called Fermi level, ϵ_F. At temperatures $T > 0$, the occupation of the states changes. The probability of a state being occupied at a certain temperature T is given by the Fermi-Dirac distribution:

$$f(\epsilon, \epsilon_F, T) = \frac{1}{\exp(\frac{\epsilon - \epsilon_F}{k_B T}) + 1} \tag{1.18}$$

Let us focus on the case $T = 0$ K and solve the equation $\epsilon_n(k) = \epsilon_F$. This equation has only solutions if the solid is a metal meaning electronic states are present at the Fermi level. The set of points in the k-space which fulfill the last relation is called Fermi surface. One of the easiest cases of a Fermi surface is the one of the free electron gas. It has the shape of a sphere since the band structure is given by $\epsilon(k) = \frac{\hbar^2 k^2}{2m_0}$ where m_0 is the free electron mass. In general the Fermi surface can consist of many disconnected pockets coming from more than one band with a broad variety in shape. The different bands that cross the Fermi level are regrouped into the generic term of "conduction band". One distinguishes between two kinds of surfaces : electron and hole surfaces. While the electron surfaces correspond to a minimum in the band structure and contain occupied states, the hole surfaces contain unoccupied states and therefore correspond to a maximum in the band structure. The electron velocity vectors are pointing inward if the Fermi surface is an hole surface and pointing outward if it is an electron surface. Another property of Fermi surfaces is that they can be open or closed. The Fermi surface is usually drawn in the first Brillouin zone, which is defined as the unit cell in the reciprocal space. Closed surfaces fit into one Brillouin zone and open surfaces extend to adjacent Brillouin zones. Close or open Fermi surfaces have consequence on magneto-transport measurements.

1.3.2 Density of states

An important quantity when dealing with materials properties determined by electronic structure is the density of states (DOS) g(ϵ). The DOS is connected to the total number of electrons per unit cell by:

$$N(\epsilon < \epsilon_F) = \int_{-\infty}^{E_F} g(\epsilon) d\epsilon = N \tag{1.19}$$

Another way to calculate the total number of electrons is calculating the volume of the Fermi surface and multiplying it with the number of allowed k-values per unit volume of k-space:

$$N(\epsilon_F) = 2\frac{V}{8\pi^3} \int_{\epsilon < \epsilon_F} d^3k = 2\frac{V}{8\pi^3} \sum_n \int \Theta(\epsilon_F - \epsilon_n(k)) d^3k \tag{1.20}$$

Where Θ is the Heavyside function and the factor of 2 is due to spin degeneracy. If the spins are not degenerates we get:

$$N(\epsilon_F) = \frac{V}{8\pi^3} \sum_{n,\sigma} \int \Theta(\epsilon_F - \epsilon_{n,\sigma}(k)) d^3k \tag{1.21}$$

We can calculate the density of state:

$$g(\epsilon) = \frac{dN}{d\epsilon} = \frac{V}{8\pi^3}\sum_{n,\sigma}\int \delta(\epsilon_F - \epsilon_{n,\sigma}(k)) = \frac{V}{8\pi^3}\sum_{n,\sigma}\int_{\epsilon} \frac{1}{\left|\frac{\partial\epsilon_{n,\sigma}(k)}{\partial k}\right|} dS \tag{1.22}$$

using the relation:

$$\delta(f(x)) = \sum_i \frac{1}{\left|\frac{df}{dx}\Big|_{x=x_i}\right|}\delta(x - x_i) \tag{1.23}$$

1.3.3 Measurement of the Fermi surface

The study of the Fermi surface can be done theoretically and experimentally. From the theoretical point of view, one can calculate the band structure and, by placing the Fermi energy with the number of conduction electrons, know which bands cross the Fermi level and participate to the Fermi surface, thus giving its topology. Depending on the compound considered, these calculations can be difficult. This is especially true in heavy fermion systems, where there are many flat bands close to the Fermi level, and a small correction on the Fermi energy or the bands themselves can completely change the Fermi surface topology. The calculations have to be compared with the experimental measurements of the Fermi surface and it is then important to measure the Fermi surface. Transport and thermodynamical quantities contain informations about the Fermi surface. For example, in the simple case of a single band material, the Hall effect is linear with magnetic field and its slope gives the carrier density. In multiband systems, such information cannot be retrieved easily and one has to use different techniques to gather informations about the electronic structure. Angle resolved photoemission spectroscopy can image directly the band structure below the Fermi level. The most used probe is the de Haas van Alphen effect and other similar effects that probe directly at the Fermi level. All the physical quantities related to the density of states will detect quantum oscillations due to the Landau quantization of the electronic levels under magnetic field.

1.3.3.1 Landau quantization

When a metal is submitted to a magnetic field along a particular direction, the energy becomes quantized in the plane orthogonal to the field. For a magnetic field along the c-axis, the movement of the electrons is quantized in the (a,b)-plane and the energy:

$$\epsilon(k_z) = \frac{\hbar^2 {k_z}^2}{2m} \tag{1.24}$$

becomes:

$$\epsilon_\nu(k_z) = \frac{\hbar^2 {k_z}^2}{2m} + (\nu + \frac{1}{2})\hbar\omega_c \tag{1.25}$$

where ν is a positive integer and ω_c is the cyclotron frequency given by:

$$\omega_c = \frac{eH}{m^*} \tag{1.26}$$

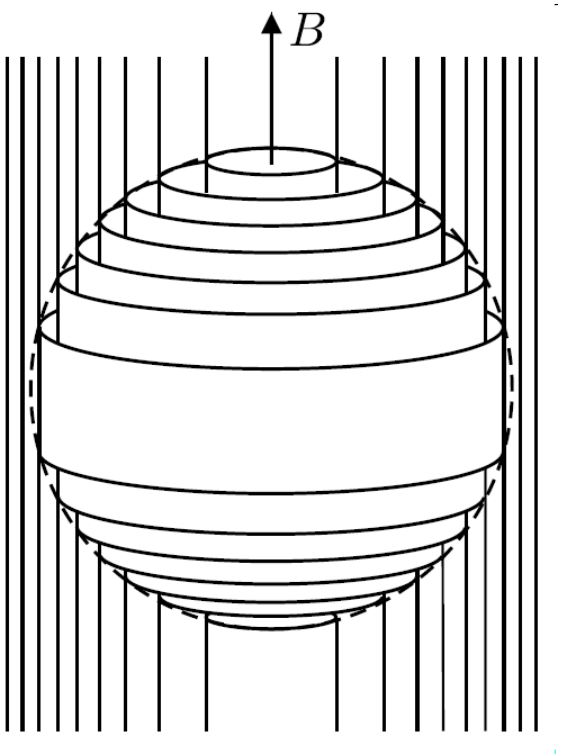

Figure 1.7: Quantization of the electronic levels under a magnetic field applied along the c-axis. The Fermi surface considered here is a sphere.

with m^* the effective mass of the quasiparticles.

In the momentum space, this quantization results in the electrons being confined into cylinders along the c-axis, as can be seen on Fig. 1.7. These cylinders are called Landau tubes or levels and the quantum number ν corresponds to the number of the Landau level. The energy spacing between two levels is $\hbar\omega_c$, therefore it increases when magnetic field strength is increasing. Since electrons cannot exist above the Fermi level, when the energy of the outer Landau tube reaches the Fermi energy, the electrons on this level drops on the next level. This gives rise to oscillations of the density of states at the Fermi level as a function of the inverse of magnetic field with a frequency F proportional to the extremal cross-section S_i of the Fermi surface in a plane orthogonal to the magnetic field direction:

$$F = \frac{\hbar}{2\pi e} S_i \tag{1.27}$$

Since the density of states is oscillating, all the probes sensitive to it (either directly proportional or indirectly so) will oscillate under the influence of the applied magnetic field.

1.3.3.2 Lifshitz-Kosevitch theory

Since many physical properties are directly proportional to the density of states at the Fermi level, such as magnetization or electrical conductivity, it is natural to expect that these quantities will oscillate when a magnetic field is applied. The oscillations are periodic

with $1/B$ and their frequencies are in units of Tesla. Lifshitz and Kosevich proposed a theory which describes the oscillations observed in the magnetization [19, Lifshitz and Kosevich, 1956] and it goes as follows:

$$M = \sum_p \sum_i \frac{1}{p^{3/2}} A_i \sin(\frac{2\pi p F_i}{B} + \phi) \tag{1.28}$$

$$\text{with} \quad A_i \propto \sqrt{B} \left| \frac{\partial^2 S_i}{\partial k^2} \right|^{-1/2} R_T R_D R_S \tag{1.29}$$

where, B is the magnetic field, p is the harmonic number, $\frac{\partial^2 S_i}{\partial k^2}$ is the curvature of the Fermi sheet considered and R_T, R_D and R_S are damping factors due to temperature, impurity scattering and spin splitting, respectively. The curvature of the Fermi surface, because it affects the way the Landau tubes are crossing the Fermi level, can reduce or increase the amplitude of the oscillations depending on whether it is small or high. If the curvature is high, then the depopulation of the Landau tube crossing the Fermi level will be almost continuous and the density of states at the Fermi energy will be almost constant, leading to small amplitude of the oscillations. Now if the curvature is low, for example if the Fermi sheet considered is a cylinder with the same axis as the magnetic field, then the electrons drops very quickly on the lower energy Landau tube when they get at the Fermi level and the oscillations should be much bigger.

The spin-splitting factor, R_S, comes from the fact that with magnetic field, the Zeeman effect will lift the spin degeneracy of the bands. This is due to the fact that the magnetic field will shift the energy of the bottom of the bands, depending on the direction of their spin, by the Zeeman energy given by:

$$E_{Zeeman} = \pm g \, \mu_B \, H \tag{1.30}$$

where g is the g-factor for the conduction electrons and μ_B is the Bohr magneton. The minus (plus) sign corresponds to a spin lying parallel (anti-parallel) to the magnetic field. This shift in energy will modify the radius of the corresponding Fermi surface and since the frequency of the oscillation is linked with the cross-section orthogonal to the magnetic field applied, it will be given by:

$$F(H) = F(H = 0) + \frac{m^*}{\hbar e} E_{Zeeman} \tag{1.31}$$

In the case of a linear Zeeman effect, this can be written as:

$$F(H) = F(H = 0) \pm \frac{m^*}{\hbar e} g \, \mu_B \, H \tag{1.32}$$

A non-linear Zeeman effect can affect the observed frequency. Indeed, the frequency measured in quantum oscillations is not the actual frequency of the band, but rather the back-projection at zero field of this frequency [124, Shoenberg 1984]. At a given field, the observed frequency is given by:

$$F_{obs}(H) = F_{true}(H) - H \frac{\partial F_{true}}{\partial H} \tag{1.33}$$

Where F_{true} is the actual frequency of the up-spin or down-spin band considered. This can be seen on Fig. 1.8. In the simple case where the Zeeman effect is linear in magnetic

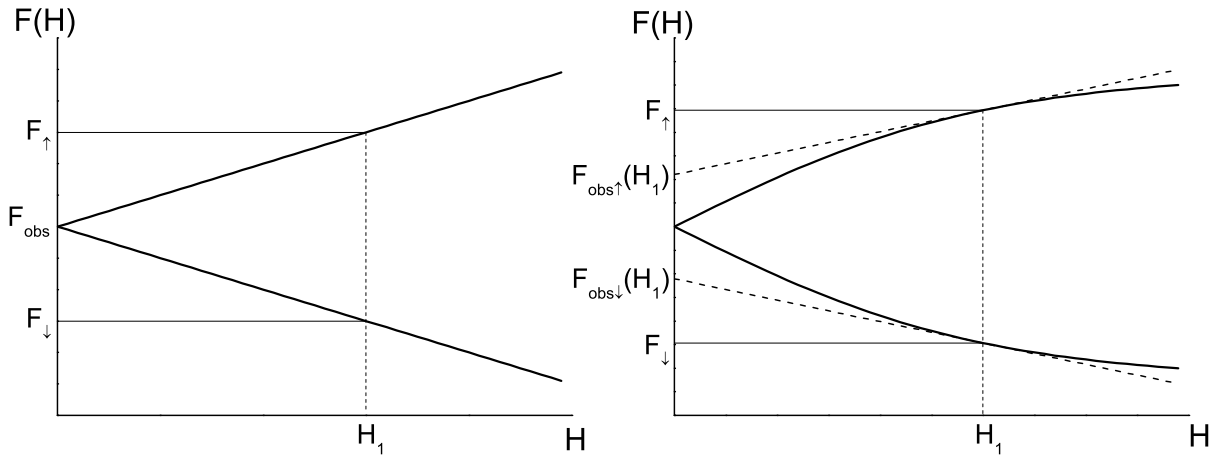

Figure 1.8: Field dependence of the up-spin and down-spin frequencies for a linear (left panel) and sub-linear (right panel) Zeeman effect.

field (left panel), then the field dependence of the true frequency also increases linearly. However, the back-projection at zero field, in this case, always gives the same observed frequency and we get $F_{obs\uparrow} = F_{obs\downarrow}$. Both frequencies are then independent of magnetic field. If the Zeeman effect is non-linear, the observed frequency of the up-spin and down-spin bands will be different (right panel). If the field dependence of the Zeeman effect is sub-linear (as in the figure), we get $F_{obs\uparrow} > F_{obs\downarrow}$ but if the Zeeman effect is super-linear (not shown here), we have $F_{obs\uparrow} < F_{obs\downarrow}$. In both cases the difference between the two observed frequencies gets larger as the magnetic field is increased. This effect will generally make the interpretation of the changes in the quantum oscillation frequency under magnetic field very difficult.

In the case of a linear Zeeman effect, the down-spin and up-spin signals can interfere, reducing the observed amplitude of the oscillations. It is given by:

$$R_S = \cos(\frac{\pi g_i p m_i^*}{2m_0}) \tag{1.34}$$

Where g_i is the g-factor of the conduction electrons of the Fermi sheet. Except in peculiar materials in which the g-factor is strongly anisotropic, this effect is rarely observed and will not be discussed here.

Impurity damping effects however play a great role in whether it is possible to detect quantum oscillations. It was shown by Dingle that the presence of impurities or crystalline defects causes a broadening of the Fermi level and acts like an additional temperature which is called Dingle temperature [20, Dingle 1952]:

$$T_D = \frac{\hbar}{2\pi k_B \tau} \tag{1.35}$$

where τ is the scattering time of the quasiparticles. The Dingle dampening factor can be written as

$$R_D = \exp\left(\frac{-\pi p r_c}{l_0}\right) \tag{1.36}$$

with $r_c = \frac{\hbar k_f}{eB}$ the radius of the cyclotron motion and l_0 the mean free path of the quasiparticles. From this we can easily understand that if the mean free path is large, the amplitude of the oscillations will also be large. Since at low temperature the mean free path of the quasiparticles is mostly due to scattering on impurities, it means that high quality samples are needed if one wants to measure quantum oscillations.

The last parameter that reduces the amplitude of the oscillations is the temperature. Like for the impurities, the finite temperature gives rise to a broadening of the Fermi level due to the broadening of the Fermi-Dirac distribution (see eq. 1.2 in chapter 1.1). If we take a magnetic field range delimited by B_{min} and B_{max}, the amplitude of the oscillations as a function of the temperature will be given by:

$$A_p(T) = A_0 \frac{\alpha p m^* T / B_{eff}}{\sinh(\alpha p m^* T / B_{eff})} \tag{1.37}$$

with $\alpha = 2\pi^2 k_B m_e / e\hbar \approx 14.69$ T/K and B_{eff} given by $\frac{1}{B_{eff}} = \frac{1}{2}\left(\frac{1}{B_{min}} + \frac{1}{B_{max}}\right)$.

This formula is very useful to determine the effective mass of the quasiparticles of this Fermi sheet. It can be obtained simply by extracting the amplitude of the corresponding frequency in the Fast Fourier Transform of the signal, plotting it against temperature and fitting with the formula. The amplitude of the oscillations, with this formula, is maximum at $T = 0$ K.

1.3.3.3 Pantsulaya-Varlamov theory

The Lifshitz-Kosevich theory can be applied fairly well to most of the quantities that can be measured, such as magnetization (de Haas-van Alphen) or conductivity (Shubnikov-de Haas). This is mainly due to the fact that all these quantities are directly proportional to the density of states. The thermoelectric power, however, does not follow this theory. As was described in chapter 1.1.1, the Mott formula states that the Seebeck coefficient is actually proportional the derivative of the density of states with respect to energy. Also, since there is no entropy left at zero temperature, the thermoelectric power as well as the oscillating part of the signal goes to zero when $T \to 0$, which cannot be taken into account with the Lifshitz-Kosevich theory. The anomalous temperature dependence of the oscillations in the Seebeck coefficient has been first observed experimentally and explained by Young and Fletcher [21, 22, 23, Young 1973, Fletcher 1981, 1983] and later properly calculated by Pantsulaya and Varlamov [30, Pantsulaya and Varlamov 1989]. Their calculations lead to the following temperature dependence of the amplitude of the oscillations :

$$A_p(T) = C\frac{\pi}{2}\frac{1}{\sinh(\frac{\alpha p m^* T}{B_{eff}})}\left(\frac{\alpha p m^* T}{B_{eff}}\coth(\frac{\alpha p m^* T}{B_{eff}}) - 1\right) \tag{1.38}$$

Where C is a constant. It is interesting to note that if we call $X = \alpha p m^* T / B_{eff}$, this formula is simply the derivative of the Lifshitz-Kosevich one with respect to X.

The schematic temperature dependence of the amplitude of the oscillations for both the Lifshitz-Kosevich and Pantsulaya-Varlamov theories are shown on Fig. 1.9. Contrary to the Lifshitz-Kosevich function, the maximum in the Pantsulaya-Varlamov function is

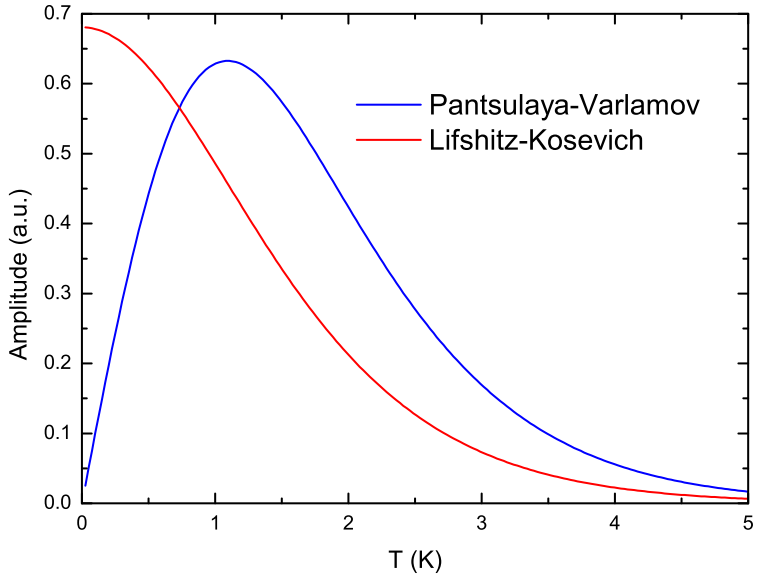

Figure 1.9: Theoretical temperature dependence of the amplitude of the oscillations for the Lifshitz-Kosevich and Pantsulaya-Varlamov formulaes, for an effective mass of 1 m_0 and an effective magnetic field of 10 T.

not at $T = 0$ K, but at a temperature $T_{max} \approx 0.11 \frac{B_{eff}}{pm^*}$ above which the amplitude decreases again and goes to zero at $T = 0$ K. T_{max} depends on the effective mass of the quasiparticles and is inversely proportional to it. Therefore, with a higher effective mass, the peak in the temperature dependence of the amplitude of the thermoelectric power oscillations will be shifted to lower temperature and become narrower. This makes the observation of high effective masses difficult, as the maximum of the amplitude will be at very low temperature and the amplitude will drop quickly as temperature is increased.

Recently, it has been shown that the Pantsulaya-Varlamov formula fits quite well the experimental temperature dependence of the thermoelectric power oscillations in UGe_2 [24, Palacio 2016].

In this thesis, all quantum oscillations of the thermoelectric power has been treated with the Pantsulaya-Varlamov theory in order to extract the effective masses.

1.4 Topological change of the Fermi surface

One can change the Fermi surface by varying the Fermi energy and/or the band structure. Possible methods for changing the band structure are, for example, the application of pressure or magnetic field. If either variation yields a topological change of the Fermi surface, one calls it a "Lifshitz transition", "Electronic topological transition" (ETT) or "$2\frac{1}{2}$ order phase transition", which takes place if a van Hove singularity (a non-smooth point in the density of states, where its derivative is discontinuous) at ϵ_c passes the Fermi level: $\epsilon_F = \epsilon_c$. The name "Lifshitz transition" arises from a publication by I. M. Lifshitz [25, Lifshitz 1960], where he considered topological changes of the Fermi surface and the resulting consequences for the density of states and other physical properties. The name

ETT is clear from its definition and the reason why this transition is sometimes called a "$2\frac{1}{2}$ order phase transition" will be described later. In a three dimensional system, only four different topological changes of the Fermi surface are possible :
- the disruption of a neck in the Fermi surface
- the creation of a neck in the Fermi surface
- the creation of a new pocket of the Fermi surface (void formation)
- the disappearance of a pocket of the Fermi surface (void disruption)

Let us now focus on the creation or disappearance of a pocket of the Fermi surface. The result can be generalized to the case of the disruption or creation of a neck.

1.4.1 Topological changes in the band structure

One can calculate the variation of the density of states in the void disruption/creation case of a Lifshitz transition. Consider the band structure ϵ_k of a solid. Assume at some region for one band $\epsilon_n(k)$ has the following form:

$$\epsilon_n(k) = \epsilon_c \pm (\frac{\hbar^2}{2m_x}(k_x - k_{0x})^2 + \frac{\hbar^2}{2m_y}(k_y - k_{0y})^2 + \frac{\hbar^2}{2m_z}(k_z - k_{0z})^2) \tag{1.39}$$

The question is now, how does the Fermi surface of such a band looks like. The term in the brackets is everywhere greater or equal to zero, so that the Fermi energy has to be greater than ϵ_c in case of the plus sign and smaller than ϵ_c in case of the minus sign to give additional pocket in the Fermi surface. For simplicity we consider here only the case with the plus sign (electron surface), the case with the minus sign (hole surface) is analogous. Another simplification, which does not affect generality, is that we shift the coordinate system so that its origin is at the point k_0. If the Fermi energy is close to ϵ_c and $\epsilon_n(k)$ is given by $\epsilon_n(k) = \epsilon_F$, then we can solve this equation for k_z:

$$k_z = \pm\sqrt{\frac{2m_z}{\hbar^2}(\epsilon_F - \epsilon_c) - (\frac{m_z}{m_x}k_x^2 + \frac{m_z}{m_y}k_y^2)} \tag{1.40}$$

The ellipsoidal Fermi surface appears when $\epsilon_F > \epsilon_c$ and disappears when $\epsilon_F < \epsilon_c$. With the minus sign in the Eq. 1.39, it will be the other way around. The density of states for such an ellipsoid can be calculated:

$$\delta g(\epsilon) = \begin{cases} \frac{V}{\pi^2\hbar^3}\sqrt{2m_x m_y m_z}(\epsilon - \epsilon_c)^{\frac{1}{2}} & \text{electron ellipsoid} \\ -\frac{V}{\pi^2\hbar^3}\sqrt{2m_x m_y m_z}(\epsilon_c - \epsilon)^{\frac{1}{2}} & \text{hole ellipsoid} \end{cases} \tag{1.41}$$

The density of state here is called δg corresponding to the electronic topological transition, so the total density of states is given by:

$$g(\epsilon) = g_0(\epsilon) + \delta g(\epsilon). \tag{1.42}$$

The part coming from all parts aside from δg of k-space with energy ϵ is called g_0. We are assuming that there are no other electronic transition in their energy range under consideration so g_0 is a smooth function of energy. Eq. 1.40 is only valid for the argument of the square root being greater than zero. Otherwise $\delta g = 0$. In conclusion, the density

of states has a kink at ϵ_c where the electronic topological transition takes place. Similarly, the density of states will exhibit an extra contribution in the case of the disruption or creation of a neck. Comparing all the results (additional ellipsoid, neck, broken neck) leads to the conclusion that in the case of an electronic topological transition, the density of states can be written as:

$$|\delta g(\epsilon)| = \begin{cases} \frac{V}{\pi^2\hbar^3}\sqrt{2m_x m_y m_z}|\epsilon - \epsilon_c|^{\frac{1}{2}} & \text{Region I} \\ 0 & \text{Region II} \end{cases} \tag{1.43}$$

Here, region I is the less connected region (one more ellipsoid in the Fermi surface or a broken neck) and in region II the neck is connected or the ellipsoid has vanished or not yet formed. The shape of the sensity of states, which has a kink at the transition due to the additional contribution on one side is plotted on Fig. 1.10. This kink in the density of states will have an effect in any quantity proportional to it, such as electrical conductivity or magnetization. The thermoelectric power, as it is the derivative of the density of states with respect to energy, will have a larger response.

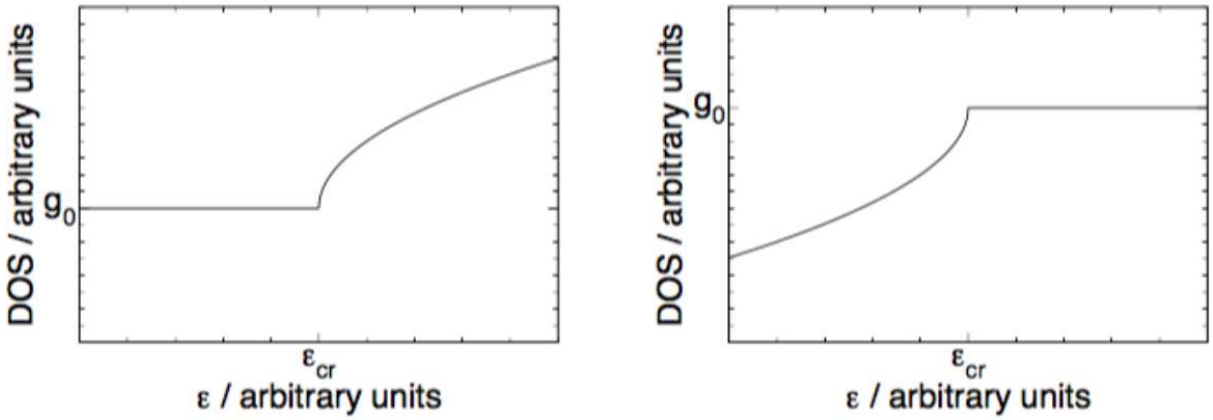

Figure 1.10: Left picture: Density of states for an electron ellipsoid appearing at ϵ_c or density of states of a neck, whose band structure has two terms with a minus sign in front, breaking at $\epsilon = \epsilon_c$. Right picture: Density of states for a hole ellipsoid disappearing at $\epsilon = \epsilon_c$ or density of states of a neck, whose band structure has one term with a minus sign in front and being created at $\epsilon = \epsilon_c$.

Since we have connected Lifshitz transitions to special shapes of the band structure, the conclusion can be drawn that Lifshitz transition can already be seen in the band structure. If a minimum (maximum) of the band structure crosses the Fermi energy, an additional electron (hole) ellipsoid will appear on that side of the transition. In the case of a Lifshitz transition, which creates or disrupts a neck, a saddle-point crosses the Fermi level. So in general one can say that if:

$$\frac{\partial \epsilon_n(k)}{\partial k} = 0 \tag{1.44}$$

is fulfilled for some band at the Fermi energy, the material is undergoing a Lifshitz transition.

1.4.2 Anomalies in the thermodynamic properties

To see the consequences of the van Hove singularity in the thermodynamic quantities, we calculate the thermodynamic potential $\Omega(\mu,\mathrm{T})$ of an electron gas in a metal. The thermodynamic potential is defined as:

$$\Omega = U - TS - \mu N \tag{1.45}$$

Here, U is the inner energy of the system, T denotes the temperature, S the entropy, μ the chemical potential and N the particle number. We consider here only the case $T = 0$. In this case the energy of the system is given by:

$$U = \int_{-\infty}^{\epsilon_F} g(\epsilon)\epsilon d\epsilon \tag{1.46}$$

At zero temperature, the chemical potential equals the Fermi energy :

$$\mu(T = 0) = \epsilon_F \tag{1.47}$$

This yields for the thermodynamic potential:

$$\Omega(\epsilon_F, 0) = \int_{-\infty}^{\epsilon_F} (\epsilon - \epsilon_F)g(\epsilon)d\epsilon \tag{1.48}$$

We can calculate the contribution of topological change of the Fermi surface to the thermodynamic potential:

$$\delta\Omega = \int_{-\infty}^{\epsilon_F} d\epsilon(\epsilon - \epsilon_F)\delta g(\epsilon) \tag{1.49}$$

So considering only the case of an additional electron surface, one gets for region I:

$$\delta\Omega = \frac{V}{\pi^2\hbar^3}\sqrt{2m_x m_y m_z}\int_{\epsilon_c}^{\epsilon_F} d\epsilon(\epsilon - \epsilon_F)(\epsilon - \epsilon_c)^{\frac{1}{2}} = -\frac{4V}{15\pi^2\hbar^3}\sqrt{2m_x m_y m_z}(\epsilon_F - \epsilon_c)^{\frac{5}{2}} \tag{1.50}$$

and for Region II, $\delta\Omega = 0$ If we consider $\Omega(\epsilon_F, 0)$ and its derivatives, we find that $\Omega(\epsilon_F, 0)$ and $\frac{\partial\Omega}{\partial\epsilon_F}$ are differentiable, $\frac{\partial^2\Omega}{\partial\epsilon_F^2}$ is continuous but not differentiable at $\epsilon_F = \epsilon_c$ due to its vertical kink, which is proportional to $(\epsilon_F - \epsilon_c)^{1/2}$ and $\frac{\partial^3\Omega}{\partial\epsilon_F^3}$ tends to infinity at $\epsilon_F = \epsilon_c$ proportional to $(\epsilon_F - \epsilon_c)^{-1/2}$. These consideration lead Lifshitz to call the topological transition of a Fermi surface $2\frac{1}{2}$ order phase transition though an electronic topological transition can only be considered as a phase transition at $T = 0$. At higher temperatures the transitionis smeared out and becomes a crossover.

1.4.3 Anomalies in the Seebeck coefficient

With the kink in the density of states, one can already expect a response from the quantities proportional to it at a Lifshitz transition. However, the thermoelectric power is

also strongly sensitive to the energy dependence of the scattering term and its contribution gives a larger response than in other transport or thermodynamic quantities.

Let us consider that an electronic topological phase transition takes place at the energy ϵ_c. This energy can represent, for example, an applied magnetic field. Then let us define z as:

$$z = \epsilon - \epsilon_c \tag{1.51}$$

which represents whether the system is situated below or above the Lifshitz transition, which takes place at $z = 0$. By using diagrammatic techniques described in Ref. [27, Varlamov 1985] (and references therein), one can demonstrate that the thermoelectric power, at finite temperature, in the vicinity of the transition, is given by:

$$S = S_0 \begin{cases} 1 + \frac{1}{4}\sqrt{\frac{\mu}{|z|}} & \text{for z} \lesssim \text{-T} \\ 0.5 + 0.18\sqrt{\frac{\mu}{T}}\frac{z}{T}\exp(-\frac{z}{T}) & \text{for z} \gtrsim \text{T} \end{cases} \tag{1.52}$$

Where T is the temperature considered, S_0 is the background thermoelectric power and μ is the chemical potential. The schematic relative variation of the Seebeck coefficient (noted Q here) for different temperatures as a function of z close to the Lifshitz transition is shown on Fig. 1.11. This represents only the enhancement of the Seebeck coefficient due to the transition.

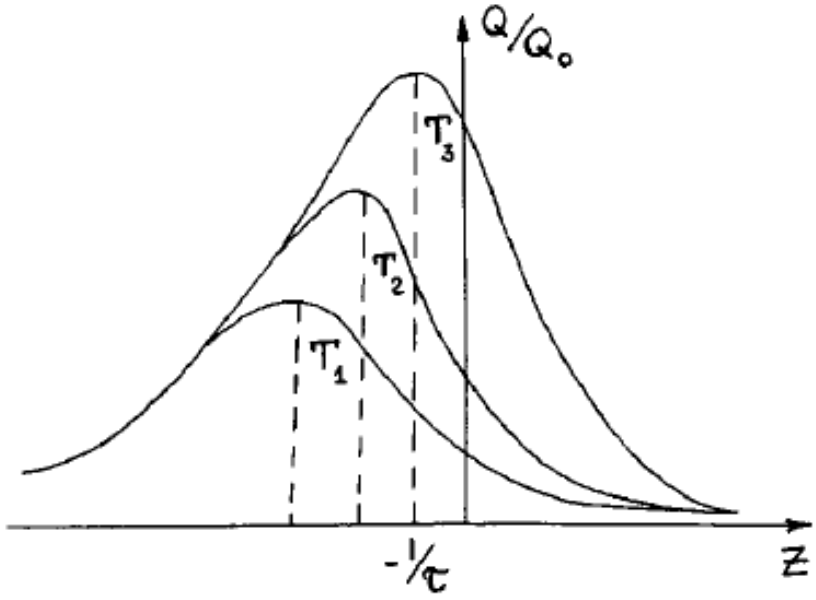

Figure 1.11: Schematic variation of the Seebeck coefficient as a function of z close to the Lifshitz transition. Three temperatures are considered with $T_1 > T_2 > T_3$. Taken from Ref. [27, Varlamov 1985].

One can immediately see that the maximum of the Seebeck coefficient is not actually situated at the point where the Lifshitz transition occurs, but at a slightly lower energy that depends on temperature : $z_{max} \approx$ -1.28×T. The amplitude of the maximum is

also decreasing as the temperature increases, which is to be expected since the Lifshitz transition is an actual transition only at zero temperature and is a crossover at finite temperature. It is given by $S_{max} \approx 0.19\ S_0\sqrt{\mu/T}$ and since μ is of the order of the Fermi energy, at low temperature S_{max} should be very large. Another interesting point is that the peak is not symmetrical with respect to the maximum. Below the transition, it increases with a power law with $S \propto |z|^{-1/2}$ and above, it decreases more rapidly with an exponential law with $S \propto \frac{z}{T}\exp(\frac{-z}{T})$. However, the higher the temperature is, the harder it is to distinguish between the power law and the exponential one. The peak also becomes much smaller as temperature is increased and experimentally, one can see it is usually quickly smeared out.

Experimentally, this particular peak in the thermoelectric power has be observed, for example, in $Bi_{1-x}Si_x$ thin films [28, Völklein 1987] or in the heavy fermion system $YbRh_2Si_2$ [71, Pourret 2013]. In this thesis, we have observed anomalies in the field dependence of the thermoelectric power in UCoGe and $CeIrIn_5$ which shape corresponds to the predictions for a Lifshitz transition. However, fitting the two sides of the peak with the expected dependence is difficult. This is due to the fact that in the calculation, the energy is considered as the control parameter and while the magnetic field can be approximated as such, it can also have additional effects that are not taken into account in the calculation. Moreover, the background Seebeck coefficient can have a large field dependence and it is then difficult to distinguish between the background and the Lifshitz transition contributions. Thus, no fitting of the anomalies with the calculated dependence was performed in this thesis.

Chapter 2

Experimental Methods

2.1 Single crystal growth and caracterization

In heavy fermion compounds, the sample quality is a very important parameter to consider when one wants to study the properties of the materials. For example, in UCoGe, ferromagnetism depends strongly on the sample quality: the Curie temperature, T_C ranges from 2 K to 3 K for most single crystals and in the samples where the quality is very bad, ferromagnetism may not show at all. More generally, it is known that unconventional superconductivity usually appears only in high quality crystals. The Dingle damping factor of the quantum oscillations is also varying with the sample quality, the amplitude being reduced in low quality samples. Therefore it is necessary to grow the highest quality samples possible, which requires a long expertise in crystal growth.

The samples of URhGe, UCoGe, UPd_2Al_3 studied in this thesis have been grown in a tetra-arc furnace, using high purity materials and under controlled argon atmosphere. A stoichiometric amount of elements are placed in a water-cooled copper crucible and melted using electric arcs. The polycrystalline ingot is then turned and melted again. This procedure is repeated several times in order to ensure the homogeneity of the ingot.

To get a single crystalline phase out of the ingot, the Czochralski pulling technique is used. A photograph of the furnace and the pulling process is shown on the left of Fig. 2.1. A water-cooled tungsten tip is put inside the melted ingot from above and then pulled up at a very low speed: the pulling rate is usually 10 to 15 mm/h. If one wants to have a particular orientation of the crystal, it is possible to put an oriented seed on the tip. The pulled material then presents itself in the form of a cylinder and is single crystalline. The single crystal of $CeIrIn_5$ have been grown by the so-called self-flux method, where stoichiometric amount of cerium and iridium have been melted in a large quantity of indium at high temperature. The mixture is then slowly cooled down during several days.

In order to know in which crystallographic direction the current (for transport measurements) and the magnetic field is applied, it is necessary to orient the sample. To do that, the Laue X-ray diffraction technique is used. The photograph taken allows us to know how to cut the sample to get the appropriate directions for current and magnetic field. A typical Laue pattern is shown on Fig. 2.2. The cutting is then done with a spark cutter.

The quality of a sample can be, at first, estimated by the clarity of the Laue photograph. Then to get a quantitative measurement one can measure the resistivity of the

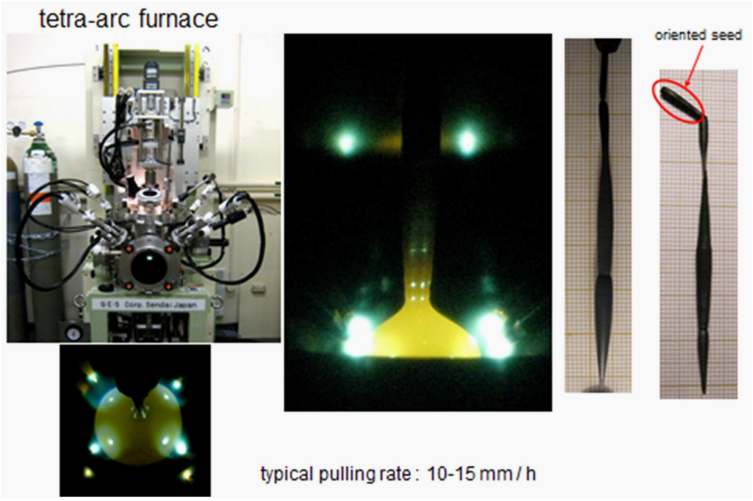

Figure 2.1: Left : Photographs of the tetra-arc furnace, the melted material and the pulling process. Right : Photographs of some single crystals pulled by this technique.

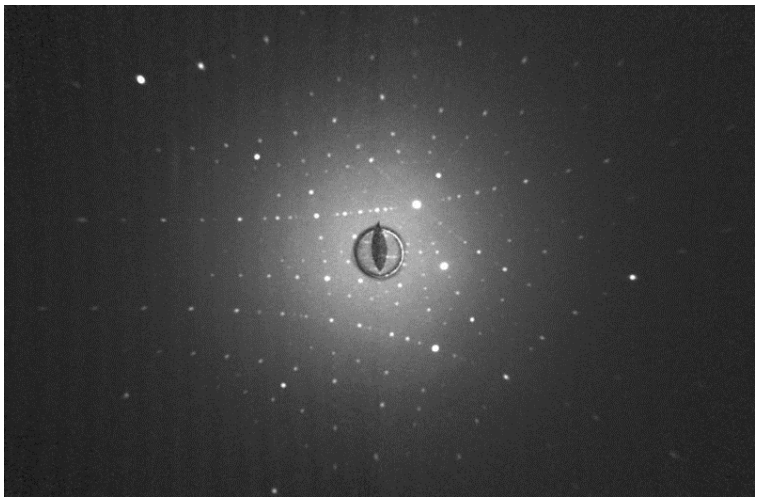

Figure 2.2: Laue photograph of a UPd_2Al_3 single crystal.

sample down to very low temperature. Indeed, when the temperature is low enough, the residual resistivity is dominated by the scattering of the electrons on the impurities and the defects of the crystal. By calculating the residual ratio of the resistivity at 300 K and the one extrapolated at 0 K, $RRR = \frac{\rho(300K)}{\rho(0K)}$, it is possible to get a rather good idea of the sample quality. Indeed, the better the quality of the sample, the lower the resistivity at very low temperature and the higher the residual ratio of resistivity.

Growing high quality samples can be, depending on the compound, very difficult. For instance, in materials such as UCoGe or URhGe, which are believed to have incongruent melting point, the 111 phase is already not easy to get, and high quality samples are usually very small. The samples studied in this thesis are the following: for UCoGe, two

samples with RRR of 105 and 190. In the case of URhGe, three samples were studied, with RRR of 23, 36 and 38 for current along c-, b- and a-axis respectively. On the other hand, UPd_2Al_3 and $CeIrIn_5$ are much easier to grow and both samples had RRR > 100. All the samples studied in this thesis were grown by Dai Aoki.

2.2 Thermoelectric measurements

As was described in chapter 1.1.1, the thermoelectric power is a longitudinal voltage arising from the application of a thermal gradient and the Nernst effect is a transverse voltage that appears if a magnetic field is applied in addition to the thermal gradient.

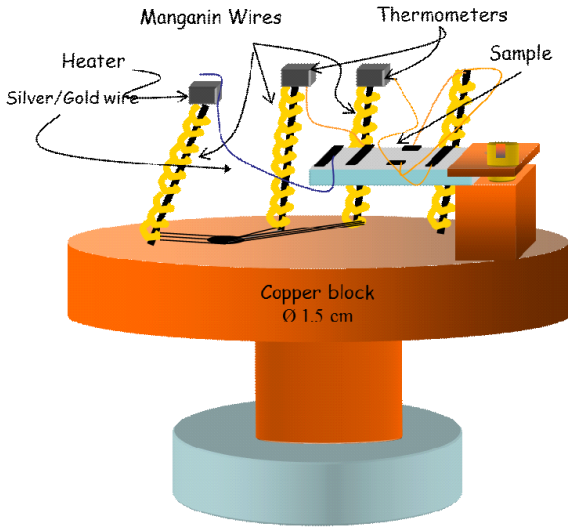

Figure 2.3: Schematic view of a typical sample holder to measure thermoelectric coefficients.

There are several ways to measure the thermoelectric coefficients. In this thesis, we used the vacuum "one heater - two thermometers" technique. The schematic view of a typical sample holder is shown on Fig. 2.3. One end of the sample is attached using silver paste to a copper block that plays the role of heat sink and the rest of the sample hangs in vacuum. In order to improve the thermal contact between the sample and the heat sink, we can add 15 μm gold wires spot welded to the sample. As heater and thermometers, we used commercial RuO_2 chips with $R(300\ \mathrm{K}) = 1\ \mathrm{k}\Omega$. These RuO_2 chips have only small magnetoresistance of the order of 1% at $H = 16$ T, making the error in temperature negligible compared to the applied thermal gradient. They have been calibrated from $T = 80$ mK to $T = 6$ K against a calibrated germanium thermometer. They are 3 mm long, 2 mm large and 1 mm thick. An electrical current is applied in the heater, generating power through the Joule effect that is transmitted by a gold or silver wire to the sample. Once the equilibrium is reached, a thermal gradient is established in the sample. The

thermometers and the heater have to be decoupled from the copper block because the heat leak must be as small as possible, in order to be sure that the thermometers recovers the correct temperature of the sample and that most of the power coming from the heater goes to the sample. To do that, the electrical wires used to measure the resistance of the thermometers and send current to the heater are 30 μm manganin wires spiraled around thin capton tubes, which have very low thermal conductivity at low temperature, to get a total resistance $R \approx 250\ \Omega$. The same kind of wires are used to recover the Seebeck and Nernst voltages. The heat leak can be minimized by using wires to bring the heat from the sample to the thermometers with a very low resistance. In this setup, we spot welded 15 μm gold wires to the sample and connected those to the thermometers using 50 μm silver wires. The spot welding ensures that the thermal contact resistance between the sample and the thermometers and the electrical contact resistance between the sample and the voltage wires are as low as possible.

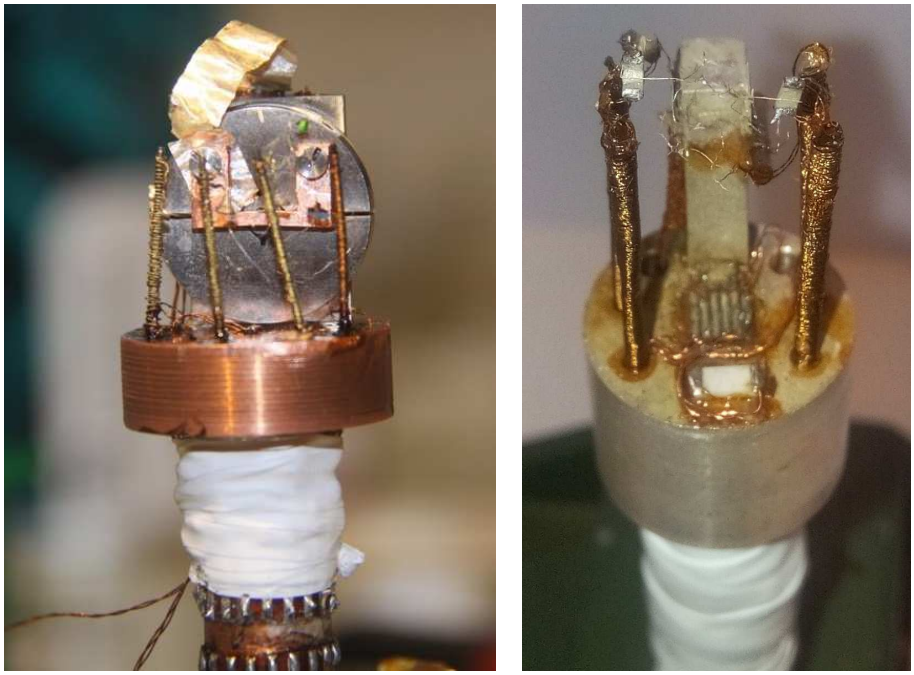

Figure 2.4: Left : Photograph of the copper sample holder with an Attocube nanopositioner. Right : Photograph of the silver sample holder used for very high field measurements.

We measured thermoelectric power with two sample holders. One, made of copper and equipped with an Attocube nano-positionner for precise field alignment, which we used in a dilution refrigerator with a base temperature of 80 mK and with a superconducting magnet up to 16 T in our laboratory. The other sample holder was made of silver, in order to minimize the nuclear specific heat under very high magnetic field. It was used for measurements in the high magnetic field facility in Grenoble (LNCMI) in which we measured with resistive magnets up to 34 T and in a ^{3}He cryostat with a base temperature of 320 mK. Photographs of the sample holders used in this thesis can be seen on Fig. 2.4. On the left is the copper one and on the right is the silver one. For a better temperature regulation, a RuO_2 thermometer is placed directly on the sample holder, along with a

stain gage, used as a regulation heater. The resistance of this thermometer was measured and converted in temperature using a commercial TRMC2 temperature controller. The temperature of the two thermometers measuring the thermal gradient was recovered using a commercial MMR3 device.

Generally, in metals, the Seebeck coefficient is rather small (of the order of 1 μV.K^{-1}). At low temperature, to avoid any non-linearity in the response of the system, the thermal gradient has to be small compared to the temperature ($\Delta T/T \approx 3\%$). At $T = 100$mK, this gives a ΔT of 3 mK, leading to a voltage of the order of 3 nV, which is very small and requires the use of nanovoltmeters to measure it properly. To reduce the noise as much as possible, one has to measure the voltage with wires that have the least soldering because it can easily give rise to a parasitic thermoelectric voltage. To avoid any soldering, we used junctions where the wires are pressed together in order to get electrical contact between them. With this method as well as with some filters, we managed to have less than 1 nV of noise in our setup.

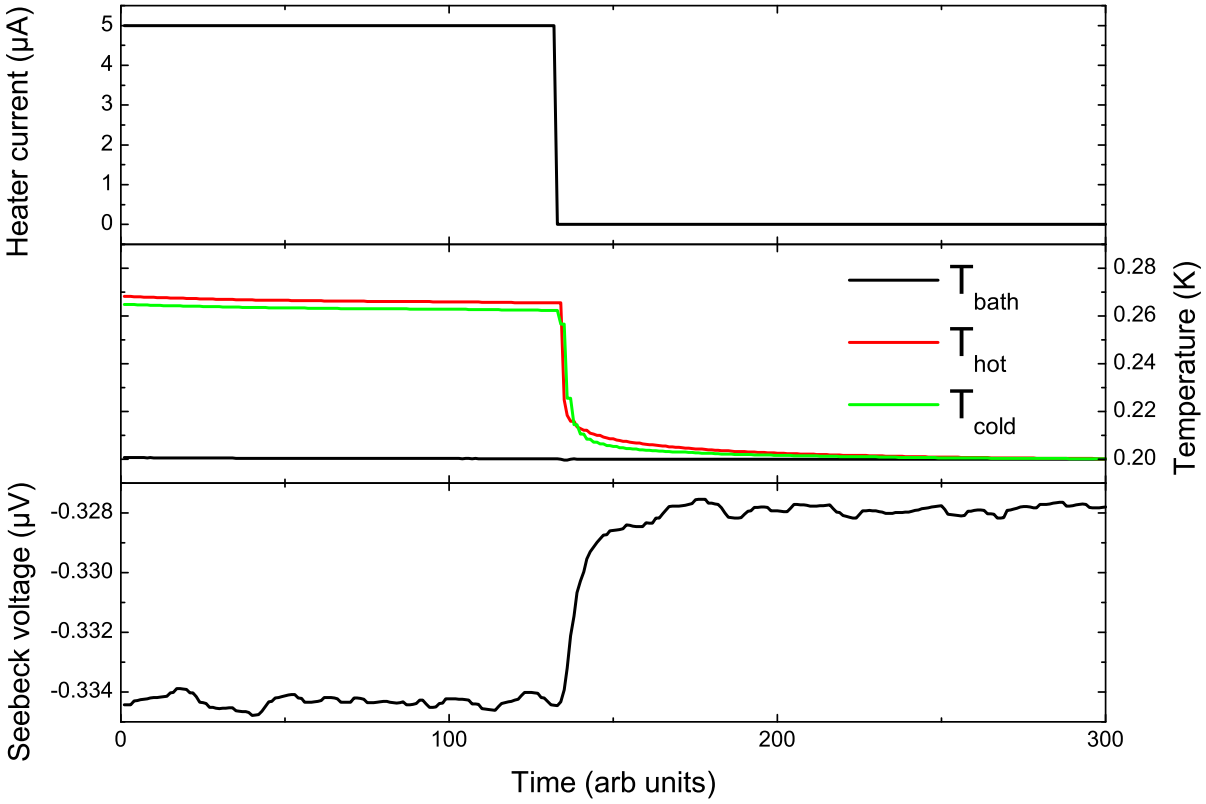

Figure 2.5: Time dependence of the current applied in the heater (top), the three thermometers T_{bath}, T_{hot} and T_{cold} (middle) and the Seebeck voltage (bottom) in the measurement sequence.

In this thesis we made two types of measurements : continuous field sweeps and averaged field steps. The averaged field steps measurement is made by stopping the magnetic field at each desired point to measure the thermoelectric voltage as well as the two thermometers, both with and without applying thermal gradient. The Seebeck is then recovered by subtracting the values of thermal gradient and thermoelectric voltage obtained with a thermal gradient by the one without. The typical signal obtained is shown on Fig.

2.5. For the continuous measurement, the field is continuously swept. The thermoelectric voltage and the temperature of the thermometers are measured before starting the sweep both with and without applying thermal gradient. Then the thermal gradient is kept applied and the field is swept. During the sweep, the thermal gradient is measured as well as the thermoelectric voltage. At the end of the sweep, the thermoelectric voltage and the thermometers are again measured both with and without thermal gradient. Usually, the residual thermal gradient and thermoelectric voltage without applied current do not change between the beginning and the end of the sweep, so a constant value can be removed from the signal with current for both quantities. Since this is a DC measurement, the magnetic field sweep generates a voltage proportional to $\frac{dB}{dt}$ which is removed as well.

2.3 Resistivity

To measure resistivity, we used the common AC four-point probe method. Four 15 μm gold wires are spot-welded to the sample, The outer ones are used to apply electrical current and the inner ones are used to recover voltage. The AC current was applied by a SR830 lock-in amplifier at a frequency of 17 Hz delivering a 1 V voltage into a 10 kΩ resistance for a current of 100 μA. We checked for heating effect of the applied current by lowering it and found that it was negligible. The voltage recovered is amplified by a factor 100 in a room temperature transformer and read on the same Lock-in used to apply current.

2.4 de Haas van Alphen measurements

The de Haas van Alphen experiment is a measurement of the magnetic susceptibility and was measured using a field modulation magnetization technique. The sample is fixed with thermal grease inside a coil used to pick up the magnetization signal of the sample. The coil is made of 5000 turns of copper wire and is 8 mm in diameter, the sample space in the center is 2 mm large. This coil is mounted on a mechanical rotator, for alignment in magnetic field and angular dependence, which is controlled by a piezoelectric motor. This is shown on the left panel of Fig. 2.6.

This setup was used with a top-loading dilution fridge with a base temperature of 25 mK and with a 15 T superconducting magnet. This cryostat is equipped with a modulation coil which can generate an alternative magnetic field of 10 mT with a frequency of 15.5 Hz delivered by a SR830 lock-in amplifier. The signal goes through a bipolar operational power amplifier and to the modulation coil with a voltage of 1.3 V. The signal from the pick-up coil is then recovered by the lock-in at the second harmonic frequency. This is the standard modulation technique. It has the advantage of getting rid of all the non-oscillating part of the signal but it also multiplies the signal by a Bessel function which amplitude first increases with magnetic field and then decreases again at higher field. The position in field of the Bessel function depends on the amplitude of the modulation field and the frequency of the observed oscillation. This is well explained in Ref. [124, Shoenberg 1984].

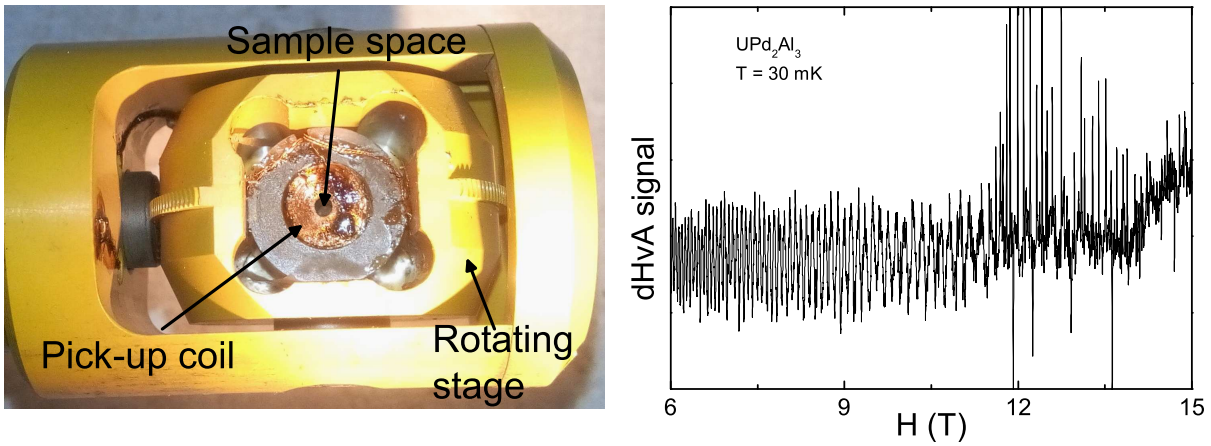

Figure 2.6: Left : Photograph of the experimental setup. Right : de Haas-van Alphen signal measured in UPd_2Al_3 at $T = 30$ mK.

The signal obtained for UPd_2Al_3 at $T = 30$ mK is shown on the left panel of Fig. 2.6. Quantum oscillations can be resolved.

2.5 Low temperatures

The measurements in this thesis, except the ones in LNCMI Grenoble and a few measurements done in a Physical Properties Measurements System (PPMS), were done at very low temperature using ^{3}He/^{4}He dilution fridge. The principle of dilution fridges is described very well in literature and will not be presented here [29, Enss and Hunklinger 2005]. The cryostat used for thermoelectric and resistivity measurements was homemade. The temperature of the mixing chamber is measured with a calibrated Germanium thermometer. For a better regulation of the sample temperature, we put a calibrated RuO_2 resistance directly on the sample holder and nearby a strain gage is used as a regulation heater.

2.6 Analysis of the quantum oscillations

As was covered in chapter 1.3.3, at low temperature and high magnetic field, the magnetic susceptibility and the thermoelectric power can show quantum oscillations. For the susceptibility, the analysis is quite straightforward. The signal is periodic with respect to the inverse of magnetic field and the frequencies observed can be easily extracted with a Fourier transform.

Therefore, in all this study, the frequencies of the quantum oscillations as well as their corresponding amplitudes were extracted using Fast Fourier Transform (FFT). To reduce the side peaks appearing because of a rectangle FFT window, we used a Hanning function

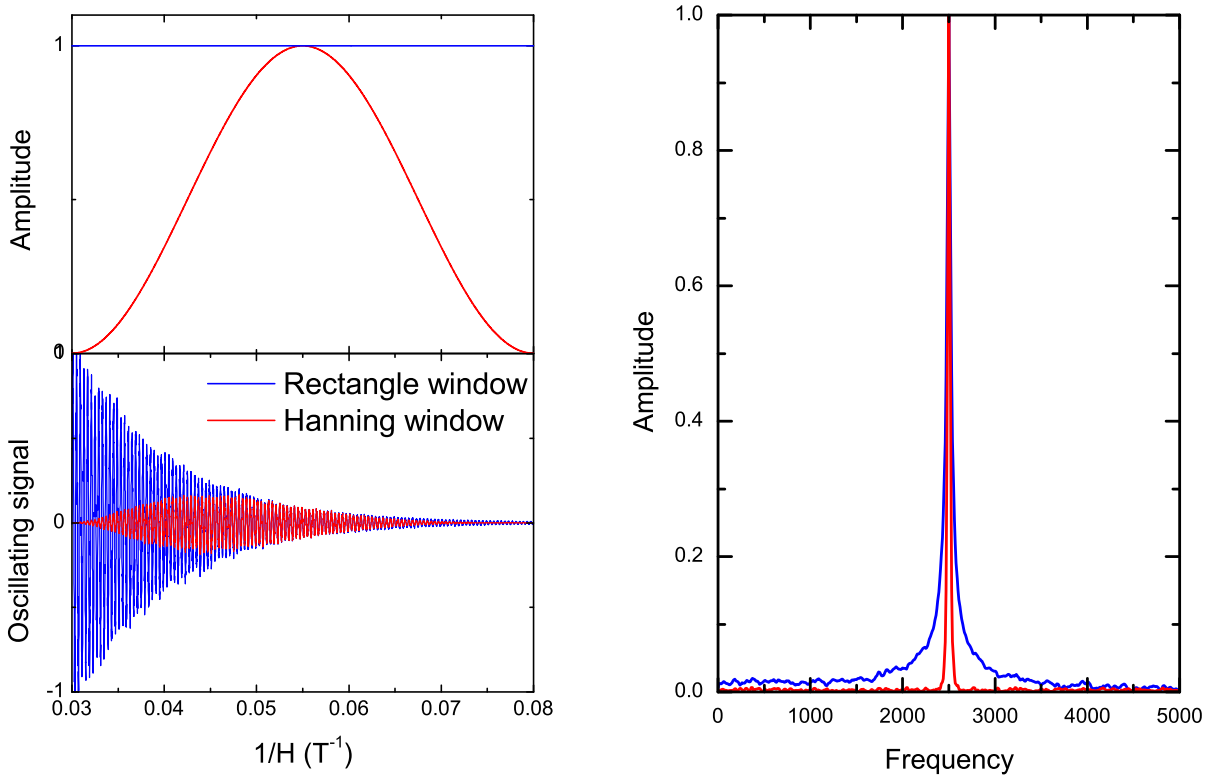

Figure 2.7: Left : Rectangle (blue curve) and Hanning (red curve) windows on an interval from $H^{-1} = 0.03$ T^{-1} to $H^{-1} = 0.08$ T^{-1} (top) and inverse field dependence of a schematic oscillation signal multiplied by the two windows on the same interval (bottom). Right : FFT spectrum of the oscillating signal on this inverse field interval with rectangle window (blue curve) and Hanning window (red curve).

for all FFTs:

$$f(t) = \begin{cases} \frac{1}{2} - \frac{1}{2}\cos(\frac{2\pi t}{T}) & \text{for t } \in[0,\text{T}] \\ 0 & \text{otherwise} \end{cases} \tag{2.1}$$

The inverse field dependence of a rectangle (in blue) and Hanning (in red) window is shown on the top left panel of Fig. 2.7 (top). A schematic inverse field dependence of a quantum oscillation with a frequency of 2500 T, multiplied by a rectangle and a Hanning window is shown on the bottom left panel of Fig. 2.7. The Fast Fourier Transform of both signal is shown on the right panel of Fig. 2.7. The peak is much more narrow when using the Hanning function than with the simple rectangle one. Therefore, in this thesis, all Fast Fourier Transforms were performed using the Hanning window.

Chapter 3

Fermi surface change with no magnetic transition

In this thesis, we have studied the effect of a magnetic polarization on the Fermi surface in heavy fermion systems. To do this we performed mainly systematic thermoelectric power measurements at low temperature and in high magnetic field. The results are separated into two chapters. In the first one, we have studied how the magnetic field can induce, through the Zeeman effect, a modification of the Fermi surface without any evidence of a magnetic transition. Two systems were studied : the ferromagnetic superconductor UCoGe, where the magnetic field was applied along the easy magnetization c-axis and the paramagnetic superconductor $CeIrIn_5$, with a magnetic field applied along the a-axis. In these two systems, evidences of magnetic field induced topological changes of the Fermi surface are given.

3.1 UCoGe

In this section, thermoelectric power measurements at low temperature and high magnetic field on the ferromagnetic superconductor UCoGe are reported. For a magnetic field applied along the easy magnetization c-axis, the presence of successive Lifshitz type transitions is demonstrated through the direct observation of quantum oscillations (see Ref. [59, Bastien 2016]). The longitudinal configuration studied with $J_Q \parallel H \parallel b$ did not show the previously reported Fermi surface changes around the S-shape in this compound.

3.1.1 State of the art

UCoGe is one of the very rare compounds where superconductivity shows a microscopic coexistence with ferromagnetism [31, Huy 2007], along with UGe_2 [32, Saxena 2000], URhGe [33, Aoki 2001] and UIr [34, Akazawa 2004]. In a conventional superconductor, magnetic field destroys superconductivity and even in the frame of unconventional superconductors magnetism competes with superconductivity. Some materials have been found to display both orders at low temperature but with a Curie temperature smaller

than the superconducting one, such as $ErRh_4B_4$ [35, Fertig 1977] or $Ho_{1.2}Mo_6S_8$ [36, Ishikawa 1977] and the magnetic order destroys the superconducting one.

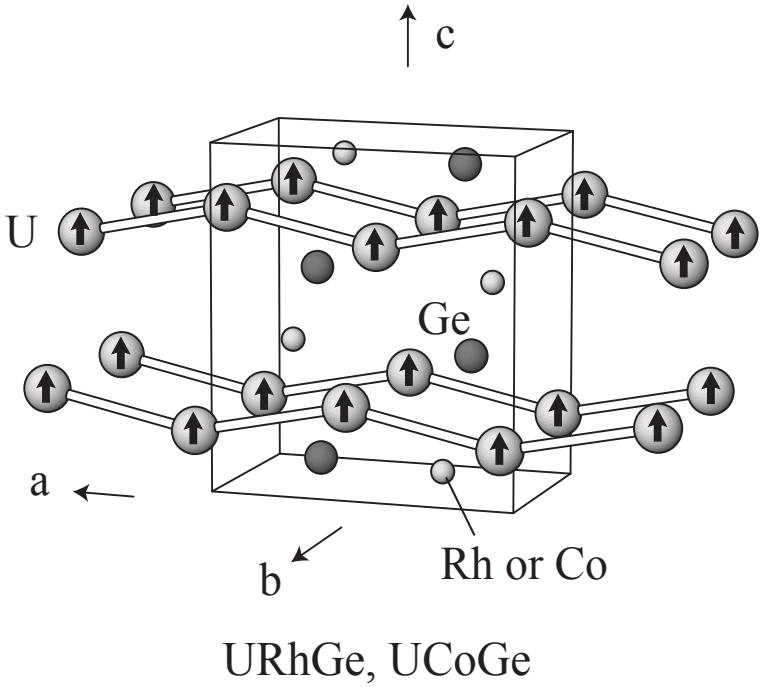

Figure 3.1: Unit cell of UCoGe and URhGe. Zig-zag chains of uranium are along a-axis and ferromagnetic moments are along c-axis.

UCoGe crystallizes in the orthorhombic TiNiSi structure with the space group Pnma. The uranium atoms form a zig-zag chain along the a-axis as shown in Fig. 3.1. It is ferromagnetic below a T_C ranging from 2.2 K to 3 K, depending on sample quality, with small ordered moments of $M_0 = 0.03\ \mu_B$ oriented along the c-axis and shows superconductivity below $T_{SC} = 800$ mK. The Sommerfeld coefficient is $\gamma \approx 65$ mJ.mol^{-1}.K^{-2} [37, Buschow 1990] showing that it is a heavy fermion system where the effective masses are moderately enhanced. The microscopic coexistence of the ferromagnetic and superconducting orders was proven using NMR [38, 39, Ohta 2008, 2010], muon spin rotation and relaxation in zero magnetic field [40, de Visser 2009].

The pressure-temperature phase diagram drawn by resistivity measurements on a single crystal sample is shown on Fig. 3.2. A collapse of the ferromagnetic order around $P_C = 1$ GPa is observed. Superconductivity exists at $P = 0$ in the ferromagnetic region, its critical temperature increases with pressure up to a maximum where the order is suppressed [42, Hassinger 2008]. Superconductivity still exists in the paramagnetic phase with no sudden variation in the superconducting temperature at the transition and extends up to 4 GPa [41, Bastien 2016].

In magnetic field, UCoGe has been found to show very large magnetic anisotropy. Field dependence of magnetization at $T = 2$ K and up to 5 T for a magnetic field along the three main crystallographic axes is shown on Fig. 3.3. The hardest magnetization axis, with a very low susceptibility $\chi_a \approx 0.0024\ \mu_B$/T, is the a-axis. The b-axis has a slightly higher susceptibility $\chi_b \approx 0.006\ \mu_B$/T. Along these two axes, the magnetization is linear in magnetic field, as can be expected since these are hard magnetization axes. On

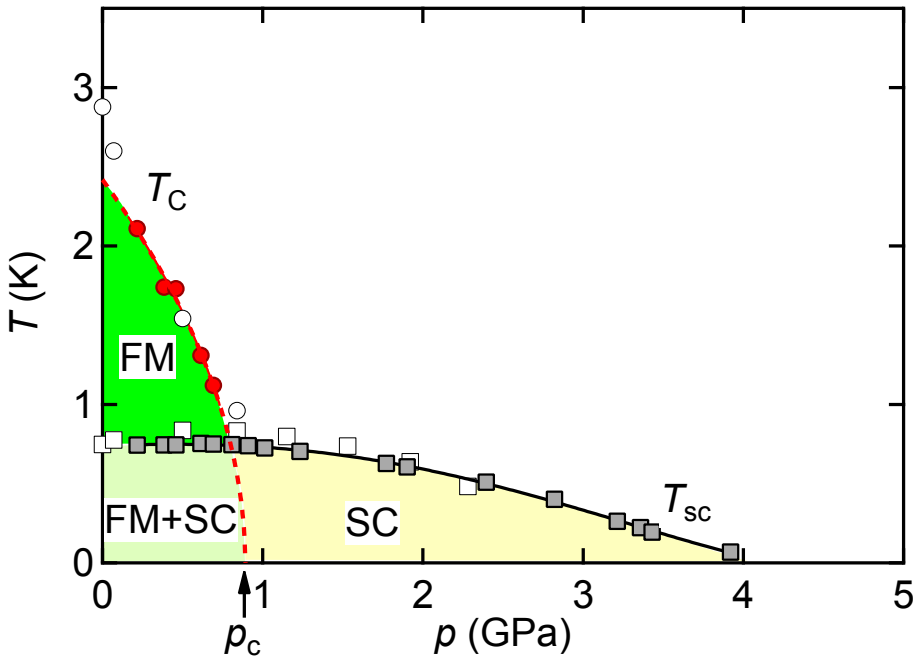

Figure 3.2: Pressure-Temperature phase diagram of UCoGe drawn by resistivity measurements, taken from Ref. [41, Bastien 2016].

the other hand, susceptibility along the easy magnetization c-axis is very high compared to the other two with $\chi_c \approx 0.029\ \mu_B$/T. Along this axis, the magnetization is finite at zero field, confirming that the magnetic moments are oriented along this direction. The inset shows the temperature dependence of the magnetization for a small magnetic field of 0.01 T applied along the c-axis. It shows the expected increase in magnetization at the Curie temperature $T_C = 3$ K. The high suscpetibility and the low spontaneous magnetization in UCoGe along the c-axis allows for a magnetic field as low as 1 T to induce a magnetization twice a large as the spontaneous magnetization [43, Huy 2008].

Superconductivity also appears to be highly anisotropic. The upper critical field along all three crystallographic directions as a function of T/T_{SC} is shown on Fig. 3.4. H_{C2} is very low when magnetic field is applied along the c-axis and becomes very large along the a- and b-axes. In all three directions, H_{C2} also appears to have initially a positive curvature with temperature. The value of the upper critical field along the c-axis is low enough to be explained by the Pauli limitation, given in the BCS theory by:

$$H_{C2}^{Pauli}(T=0) = \frac{\sqrt{2}\Delta_0}{g\mu_B} \approx 1.85\ T_{SC} \approx 1.48T. \tag{3.1}$$

where Δ_0 is the amplitude of the superconducting gap at $T = 0\ K$. It shows however a very different temperature dependence. The value for the a- and b-axes are far greater than what can be explained by the Pauli limitation. Therefore, it is believed that the Cooper pairs in this system form a triplet state [31, Huy 2007] and the only limitation to the critical field is the pair breaking by the Lorentz force, known as the orbital limit [44, Klemm and Scharnberg 1985]. Moreover, the shape of the critical field along the b-axis is very unusual, showing the so-called S-shape [45, Aoki 2009], where $T_{SC}(H{=}12\text{ T}) > T_{SC}(H{=}5\text{ T})$.

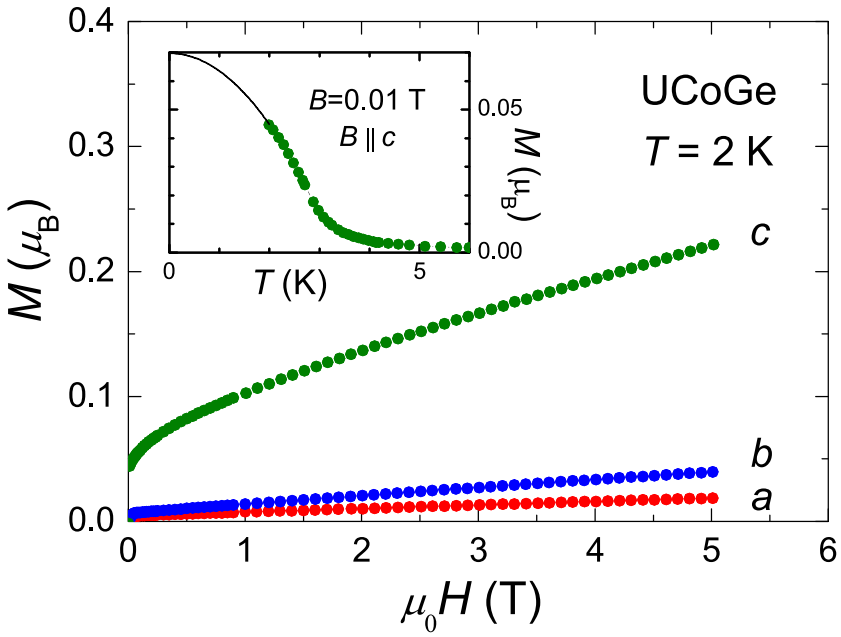

Figure 3.3: Magnetization at $T = 2$ K in the three crystallographic directions up to 5 T. In the inset the temperature dependence of magnetization for $H = 0.01$ T along c-axis. Taken from Ref. [43, Huy 2008].

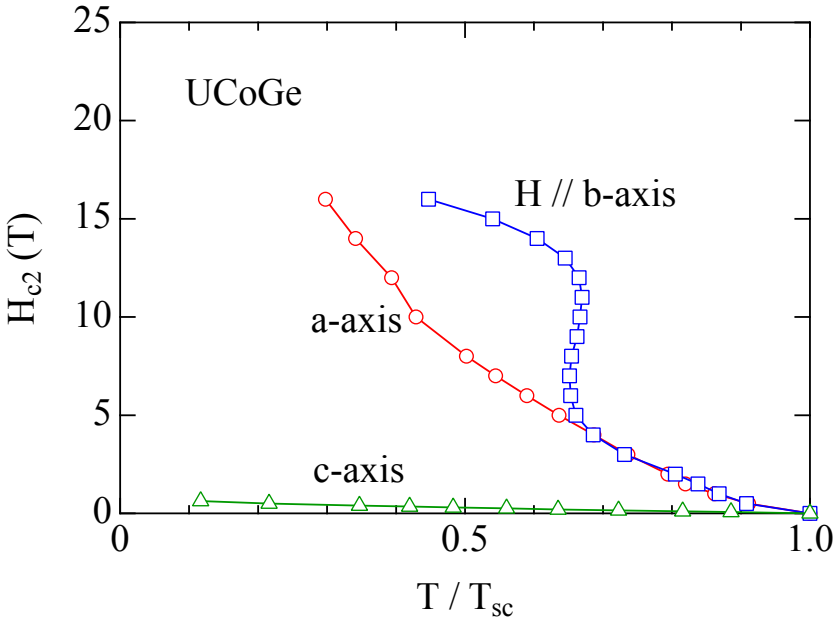

Figure 3.4: Upper critical field in UCoGe for a magnetic field applied along all three crystallographic directions, taken from Ref. [45, Aoki 2009].

This unusual behavior of the upper critical field not predicted by electron-phonon interaction for $H \parallel b$ is most probably linked to the field change of the magnetic fluctuations. In the frame of unconventional superconductivity, the superconducting critical

temperature can be estimated through the McMillan formula:

$$T_{SC} = T_0 \exp\left(\frac{1}{\lambda - \mu^*}\right) \tag{3.2}$$

where μ^* is the Coulombian repulsion and λ is the superconducting coupling parameter. This parameter is related to the enhancement of the effective mass by the fluctuations through the relation:

$$m^* = m_B(1 + \lambda) \tag{3.3}$$

where m_B corresponds to the band mass, and m^* is the total effective mass of the quasi-particles. Assuming that the band mass does not change too much in magnetic field, it was recently proposed [92, Wu 2016] that an increase of the superconducting temperature is linked to an increase of λ. From Eq. 3.2, one can understand λ as a "fluctuation mass". The A coefficient of the resistivity normalized by its value at zero magnetic field is shown on Fig. 3.5. As was seen in chapter 1.1, far from a magnetic instability, the A coefficient is proportional to the square of the total effective mass and even close to one, a variation in this quantity may indicate a similar change in the effective mass. Still assuming that the band mass is independent of magnetic field, the variation of the A coefficient can be directly linked to a variation of the magnetic fluctuations in this system. The A coefficient shows a sharp decrease for field along the c-axis, that has been recently attributed to the suppression of the magnetic fluctuations and hence a decrease of the superconducting coupling parameter λ [92, Wu 2016]. For field along the a-axis, it decreases slightly up to 10 T and is constant for higher field. With magnetic field along the b-axis, the A coefficient decreases at first and then shows a broad maximum around 14 T, which corresponds to where the S-shape is located. The λ parameter follows the field dependence of the A coefficient, and so using the McMillan formula, the shape of H_{C_2} can be qualitatively obtained.

Additionally, it has been suggested from thermoelectric power measurements [46, Malone 2012] that a Fermi surface reconstruction appears around the field of reentrant superconductivity for a magnetic field applied along the b-axis, which most likely indicates that the Fermi surface plays a role or at least is linked to the magnetic correlations. The Seebeck coefficient renormalized by temperature at different temperatures as a function of magnetic field applied along the b-axis and for a thermal gradient applied along the a-axis is shown on Fig. 3.6 . At low temperature ($T = 350$ mK), it shows a large peak at $H^* = 11.1$ T and a smaller one at $H^{**} = 14.6$ T, then drops quickly to change sign around 17 T. With increasing temperature, the peak at H^* becomes smaller and the the one at H^{**} also becomes smaller and then is no longer visible at $T = 2.9$ K. Considering that the Seebeck effect is sensitive to changes in the Fermi surface and its sign is directly related to the relative contribution of electron and hole pockets, it shows that the Fermi surface is somehow different in the high field region compared to the low field one. If one assumes that one or more pockets are shrinking with field while considering the effective mass as constant on these pockets, one can find that the Fermi velocity has to decrease, therefore increasing the orbital limit and seemingly raising the superconducting temperature with field.

Very high pulsed field magnetization measurements at $T = 1.5$ K for magnetic field up to 50 T along all three directions are shown on the left panel of Fig. 3.7 [48, Knafo

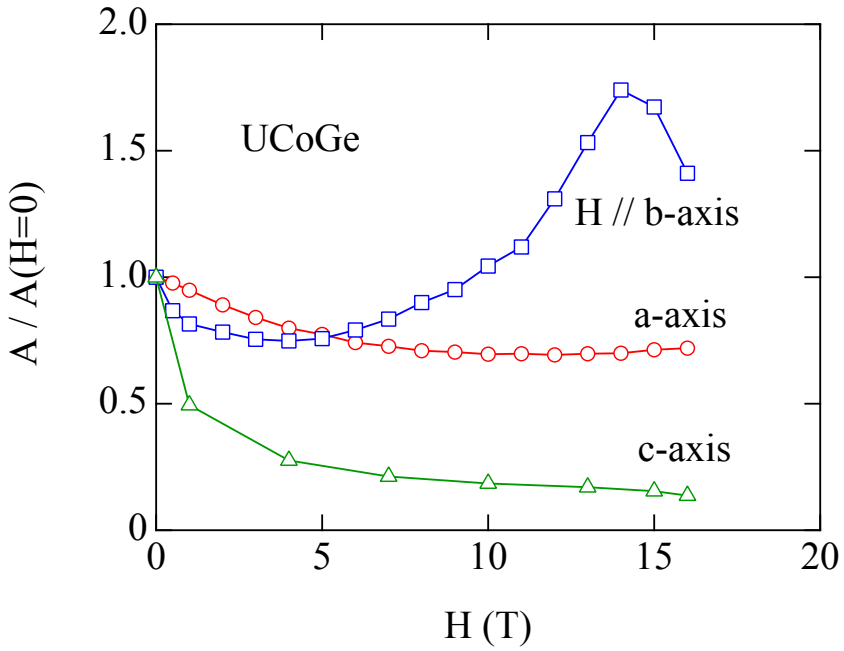

Figure 3.5: A coefficient of resistivity normalized by the zero field value as a function of magnetic field for all three crystallographic directions. Taken from Ref. [45, Aoki 2009].

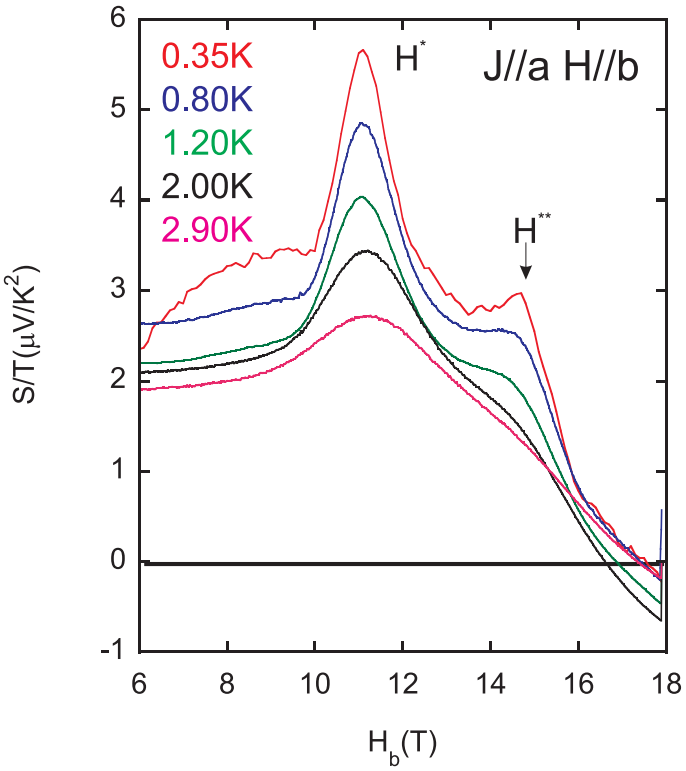

Figure 3.6: Thermoelectric power as a function of magnetic field for $J \parallel a$ and $H \parallel b$. Two anomalies are detected at 11.1 T and 14.6 T. Taken from Ref. [46, Malone 2012].

2012]. It confirms that the magnetization along the a-axis increases linearly and slowly. Along the b-axis, it also increases linearly but slightly faster and a small kink appears at $H \approx 45$ T where the slope of the magnetization increases. The magnetization along the c-axis increases very fast, non-linearly and never reaches a saturation even up to $H = 50$ T. This behavior is very unusual and cannot be described by a simple model. Aside from a small kink around 20 T, no thermodynamic transition is detected for field along the c-axis. Resistivity in a sample with $J \parallel c$ as a function of magnetic field along the b- and c-axes is shown on the right panel of Fig. 3.7. The transverse configuration shows that at $T = 1$ K, magnetoresistance for field along b-axis, two kinks are detected around 10 T and 15 T. Longitudinal magnetoresistance, with field along c-axis and at $T = 40$ mK, displays several anomalies at 9, 17, 24 and 30 T [49, Aoki 2011].

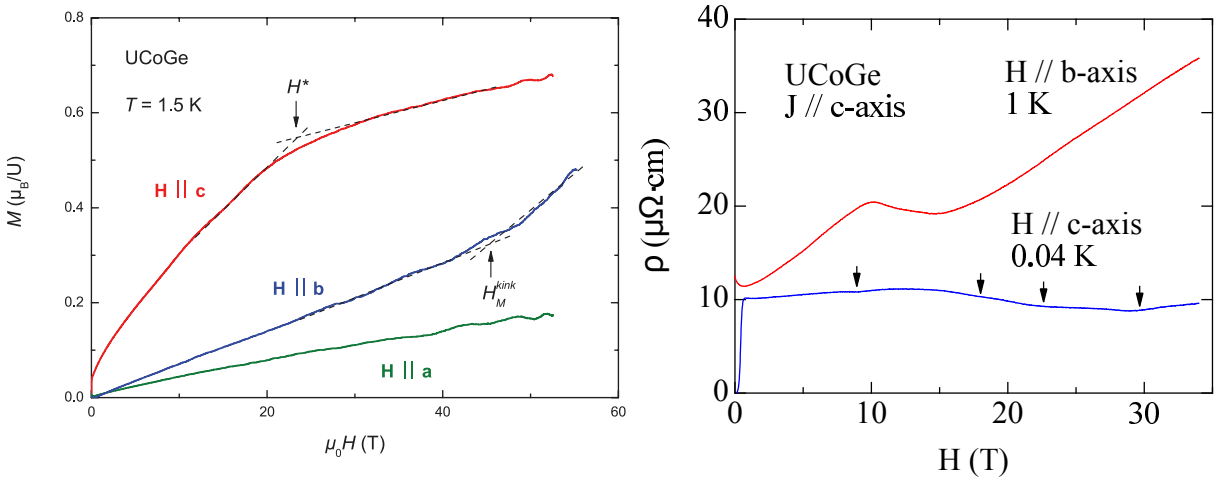

Figure 3.7: Left : Magnetization at 1.5 K up to 50 T for all three directions. For $H \parallel c$, only one kink is observed around 23 T. Taken from Ref. [48, Knafo 2012]. Right : resistivity for $H \parallel b$ at $T = 1$ K and $H \parallel c$ for $T = 40$mK up to 34 T. Many small anomalies are observed for $H \parallel c$. Taken from Ref. [49, Aoki 2011].

Up to now, the nature of these anomalies for a magnetic field applied along the c-axis remains unclear. However, the lack of any thermodynamic signature of a transition suggests that it could be related to the Fermi surface and hence that these anomalies would be of Lifshitz nature.

In order to demonstrate the presence of a Lifshitz transition, the most pertinent way is through the direct observation of quantum oscillations. Knowing the topology of the Fermi surface, it is then possible to observe directly any change or reconstruction of the Fermi surface through the change of the observed oscillation frequencies. As already mentioned, high quality single crystals are needed to observe quantum oscillations. However, the single crystal growth of UCoGe is difficult and high quality samples are hard to achieve. Actually, only one Shubnikov-de Haas measurement has been successfully performed at very low temperature and it shows a rather large pocket with a frequency around 1000 T which seems almost spherical when rotating from b to c-axis[49, Aoki 2011]. This branch was observed above $H = 24$ T and its effective mass goes from $m^* = 25\ m_0$ along the b-axis to $m^* = 18\ m_0$ along the c-axis. Another branch was also detected at lower magnetic fields with a frequency $F = 250$ T and an effective mass $m^* = 11\ m_0$ [50, Aoki 2014].

The only angle resolved photo-emission spectroscopy experiment study is in the paramagnetic state of UCoGe [51, Fujimori 2015], because the lowest temperature that can be achieved is higher than the Curie temperature of the compound. Also, while the band structure deep below the Fermi level can be studied and compared with calculations, the numerous flat bands at the Fermi energy would require a resolution that is, up to now, beyond the reach of experimental apparatus available. However, this study confirms the itinerant character of the $5f$-electrons in this system, and their spectra fit rather well with the band calculation they performed.

Band calculations have been made by different groups [53, 51, Samsel-Czekała 2010, Fujimori 2015]. The calculated Fermi surface of Ref. [51, Fujimori 2015] is shown on Fig. 3.8. It shows interesting topology, with cylinders centered at the S point on the border of the Brillouin zone along the c-axis, a rather large closed surface with a complicated structure more oriented along the b-axis at the Y point, two smaller pockets at the X point and a small one at the Γ point. The calculated band structure has been found to be in rather good agreement with the angle resolved photoemission spectroscopy measurement for the bands below the Fermi level. It is interesting to note that some pockets of this Fermi surface has a partial two dimensional character, which in the frame of itinerant Ising ferromagnetism may be relevant. It was suggested that the dimensionality of the Fermi surface may play an important role in the emergence of unconventional superconductivity, a two dimensional Fermi surface, for example a cylinder, being more favorable than a three dimensional one, for example a sphere [52, Monthoux 2001].

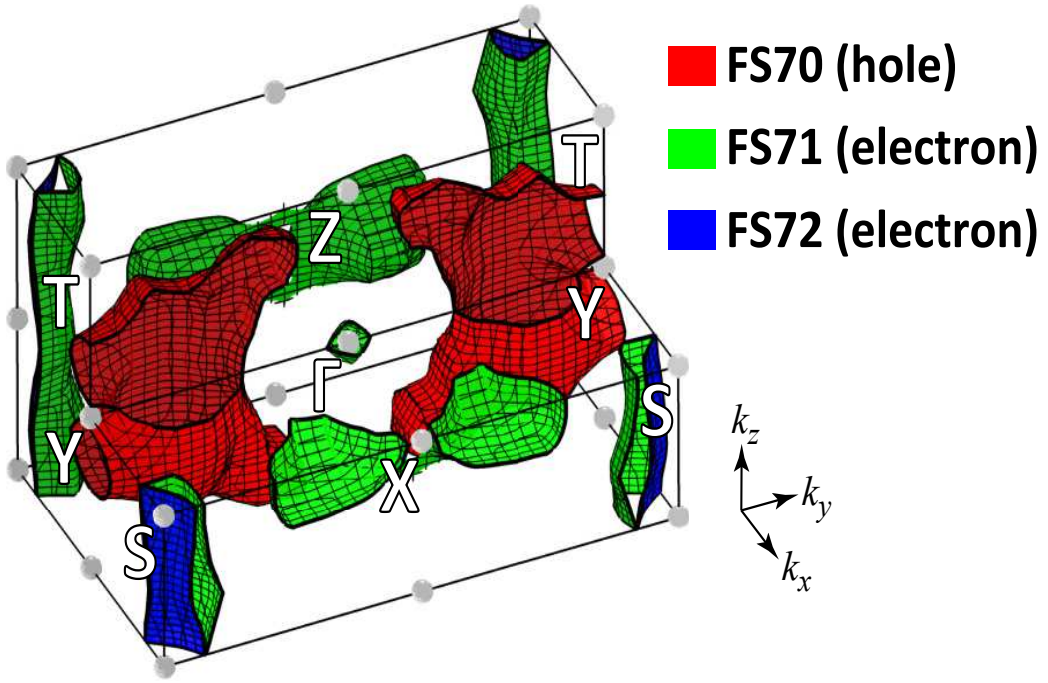

Figure 3.8: Calculated Fermi surface of UCoGe, taken from Ref. [51, Fujimori 2015].

The aim of this study was to understand the nature of the anomalies observed in

longitudinal resistivity for a magnetic field applied along the easy magnetization c-axis and study of the Fermi surface across those. Therefore we chose to use thermoelectric power, as this probe is known to be very sensitive to modifications of the Fermi surface and show a large response at a Lifshitz transition.

3.1.2 Fermi surface and magnetic polarization along the easy magnetization axis

The thermoelectric power measurements on a UCoGe single crystal with the heat current along the b-axis and magnetic field along the c-axis were performed both in a superconducting magnet (up to 16 T) and low temperature (down to 180 mK) in a dilution fridge in the laboratory and these measurements have been extended in a resistive magnet (up to 33 T) and in a ^{3}He cryostat (down to 450 mK) in LNCMI Grenoble. The measured sample was plate-like with a length of 2 mm for a width of 0.9 mm and a thickness of 0.15 mm and was of very high quality (RRR = 105).

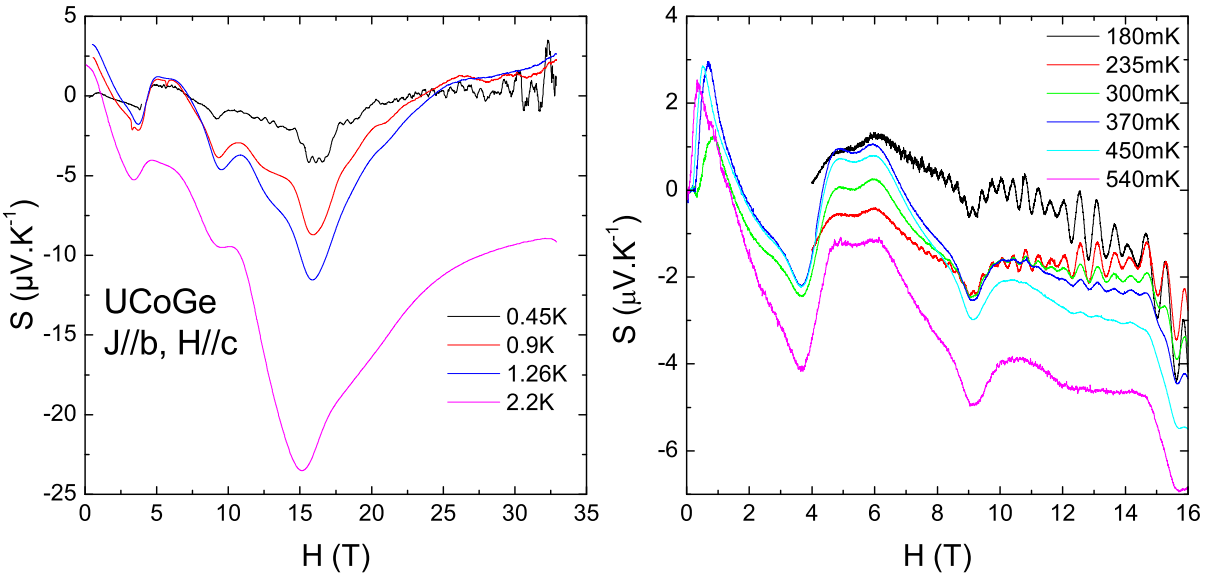

Figure 3.9: Field dependence of the thermoelectric power at high magnetic field up to 33 T and for temperatures from 0.45 K to 2.2 K (Left) and up to 16 T and for temperatures from 0.18 K to 0.54 K (Right).

The field dependence of the Seebeck coefficient at low temperatures is shown on Fig. 3.9. The left panel shows the measurements performed in high magnetic field up to 33 T. At T = 450 mK, anomalies are visible in the thermoelectric power and quantum oscillations are detected. When the temperature is increased, the field at which the anomalies occur do not seem to change with temperature but they become less visible. Also, at T = 900 mK, the quantum oscillations have vanished. The right panel presents the same measurement but performed in a superconducting magnet (up to 16 T) and at lower temperature (down to 180 mK). The noise level on this experiment is also much better. At T = 180 mK, quantum oscillations are clearly visible as well as a modulation

of these. At higher temperature, the amplitude of the oscillations is reduced and the anomalies are the same as the one observed in the high field measurements. A more detailed analysis of the anomalies and of the quantum oscillations will be presented later. This work completes the resistivity and Hall effect measurements done in the laboratory, which will be presented along with the thermoelectric power measurements.

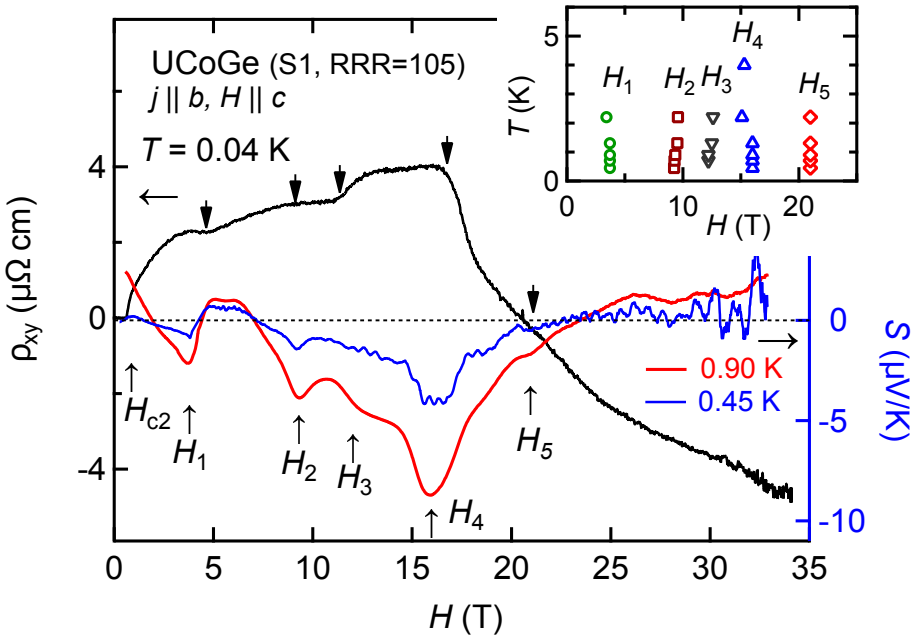

Figure 3.10: Hall effect at $T = 40$ mK (left scale) and Seebeck coefficient at $T = 450$ mK and $T = 900$ mK (right scale) as a function of magnetic field. In the inset is the magnetic field-temperature phase diagram of these anomalies. Taken from Ref. [59, Bastien 2016].

The field dependence of the Hall effect at $T = 40$ mK and the thermoelectric power at $T = 450$ and 900 mK is shown on Fig. 3.10. Both quantities show clear anomalies at $H_1 = 4$ T, $H_2 = 9$ T, $H_3 = 12$ T, $H_4 = 16$ T. Another anomaly at $H_5 = 21$ T is observed only in the Seebeck coefficient. As can be seen in the inset, the magnetic field at which these anomalies occur is very little temperature dependent. At $T = 450$ mK, in the thermoelectric power quantum oscillations can be observed for $H > 12$ T. At low temperature, both quantities change sign around $H_5 = 21$ T.

The analysis of the quantum oscillations gives more insight on the nature of these anomalies. On Fig. 3.11 are represented the oscillating part of the signal for resistivity (top) and thermoelectric power (bottom). It is clear that a change in frequency is observed at H_4 and H_5. Below H_4, a frequency of 300 T is detected (as will be discussed later, these quantum oscillations actually contain two close frequencies, called γ and β). At H_4, this frequency of 300 T seems to grow faster to reach a frequency of 600 T (called ω). This branch has only been observed in the Seebeck signal. In resistivity, the low field oscillation ($\gamma + \beta$) abruptly disappears at H_4 and the ω branch is not observed. At H_5, in the thermoelectric power signal, the branch at $F = 600$ T suddenly disappears and a new one at $F = 980$ T (called α) appears.

While even a sudden appearance of a new pocket in quantum oscillations cannot demonstrate the presence of a Lifshitz transition, the abrupt disappearance of one makes

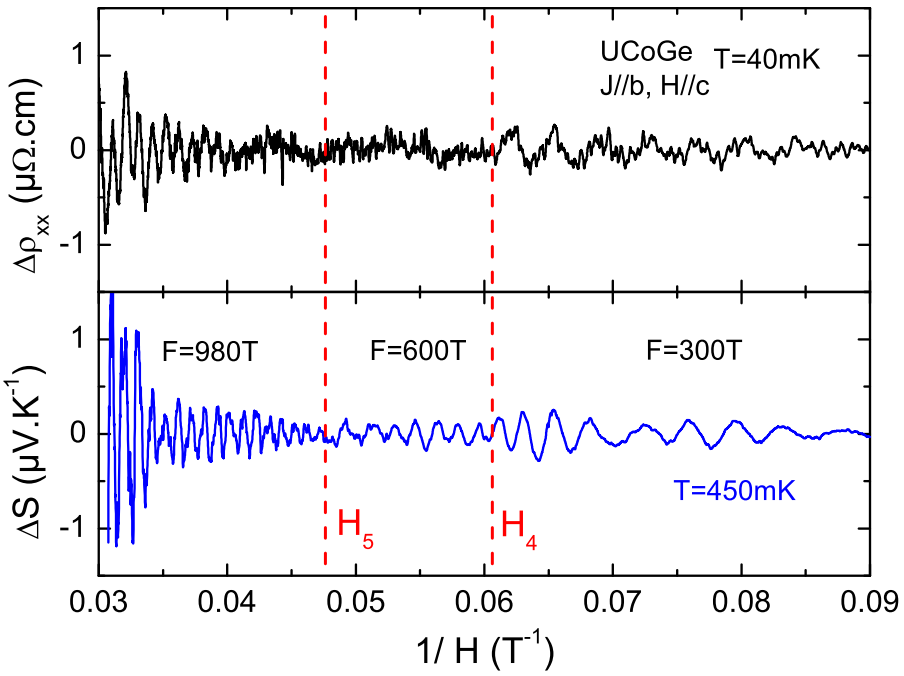

Figure 3.11: Inverse field dependence of the oscillating part of the resistivity (top) and of the Seebeck effect (bottom). Clear changes occur at H_4 and H_5.

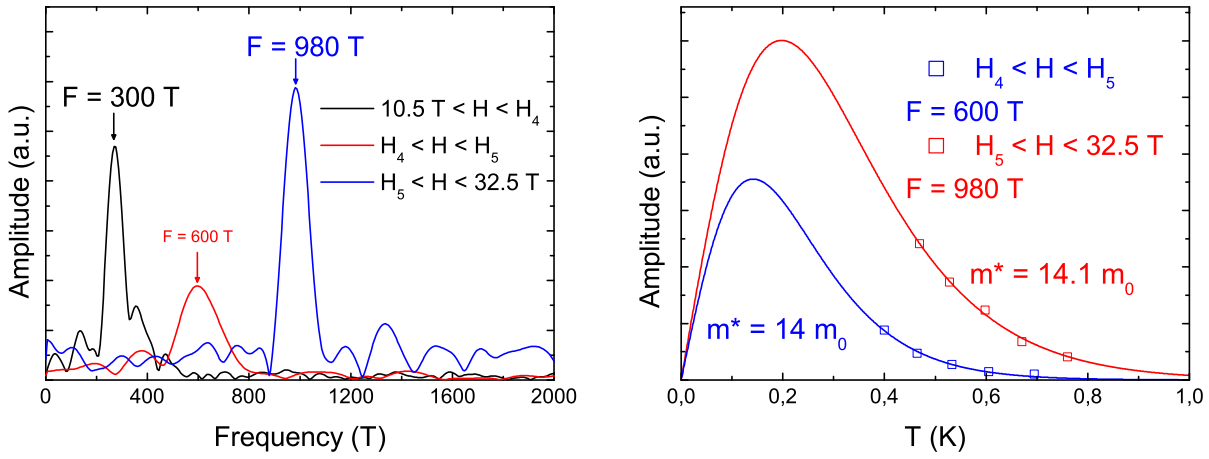

Figure 3.12: Left : Fast Fourier Transform of the Seebeck signal on three field ranges: 10.5 T $< H <$ H_4 (in black), $H_4 < H < H_4$ (in red) and $H_5 < H <$ 32.5 T. Right: Temperature dependence of the amplitude of the oscillations and Pantsulaya-Varlamov fits performed to extract the effective masses.

it very likely (although without knowing the full topology of the Fermi surface, it is difficult to conclude). The FFT of the Seebeck signal on the three field range H $\leq H_4$, $H_4 \leq$ H $\leq H_5$ and H $\geq H_5$ is shown on left of Fig. 3.12, demonstrating the different appearances and disappearances of the previously mentioned frequencies.

Using the Pantsulaya-Varlamov theory (described in chapter 1.3.3.3), we extracted the effective mass for the α and the ω branches by plotting the amplitude of the quantum

oscillations as a function of temperature. The values found are $m^* = 14.1\ m_0$ and $m^* = 14\ m_0$, respectively. The fits are shown on the right panel of Fig. 3.12 and the fitting is very good in both cases even if the temperature is not low enough to observe the decrease of the quantum oscillations amplitude. The low field experiment at lower temperature shows that the 300 T branch observed below H_3 is in fact composed of two oscillations with close frequencies that we could not resolve in the high field experiment. On Fig. 3.14 a clear modulation of the signal can be seen on the left and the Fast Fourier Transform on the right shows that there are two frequencies, one of 240 T and 310 T, called β and γ, respectively. The inset shows the mass fit which gives an effective mass $m^* = 12.4\ m_0$ and $m^* = 12.8\ m_0$ for the β and γ branches, respectively. The oscillating part of the signal was extracted using an envelope that fits both side of the signal on the minima and maxima, as shown in Fig. 3.13. The average of the upper and lower envelope is then subtracted from the signal. This technique was used because the polynomial fit we usually use was not good enough to remove the rapidly changing background properly.

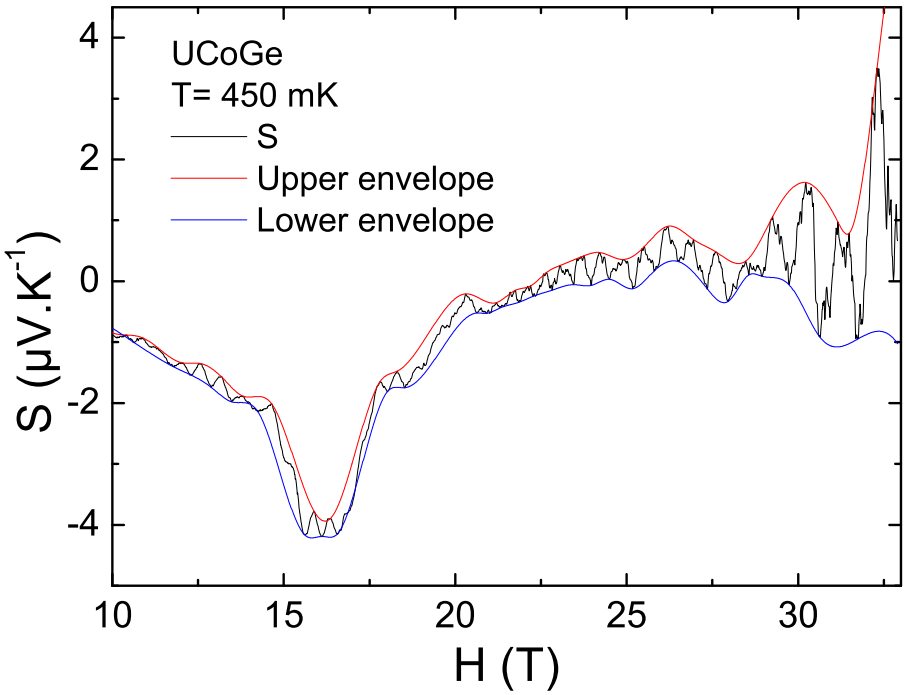

Figure 3.13: Thermoelectric power at $T = 450$ mK (in black) and the upper (red) and lower (blue) envelope used to remove the background and extract the oscillating part of the signal.

The frequencies observed are in very good agreement with the Shubnikov-de Haas measurements and the effective masses are in fairly good agreement as well. The results for Shubnikov-de Haas and thermoelectric power measurements are summarized in Table 3.1.

Angular dependence of the TEP on Fig. 3.15 shows that when the magnetic field is rotated from the b- to c-axis, the anomalies H_1 and H_2 are shifted to higher field. In accordance with the angular dependence of the magnetoresistance, the anomalies H_1, H_2 and H_3 follow rather well $1/\cos(\theta)$ law, as shown on Fig. 3.16, indicating that the only relevant field direction is the easy magnetization axis c and the subsequent polarization

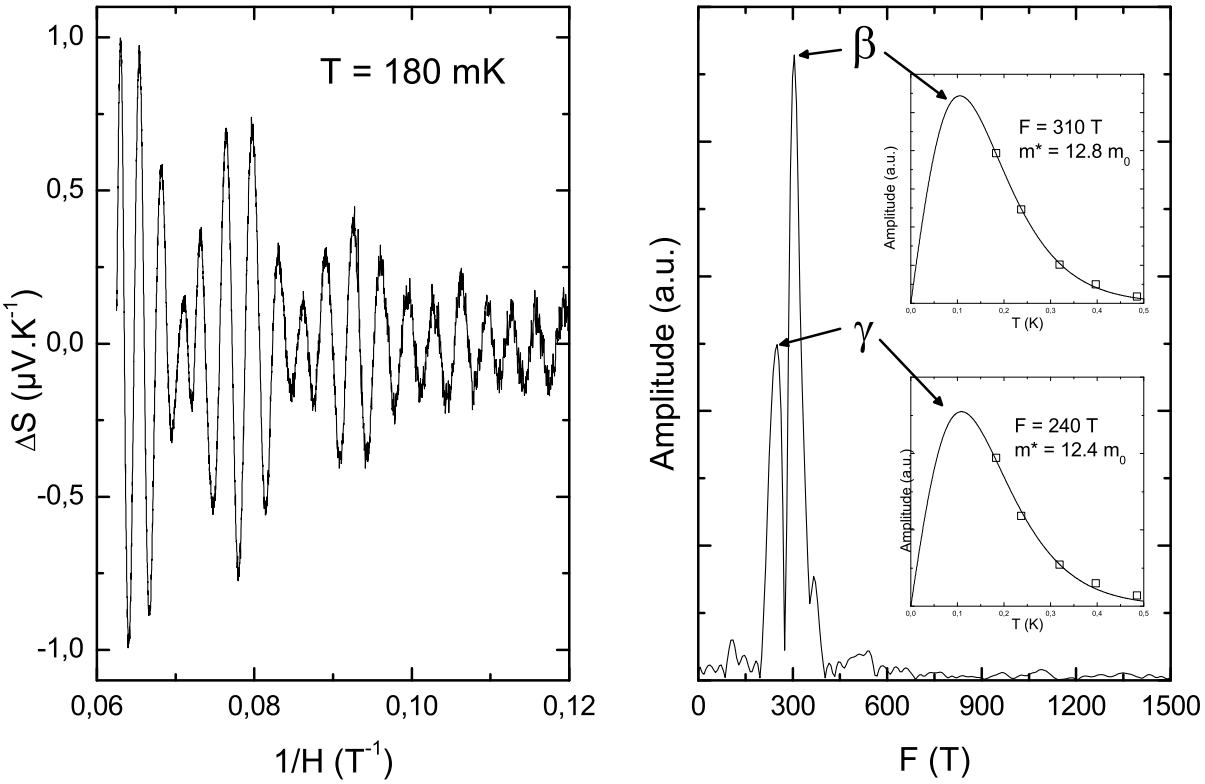

Figure 3.14: Left : Oscillating part of the Seebeck as a function of $1/H$ at $T = 180$ mK. Right : Fast Fourier Transform spectrum of the signal and fit of the corresponding temperature dependence for the β (top) and γ (bottom) branches in inset.

that is induced along this axis. Similarly, the effects of magnetic polarization on the Fermi surface have been studied in detail in $YbRh_2Si_2$ [72, Pfau 2013], URu2Si$_2$ [54, Pourret 2013] or $CeRu_2Si_2$ [55, 56, Daou 2006, Boukahil 2014].

These measurements, along with the previously reported magnetization data, clearly demonstrate that the anomalies observed correspond to strong reconstructions of the Fermi surface induced by the magnetic field along the c-axis. The appearance and disappearance of some pockets of the Fermi surface strongly suggest that these are Lifshitz transitions. However, it is often difficult to confirm experimentally that a Lifshitz transition is occurring because it would require the knowledge of the full topology of the Fermi surface. Without many branches of the Fermi surface directly observable, band calculations and especially field dependent ones would be required to confirm the presence of a Lifshitz transition. In UCoGe, the observation of all branches participating in the Fermi surface is challenging because of the difficulty to get high quality samples and the large effective masses require very low temperature and high magnetic field. Additionally, band calculations are not very reliable due to the dual character of the $5f$ electrons (localized/itinerant) and the low symmetry of the UCoGe unit cell. Therefore, the knowledge of the topology of the Fermi surface is not a trivial task.

Table 3.1: Quantum oscillations frequencies and effective masses in UCoGe from resistivity and Seebeck effect measurements for field along the *c*-axis. Different field intervals are considered, they are delimited by the anomalies observed in transport measurements.

		SdH Sample 1		SdH Sample 2		Seebeck (Sample 1)	
H range	orbit	F(T)	m*(m_0)	F(T)	m*(m_0)	F(T)	m*(m_0)
4T<H<9T	γ			230	7		
	β	270		280		285	
9T<H<16T	γ	240	11	240	8	240	12
	β	310	11	310	11	310	13
16T<H<21T	ω					600	14
H>21T	α	970	17	955		980	14.1

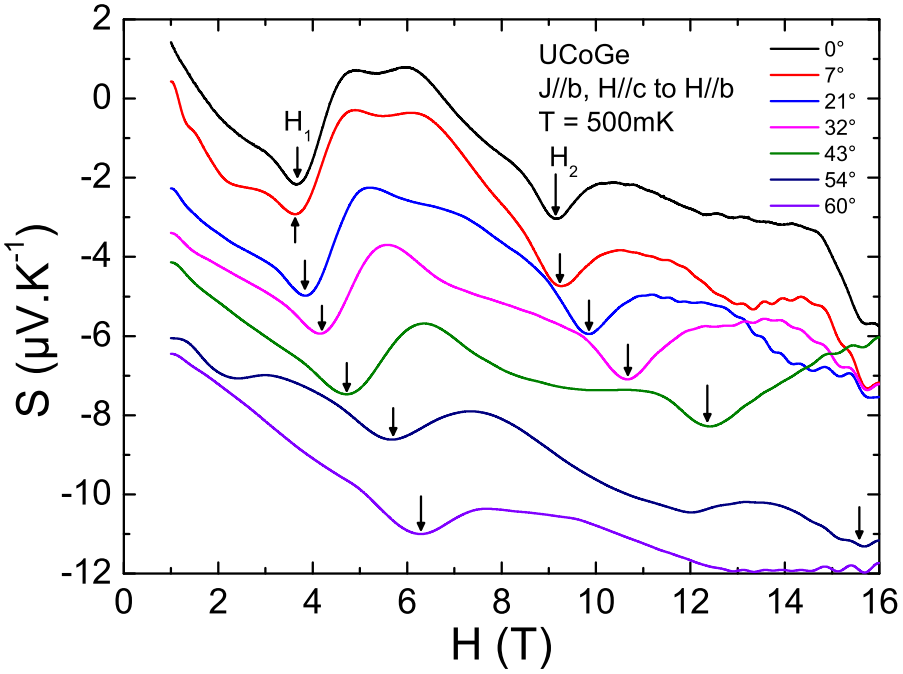

Figure 3.15: Field dependence of the thermoelectric power for different angles rotated from *c*-axis (0°) to *b*-axis (90°).

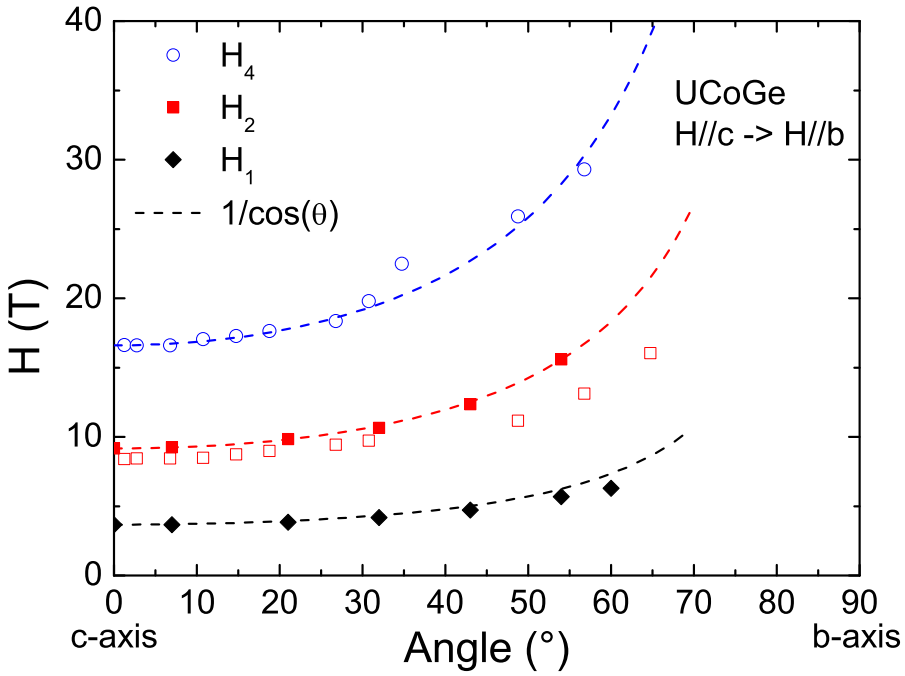

Figure 3.16: Angular dependence of the H_1, H_2 and H_4 anomalies rotating the field from the c to the b-axis. Open symbols are from resistivity and filled ones are from thermoelectric power. Dashed line shows the $1/\cos(\theta)$ dependence for each anomaly.

3.1.3 Results for H||b

The clear demonstration of the Lifshitz nature of the anomalies for $H \parallel c$ that the thermoelectric power was able to provide lead us to study the possible Fermi surface reconstruction suggested in Ref. [46, Malone 2012]. The aim of this study was to understand if and how the Fermi surface is modified close to the S-shape of H_{C2} in this system.

The UCoGe single crystal thermoelectric power was measured on a sample of very high quality, with a residual resistivity ratio RRR $= \frac{\rho(300K)}{\rho(T\to 0)} = 190$. It was measured in the longitudinal configuration with the thermal current $J_Q \parallel b$ and the magnetic field applied along the same direction $H \parallel b$. The aim of this study was to observe the possible Fermi surface reconstruction suggested in Ref. [46, Malone 2012] with a longitudinal configuration in order to avoid all orbital effects. For resistivity, a simple picture of the orbital effect is that under the influence of an external magnetic field, the quasiparticles are orbiting in the plane orthogonal to the field, forcing them to travel a path longer than they normally would, increasing the observed resistivity. If the sample quality is low, the scattering time is too low to allow the quasiparticles to have a real orbiting motion, the orbital effect is low, and the magnetoresistance is weak. On the other hand, for very high quality samples, where the scattering time is high, the orbital effect can increase the resistivity by a factor of more than ten at high field. In the thermoelectric power, there is no general variation in magnetic field. Indeed, in a multiband system such as UCoGe, each band may have a different scattering time and therefore the orbital effect vary from

one band to another, making an estimation difficult.

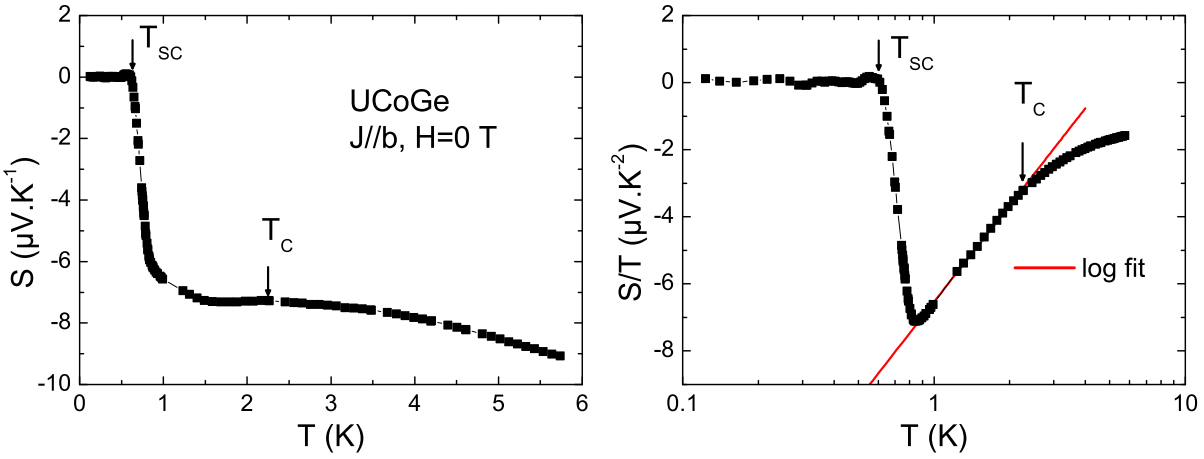

Figure 3.17: Temperature dependence at zero magnetic field of the thermoelectric power (left panel) and the thermoelectric power renormalized by temperature on a logarithmic scale (right panel). The red curve is a logarithmic fit of the divergence of S/T.

The temperature dependence at zero field of the thermoelectric power (left panel) and the thermoelectric power renormalized by temperature (right panel) for $J_Q \parallel b$ is shown on Fig. 3.17. The Seebeck coefficient shows a small maximum at the Curie temperature T_C = 2.25 K and superconductivity below T_{SC} = 0.8 K. In this compound, the transition at T_C is hard to detect, probably due to the very weak character of the ferromagnetic order. The Seebeck renormalized by the temperature shows no anomaly at T_C but is diverging with a logarithmic dependence $S/T \propto log(T)$ down to the onset of the superconducting transition.

The temperature dependence of the thermoelectric power renormalized by temperature for a magnetic field applied along the b-axis is shown on Fig. 3.18. The logarithmic divergence is still observable up to H = 16 T. When the magnetic field is increased, the range where $S/T \propto log(T)$ is shifted to higher temperature and S/T seems to tend to a constant value at low temperature, as is expected in a Fermi liquid regime. However, the presence of superconductivity makes the estimation of the behavior of S/T at very low temperature difficult. This logarithmic divergence was already observed in Ref. [46, Malone 2012]. However, in their study the divergence was weak at zero field and strong around H^* = 11 T. Here it is already strong at zero field and stays that way up to H = 16 T. This suggests the presence of magnetic fluctuations between T_C and T_{SC}, with an energy scale moving to higher temperature as the magnetic field is increased. Indeed, a logarithmic dependence of S/T is theoretically expected when quantum magnetic fluctuations are present in the system [47, Paul 2001]. However, recent resistivity measurements [41, Bastien 2016] showed that at ambient pressure and zero magnetic field, the Fermi liquid T^2 behavior is achieved between T_C and T_{SC}, ruling out the quantum fluctuations associated with second order quantum critical points. It should be noted that, in a multi-band system, the Fermi liquid regime with S/T independent of temperature is usually achieved at temperatures lower than the one of the T^2 of resistivity. Indeed, in order to have S/T constant, one band has to completely dominate the entropy transport in the system and this often requires very low temperatures.

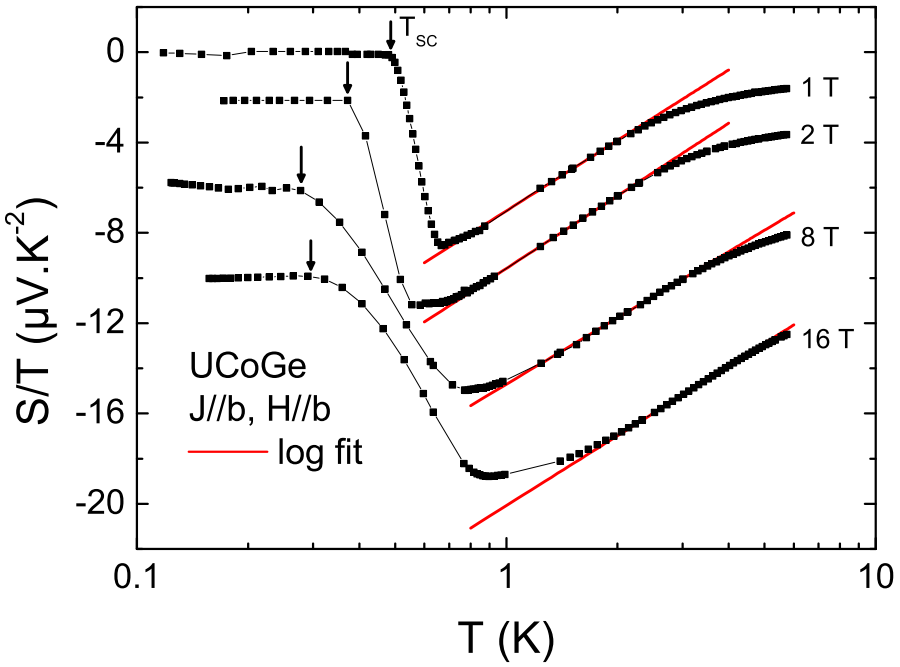

Figure 3.18: Temperature dependence the thermoelectric power renormalized by temperature for magnetic field of 1, 2, 8 and 16 T applied along the b-axis. The curves are shifted for visibility and the constant part at low temperature is the superconducting phase. The red curves are logarithmic fits of the divergence of S/T.

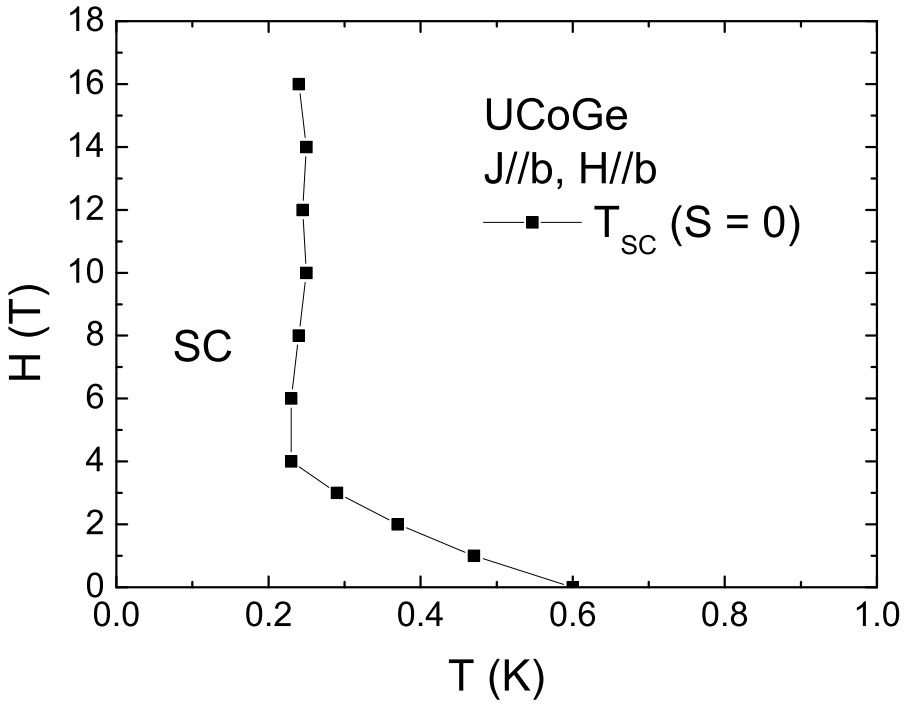

Figure 3.19: Superconducting phase diagram obtained by thermoelectric power measurements in UCoGe.

The superconducting phase diagram of UCoGe drawn by thermoelectric power measurements is shown on Fig. 3.19. The superconducting temperature decreases quickly for low magnetic fields up to 4 T and increases slightly up to 10 T where it decreases again up to 16 T, showing the so-called S-shape.

Although it is difficult in UCoGe, one can roughly estimate the value of S/T in the zero temperature limit. It is then interesting to note that while the Sommerfeld coefficient in UCoGe is not very large for a heavy fermion system ($\gamma = 65$ mJ.mol^{-1}.K^{-2}), an estimation value of the Seebeck coefficient renormalized by temperature at zero temperature is large ($S \approx$ -2 μV.K^{-1} at 1 K). The q-ratio, described in chapter 1.1.1, is in this case $q \approx$ -3. This value is rather large compared to the one of the free electron gas (q = -1) with one electron per formula unit. It is close to the one found in URu_2Si_2 (q = -4.5) [58, Bel 2004] and the one in Ref. [46, Malone 2012], where they found $q \approx 5$. The sign difference between our calculation of q and the one done in Ref. [46, Malone 2012] shows that the pocket of the Fermi surface dominating the entropy transport is not the same when the thermal gradient is applied along the a- or the b-axis. The difference in the magnitude of q may come from the difficulty in our measurement to determine how S/T would extrapolate at zero temperature in the absence of superconductivity. The q-ratio being inversely proportional to the density of carrier, we can deduce that UCoGe has a low number of carriers and the dominant type is electron-like at low temperature for the heat current along the b-axis (hole-like along the a-axis, as found in Ref. [46, Malone 2012]). One of the band calculations in UCoGe also shows that the Fermi surface is mainly composed of small pockets [53, Samsel-Czekała 2010], indicating that it is a low carrier density system.

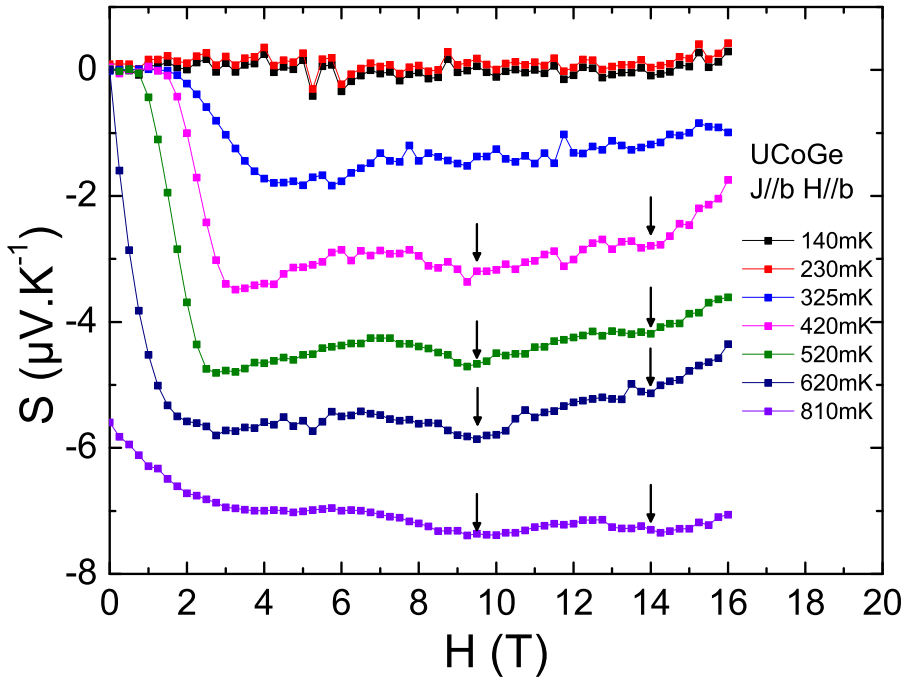

Figure 3.20: Field dependence of the Seebeck effect for temperatures from 140 mK to 620 mK. Superconductivity exists at all fields for $T \leq 230$ mK. Two anomalies are visible at higher temperature (black arrow) at 9.5 T and 14 T.

The field dependence at low temperature of the Seebeck coefficient is shown on Fig. 3.20. Below 230 mK, the sample is superconducting at all fields up to 16 T, in accordance to the exotic S-shape of the upper critical field H_{C_2} curve (see Fig. 3.4). At temperatures between 325 and 620 mK, the superconducting transition is seen at a rather low field. Comparing this measurement with previous transport measurements obtained with a very well aligned sample, indicates that the sample misalignment from the b- to c-axis is probably less than 1°. Some small anomalies are also detected at higher field: one around 9.5 T and one around 14 T. While the anomaly at 14 T probably corresponds to the H^{**} of Ref. [46, Malone 2012], the other one occurs at much lower field than $H^* = 11.1$ T.

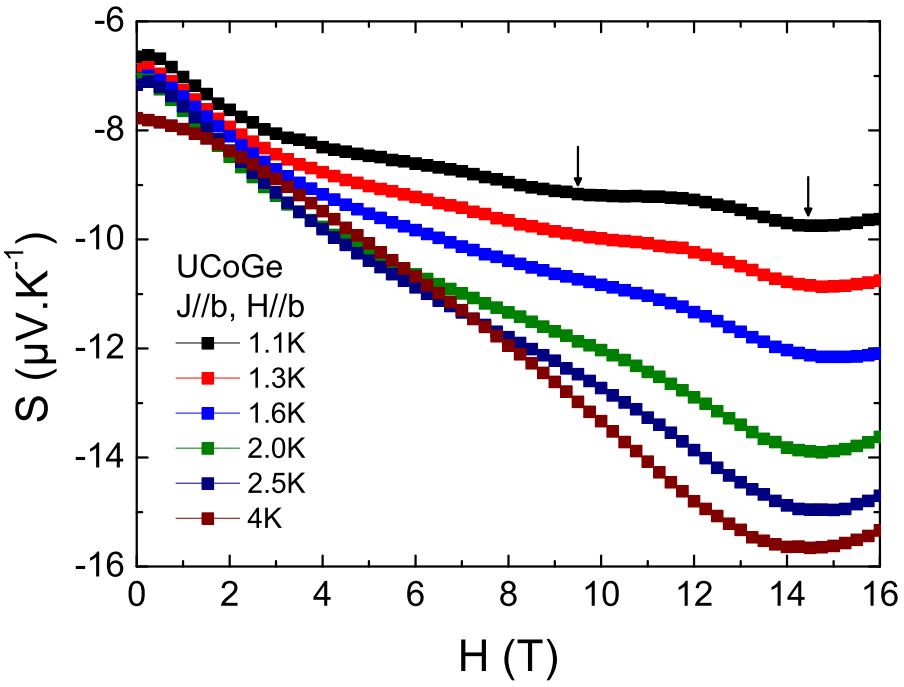

Figure 3.21: Field dependence of the Seebeck effect for temperatures from 1.1 K to 4 K. Two anomalies are visible at 1.1 K but the low field one disappears as temperature increases.

At higher temperature, on Fig. 3.21, the overall thermoelectric power signal becomes rather smooth with field and the low field anomaly disappears probably because the variation with magnetic field is increasing. The higher field one is still visible up to 4 K.

Due to the high anisotropy of UCoGe and the big dependence of transport properties with sample quality, it is not surprising to find that the thermoelectric response for $J_Q \parallel b$ that we measured is very different from the one previously reported for $J_Q \parallel a$. The fact that we could not reproduce the rather large peaks from Ref. [46, Malone 2012] is therefore not conclusive. Additionally, below $T = 0.23$ K, the sample is superconducting up to $H = 16$ T. Therefore no quantum oscillations were observed in this configuration, as the high effective mass branches of the Fermi surface would require lower temperatures to be detected for $H < 16$ T. This prevents us to draw a definitive conclusion on the reconstruction of the Fermi surface close to the S-shape.

3.1.4 Conclusion

The study of the thermoelectric power in UCoGe with a magnetic field applied along the easy magnetization c-axis shows that the anomalies first observed in the resistivity [49, Aoki 2011] and also observed in Hall and Seebeck effects can be interpreted as Lifshitz transitions. The analysis of the quantum oscillations indicates that the β and γ branches, observed below $H_4 = 16$ T, disappear at this field and another branch, ω, appears. This branch disappears at $H_5 = 21$ T and the α branch is observable above this magnetic field. This demonstrates that the anomalies detected in the Seebeck coefficient at H_4 and H_5 are linked with a modification of the Fermi surface, and since no thermodynamic transition could be detected in magnetization, it suggests that they may be Lifshitz transitions. The situation of the anomalies at H_1, H_2 and H_3 is not clear. No change in the quantum oscillations could be detected in the thermoelectric power. However, Shubnikov-de Haas measurements showed a slight change in the frequency of the β and γ branches at H_2 [59, Bastien 2016].

To further complete this study, it would be interesting to measure the magnetic field dependence of the specific heat at low temperature up to at least 30 T, in order to observe the influence of a Lifshitz transition on the Sommerfeld coefficient. A precise measurement of the magnetization at very low temperature may show more clearly the position of the anomalies as well as maybe detect more branches of the Fermi surface.

3.2 $CeIrIn_5$

In this section, we present thermoelectric study at low temperature and under high magnetic field in $CeIrIn_5$, along with torque magnetometry measurements for a magnetic field applied along the c-axis. The torque measurements were performed by I. Sheikin at LNCMI Grenoble, for more details see Ref. [60, Sheikin 2014]. The Seebeck coefficient places two anomalies at $H_{M_1} = 28$ T and $H_{M_2} = 32$ T. Additionally, the quantum oscillations observed in torque shows that the topology of the Fermi surface is modified at H_{M_1}, showing that it is a Lifshitz transition (see Ref. [74, Aoki 2016]).

3.2.1 State of the art

$CeIrIn_5$ is a heavy fermion superconductor belonging to the well known 115 family, along with $CeCoIn_5$ and $CeRhIn_5$. While $CeRhIn_5$ displays an AF ground state at low temperature [61, Hegger 2000], it is not the case for $CeIrIn_5$ and $CeCoIn_5$ which are paramagnetic down to the lowest temperature.

$CeIrIn_5$ crystallizes in the tetragonal $HoCoGa_5$ structure with the P4/mmm space group, as shown on Fig. 3.22. The measured Sommerfeld coefficient $\gamma = 750$ mJ.mol^{-1}.K^{-2} indicates that it is a heavy fermion system with large renormalized masses [64, Movshovich 2001]. This was confirmed by de Haas van Alphen experiments where effective masses of the order of 30 m_0 where found [65, Haga 2001]. It shows superconductivity below a temperature of $T_{SC} = 1.2$ K in resistivity but bulk superconductivity appears below $T = 0.4$ K. No magnetic order was detected down to $T = 50$ mK [63, Petrovic 2001].

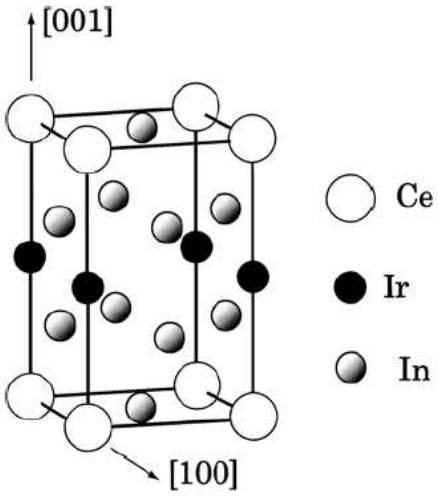

Figure 3.22: Crystal structure of $CeIrIn_5$ taken from Ref. [66, Takeuchi 2001].

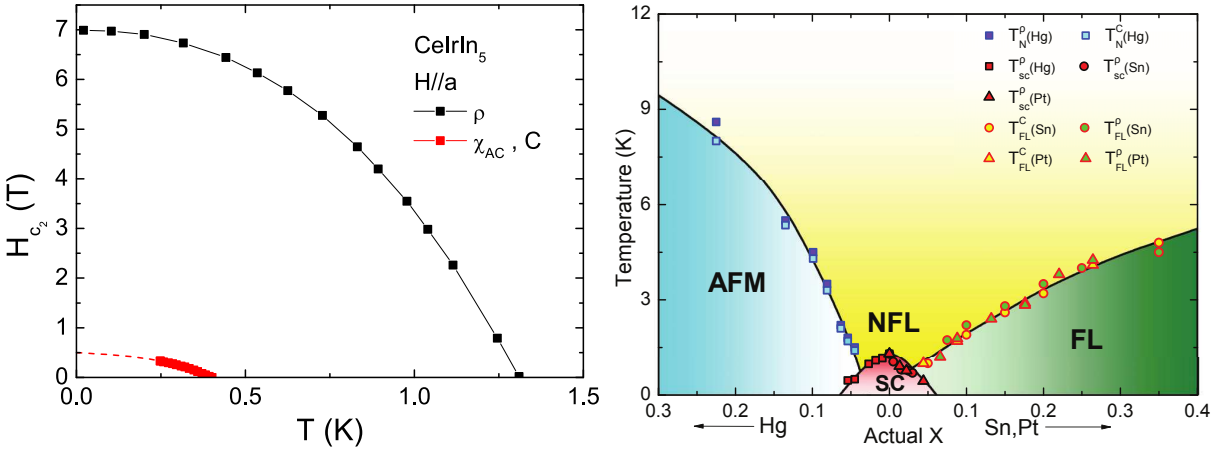

Figure 3.23: Left: Temperature-magnetic field superconducting phase diagram drawn by resistivity (black), specific heat and AC susceptibility (red), adapted from Ref. [63, Petrovic 2001]. Right: Phase diagram obtained by substituting In by Hg, Sn and Ir by Pt, by measurements of resistivity and specific heat, taken from Ref. [62, Shang 2014].

The temperature-magnetic field superconducting phase diagram is shown in the left panel of Fig. 3.23. The black squares are obtained by resistivity measurements and the red squares by susceptibility and specific heat measurements. The upper critical field for $H \parallel a$ of resistivity is around $H_{C_2}(\rho) = 7$ T, and may be extrapolated for bulk measurements around $H_{C_2}(\text{Bulk}) = 0.5$ T. The discrepancy between the superconducting temperatures from resistivity and bulk measurements is very high compared to what is usually observed in other superconductors. This effect may be due to the presence of superconducting filaments in the system far above the bulk T_{SC}, which can be associated to the 2D character of the material [63, Petrovic 2001]. It is believed that in this compound, superconductivity arises from the magnetic fluctuations due to a closeness to an antiferromagnetic instability and the resistivity was observed to have a non-quadratic temperature dependence, with

instead $\rho \propto T^n$ with $n = 1.3$, which was attributed to scattering with antiferromagnetic fluctuations. The phase diagram obtained by doping was reported in Ref. [62, Shang 2014] and is shown on the right panel of Fig. 3.23. The substitution of In with Hg kills superconductivity and an antiferromagnetic order develops with just a few percentage of doping, confirming that the pure system is close to the magnetic instability. The substitution of In with Sn and Ir with Pt also kills the superconductivity with about the same percent as in the Hg-doping case. However, at higher doping, no magnetic ordering develops but the resistivity gets back its quadratic temperature dependence indicating that the Fermi liquid state is restored as the system moves away from the magnetic instability.

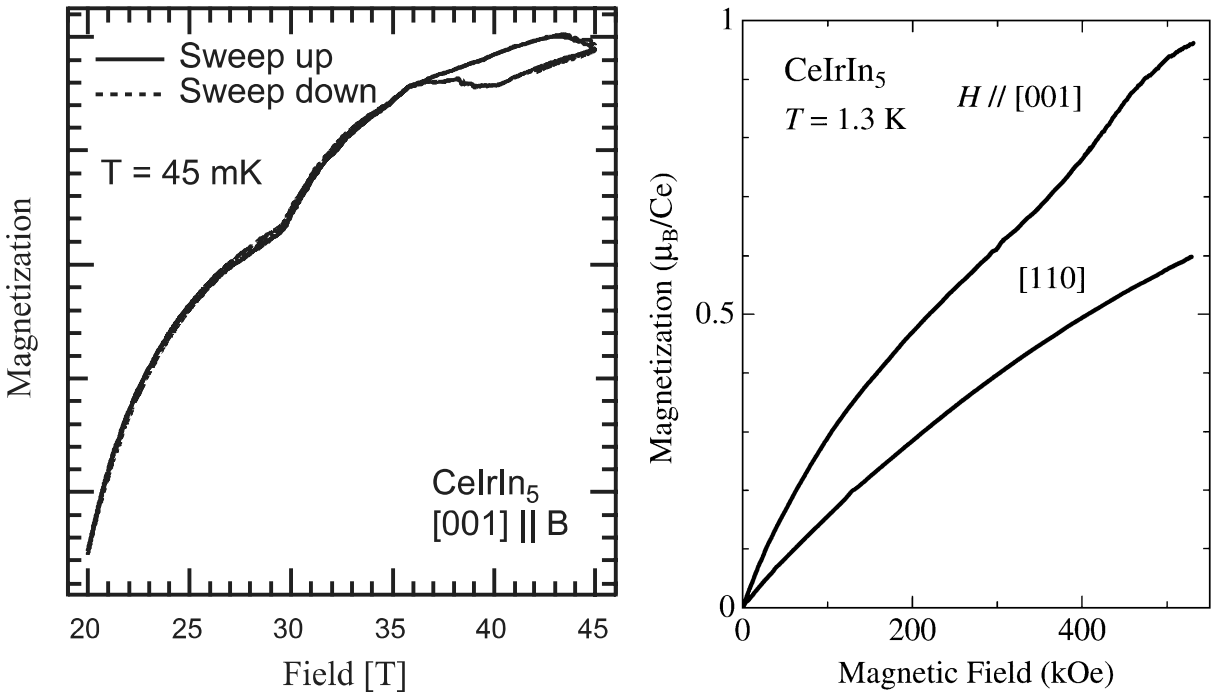

Figure 3.24: Field dependence of the magnetization in $CeIrIn_5$ at $T = 40$ mK for 20 T $< H <$ 45 T along the c-axis (right), taken from [67, Palm 2003], and at 1.3 K and up to 50 T along the c- and [110] directions (right), taken from [66, Takeuchi2001].

Magnetization measurements in $CeIrIn_5$ are shown in Fig. 3.24. On the left panel is the measurement reported in Ref. [67, Palm 2003], performed with magnetic field applied along the c-axis from 20 to 45 T and at $T = 40$ mK. The magnetization shows a strong upturn at $H_M = 30$ T and an hysteresis at $H = 35$ T. The anomaly at $H_M = 30$ T was interpreted as a metamagneticlike transition. The right panel shows the magnetization reported in Ref. [66, Takeuchi 2001] with the magnetic field applied along the c- and [110] directions up to $H = 50$ T at $T = 1.3$ K. Along the [110] direction, the magnetization is non-linear, but otherwise there is no anomaly detected. For a magnetic field along the c-axis, only a small change in the slope of the magnetization can be observed around $H = 40$ T, but no metamagneticlike transition is detected at $H_M = 30$ T at this temperature. Specific heat measurements showed the presence of a transition at high magnetic field [68, Kim 2002]. The temperature where this transition occurs increases with magnetic field, being located at $T = 1.8$ K at $H = 35$ T and $T = 4$ K at $H = 45$ T.

However, it is not clear if the anomalies detected in magnetization and specific heat are originating from the same transition. Additionally, the metamagneticlike character of the transition reported in Ref. [67, Palm 2003] is also not so clear, as even at $T = 45$ mK, there is no jump in the magnetization but rather a strong upturn. The sudden change in the magnetic susceptibility could be related to a modification of the topology of the Fermi surface, namely a Lifshitz transition. The most simple way to demonstrate if there is or not a Lifshitz transition is through the study of the Fermi surface.

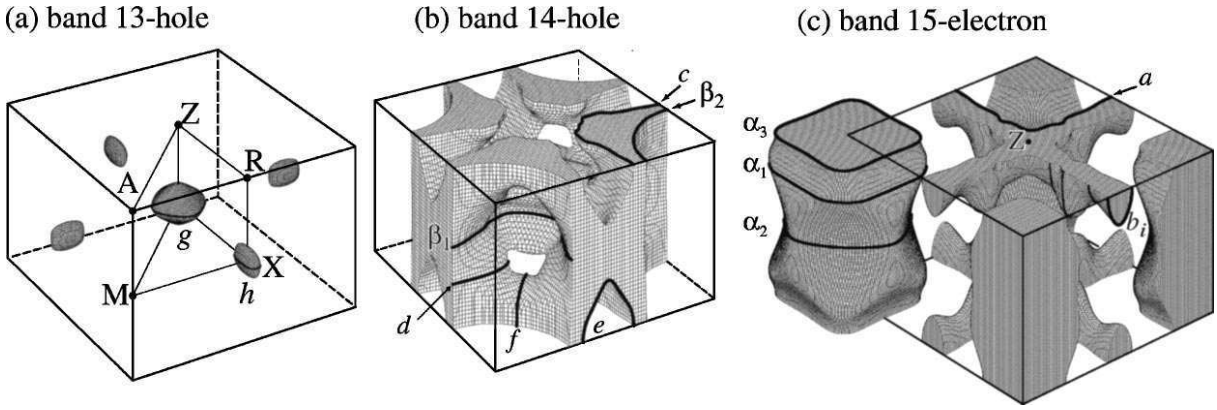

Figure 3.25: Calculated Fermi surface of $CeIrIn_5$, taken from Ref. [69, Haga 2001].

In $CeIrIn_5$, the Fermi surface is already well known. Experimental determination by de Haas-van Alphen oscillations as well as theoretical band structure calculations were performed with good agreement [69, 70, Haga 2001, Elgazzar 2004]. The Fermi surface calculated by H. Harima in Ref. [69, Haga 2001] is shown on Fig. 3.25. It consists of three bands, two mainly of holes and one mainly of electrons. It is quasi two-dimensional, as of most of the Fermi sheets are cylinderlike shaped.

With a magnetic field applied along the c-axis, many large orbits are available: the h and g branches from the band 13, centered at the Γ and X point, respectively. The β_1 branch, centered at the M point, the β_2 and c branches, centered at the A point, and the d branch centered at the X point, from the band 14. The α_1, centered between the M and the A points, the α_2, centered at the M point, the α_3 and a branches, centered between at the A point, from the band 15. Experimentally, the α_1, α_2, α_3, β_1 and β_2 branches have been observed, as shown on Fig. 3.26. The measured angular dependence of the frequencies of these branches fits well with the calculated Fermi surface. The calculations are therefore a solid ground to study the evolution of the Fermi surface under magnetic polarization. In this study, the aim was to understand the exact nature of the transition occurring at $H_M = 28$ T and especially the evolution of the Fermi surface of $CeIrIn_5$ through this transition.

3.2.2 Thermoelectric power and magnetic torque evidence of a field induced Lifshitz transition.

As we have seen before, thermoelectric power is very sensitive to Fermi surface modifications. The field dependence of the Seebeck coefficient for magnetic field applied along

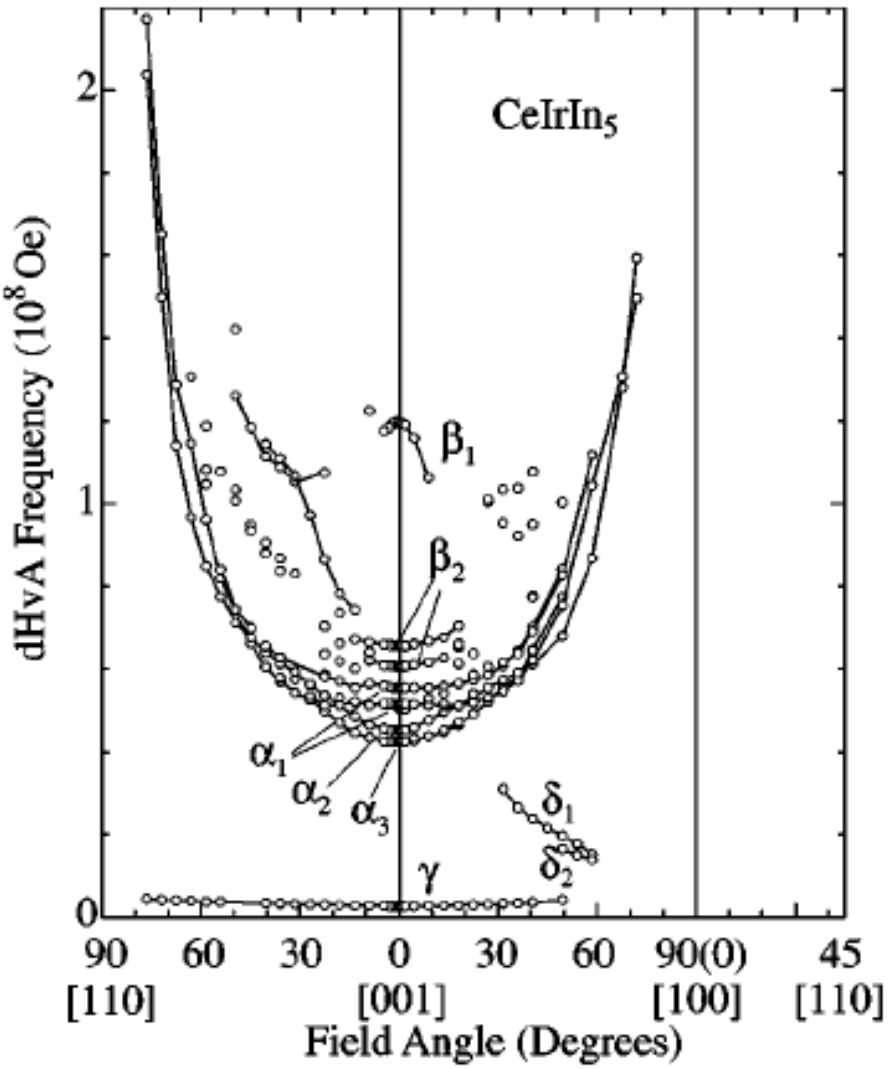

Figure 3.26: Angular dependence of the de Haas-van Alphen frequencies obtained by quantum oscillations measurements, taken from Ref. [69, Haga 2001].

the c-axis is shown in the left panel of Fig. 3.27. A clear anomaly is seen at $H_{M_1} = 28$ T at $T = 540$ mK and is followed up to 1.6 K where it is shifted to 32 T. Another anomaly can be seen at $H_{M_2} = 32$ T at $T = 540$ mK and moves slowly up to 33 T at 1 K where it disappears. Unfortunately, no direct observation of the Fermi surface topology has been possible through the direct observation of quantum oscillations in the thermoelectric power. Our measurements came as a complement of a torque magnetometry study which was performed on the same sample in the same magnetic field range but at lower temperature ($T = 50$ mK). The magnetic torque also detect anomalies in its field dependence, although with a slightly lower value of $H_{M_1} = 27.5$ T. The anomaly at H_{M_2} was not observed in the torque signal.

The temperature-magnetic field phase diagram drawn with the thermoelectric power and the torque magnetometry is shown in the right panel of Fig. 3.27. Also on this phase diagram is shown the transitions observed by specific heat in Ref. [68, Kim 2002] and the anomaly observed in the low temperature magnetization in Ref. [67, Palm 2003].

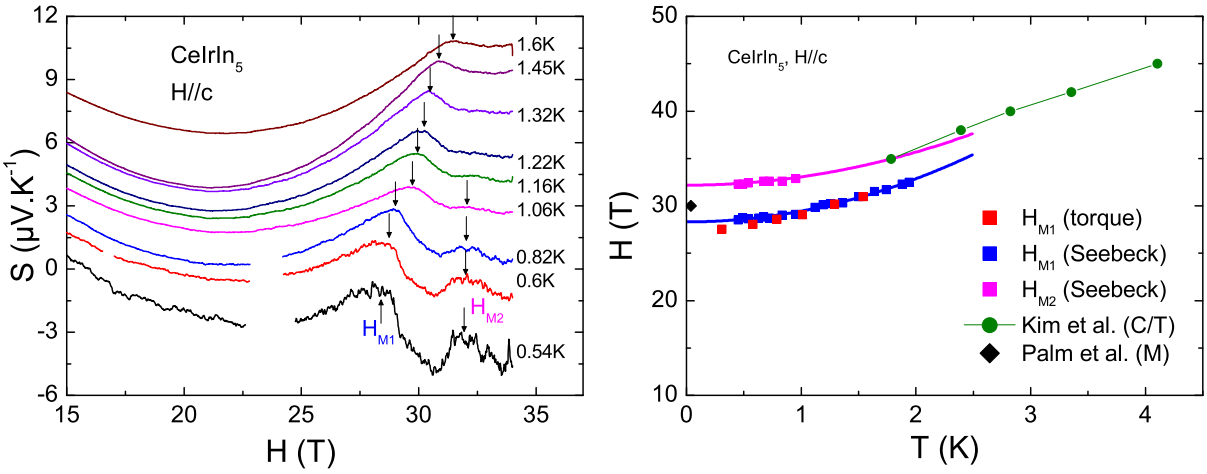

Figure 3.27: Left : Field dependence of the thermoelectric power for various temperatures. Magnetic field is along c-axis. Both anomalies are marked by arrows and the high field one disappears when temperature goes above 1 K. Right : Temperature-magnetic field phase obtained from thermoelectric power and torque measurements along with previously reported transitions. Blue squares are for H_{M_1} (Seebeck), pink squares for H_{M_2} (Seebeck), red squares for H_{M_1} (torque), green circles for specific heat data from [68, Kim 2002] and black diamond for magnetization data from [67, Palm 2003]. Solid lines are guides to the eye.

Interestingly, the data points from specific heat seems to connect with the H_{M_2} line, indicating that a phase transition may be occurring at this field. On the other hand, the transition detected by very low temperature magnetization is located just between H_{M_1} and H_{M_2}. It is therefore difficult to determine to which anomaly in the thermoelectric power it corresponds. It is however similar to what is observed in $YbRh_2Si_2$ where a Lifshitz transition is detected at $H = 10$ T [72, Pfau 2013].

At low temperature, quantum oscillations could be resolved in the torque signal. The oscillating part of the magnetic torque signal as a function of inverse magnetic field for temperatures from 50 mK to 200 mK and magnetic field $H > H_{M_1}$ is shown on the left panel of Fig. 3.28. The amplitude of the oscillation is rather high at $T = 50$ mK but decreases rapidly with increasing temperature. As shown in the top inset, a zoom on the low frequency part of the Fast Fourier Transform indicates a low frequency of 367 T. The bottom inset shows the amplitude plotted against temperature which is fitted with the Lifshitz-Kosevich formula to extract a high effective mass $m^* = 54\ m_0$. This branch of the Fermi surface was not observed below H_{M_1}, suggesting that this branch appears at the transition. However, since the amplitude of the oscillations increases with magnetic field, one could argue that the sensitivity of the measurement was just not good enough to detect this branch at lower field. Therefore the appearance of a branch is usually not a definitive proof of the presence of a Lifshitz transition.

The Fast Fourier Transform spectrum of the de Haas-van Alphen signal for 17.8 T $< H <$ 27.95 T ($H < H_{M_1}$) (a) and 27.95 T $< H <$ 34 T ($H > H_{M_1}$) (b) is shown on the right of Fig. 3.28. It shows many branches at rather high frequencies. The branch which is the most interesting is the one labeled β_1, with a frequency of 11.5 kT, which exists

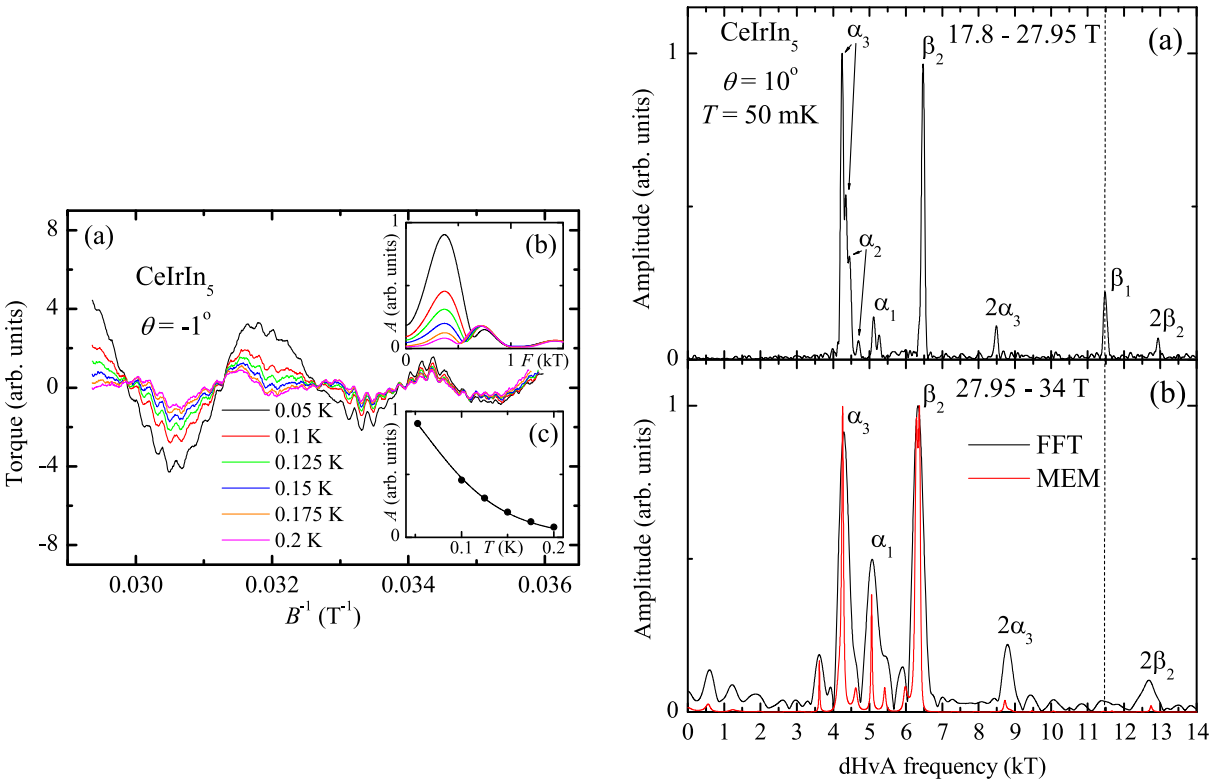

Figure 3.28: Left : Oscillating part of the torque signal for $H > H_{M_1}$ at temperatures from 50 mK to 200 mK. In insets the Fast Fourier Transform of the signal (top) and the Lifshitz-Kosevich mass plot (bottom). Right : Fast Fourier Transform of the signal for (a) 17.8 T $< H <$ 27.95 T ($H <$ H_{M_1}) and (b) 27.95 T $< H <$ 34 T ($H >$ H_{M_1}). Taken from Ref. [74, Aoki 2016]

in the low magnetic field region (panel (a), H$<$ H_{M_1}) and has disappeared in the high magnetic field region (H$>$ H_{M_1}). This result shows that this frequency is disappearing at the transition at H_{M_1}.

In order to understand how the topology of the Fermi surface changes at this transition, we compared the experimental results with the band calculation. The β_1 branch that disappears at the Lifshitz transition belongs to the band 14 (see Fig. 3.25). A sectional view of this surface is shown on Fig. 3.29, where the β_1 orbit can be seen much more clearly.

Considering the shape of the β_1 orbit, the most probable scenario for its disappearance would be a neck breaking at certain points in the Fermi sheet of this band. The Fermi sheet of the band 14 is shown in the left panel of Fig. 3.30. The possible location of the neck breaking is shown by green lines. Taking into account the symmetries of the crystal structure, if one of the necks is broken, all four of them should be. Therefore the quasiparticles are no longer allowed to make the β_1 orbit, and the frequency of this branch disappears from the Fast Fourier Transform spectrum (see Fig. 3.28). However, in this scenario, the neck breaking allows for two new orbits to appear, β_x and β_y. An estimation of their cross-section would give for these two branches frequencies around 2000 or 3000 T. The right panel of Fig. 3.30 shows the Fast Fourier Transform spectrum above H_{M_1}.

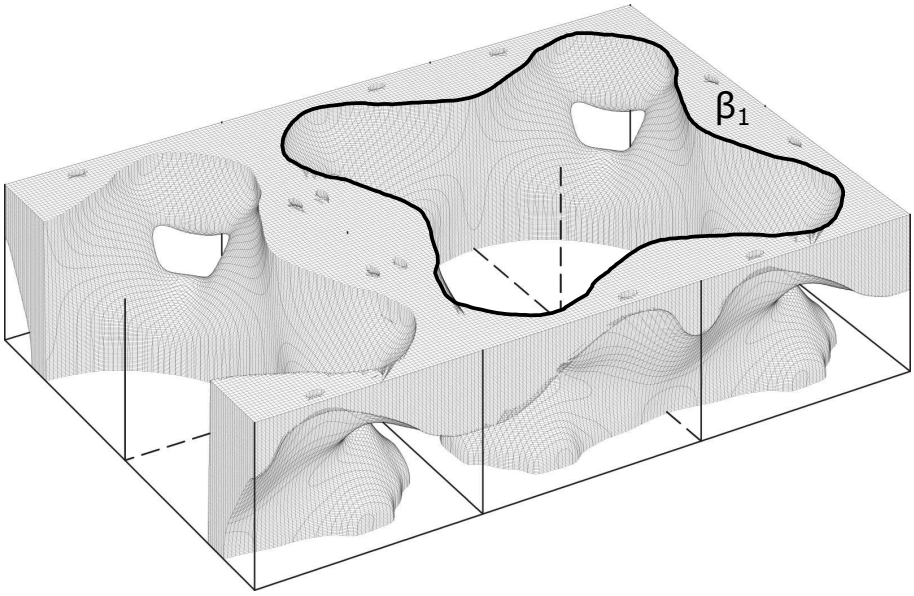

Figure 3.29: Sectional view of the Fermi surface of the band 14, showing the orbit of the β_1 branch. Taken from Ref. [73, H. Harima private communication].

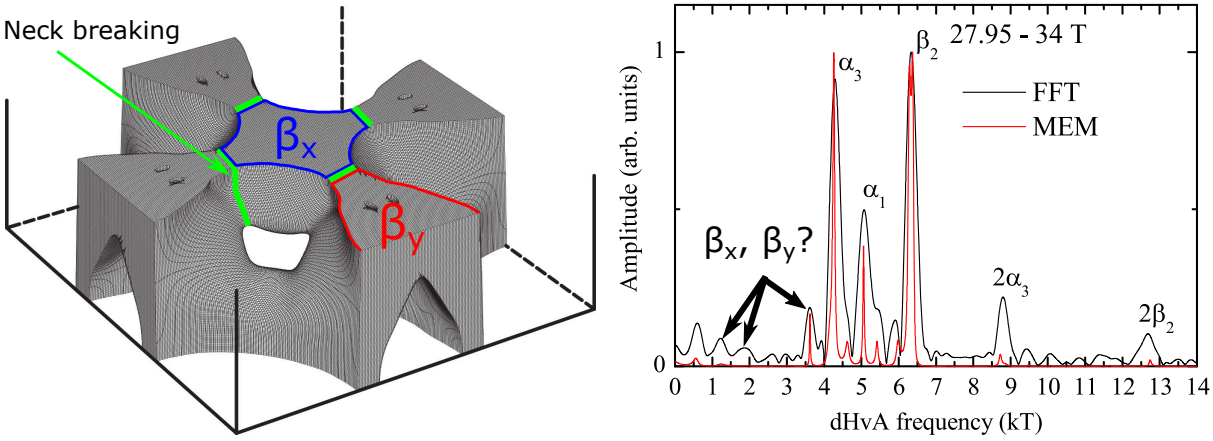

Figure 3.30: Left: Sectional view of the Fermi surface of the band 14 in the first Brillouin zone. The green lines show the possible location of neck breaking. The blue and red shows the resulting possible orbits β_x and β_y, respectively. Taken from Ref. [73, H. Harima private communication]. Right : Fast Fourier Transform spectrum for $H > H_{M_1}$. Arrows mark the possible frequencies of the β_x and β_y branches. Taken from Ref. [74, Aoki 2016].

Several peaks can be observed around 1000, 2000 and 3500 T, the latter having a good signal to noise ratio, that could correspond to either the β_x and β_y branches. However, even if we assume that there is indeed a neck breaking at this Lifshitz transition, we do not know precisely how the rest of this Fermi sheet is modified at the transition. Nevertheless, this is the most likely scenario we have found explaining the disappearance of the β_1 branch for a magnetic field along the c-axis.

3.2.3 Conclusion

We have measured the thermoelectric power in $CeIrIn_5$ for a magnetic field applied along the c-axis, completing a magnetic torque study. Two anomalies were detected in the Seebeck coefficient at $H_{M_1} = 28$ T and $H_{M_2} = 32$ T. These two anomalies move to higher field when the temperature is increased. Like in UCoGe, magnetization showed no sign of these transitions. Quantum oscillations were detected in the magnetic torque, corresponding to several branches of the Fermi surface. By performing a Fast Fourier Transform analysis of the oscillating signal on two different windows, one for $H < H_{M_1}$ and the other for $H > H_{M_1}$, a new branch with a low frequency of 370 T is detected only above H_{M_1}. It has a high effective mass $m^* = 54$ m_0 and therfore, it is difficult to know if this branch appears at the transition or is simply not detected at lower field. Additionally, the β_1 branch, which has a frequency of 11.5 kT, disappears at H_{M_1}. Comparison with the calculated Fermi surface shows that the most probable scenario explaining these results is a neck breaking in the band 14 surface. This breaking should also lead to the appearance of two lower frequencies, β_x and β_y, estimated at $F \approx 2000$ or 3000 T. A new branch is indeed observed at $F = 3500$ T, close to our estimation, but it is difficult to know precisely how the Fermi surface and field dependent calculations would be required to clarify this point. These results are evidence that the topology of the Fermi surface is modified at H_{M_1}, demonstrating that it is a Lifshitz transition.

Chapter 4

Fermi surface reconstruction at a magnetic transition

In this second section, we have studied magnetic transitions induced by magnetic polarization and Fermi surface modifications associated to it. There again we have studied two different compounds : the ferromagnetic superconductor URhGe where a magnetic field applied along the hard magnetization b-axis reorient the magnetic moments and gives rise to the so-called reentrant superconductivity and UPd_2Al_3, an antiferromagnetic superconductor where a metamagnetic transition takes place for a magnetic field applied in the basal plane. In these two systems, the aim was to study the link between the magnetic polarization of the Fermi surface and the magnetic transitions induces by magnetic field.

4.1 URhGe

In this section we will report on systematic thermoelectric and resistivity measurements under high magnetic field in the ferromagnetic superconductor URhGe. This study focused mainly on the spin reorientation transition at H_R for $H \parallel b$. A sharp change of the Fermi surface was detected in the longitudinal configuration and the position of the tricritical point, where the ferromagnetic transition changes from second to first order, was determined. The temperature dependence of the resistivity and especially the n-exponent confirms the first order character of the transition at low temperature as well as the location of the tricritical point (see Ref. [103, Gourgout 2016]).

4.1.1 State of the art

Very similar to UCoGe, URhGe displays coexistence of ferromagnetism and superconductivity. However the Curie temperature $T_C = 9.5$ K is higher than in UCoGe and the superconducting temperature $T_{SC} = 0.25$ K is lower [33, Aoki 2001]. The Sommerfeld coefficient extrapolated at $T = 0$ K is $\gamma = 155$ mJ.mol^{-1}.K^{-2}, indicating that it is a heavy fermion system with moderately enhanced effective masses [75, Prokes 2002]. Inside the ferromagnetic state, the magnetic moments are oriented along the c-axis and the spontaneous macroscopic magnetization is $M_0 = 0.4\ \mu_B$/U [78, Hardy 2011]. A DC

magnetization study demonstrated that although the magnetization shows strong uniaxial anisotropy, the universal class of the critical phenomenon does not belong to the 3D Ising system [79, Tateiwa 2014]. The unconventional critical scaling of magnetization seems to be inherent to the ferromagnetic superconductors (UGe_2, UIr) due to the dual character of the 5f electrons. URhGe crystallizes in the same orthorhombic TiNiSi structure as UCoGe with the uranium chains along the a-axis [76, 77, Troc 1988, Chevalier 1990] (see Fig. 3.1). Unlike the other ferromagnetic superconductors UGe_2 and UCoGe and most of the ferromagnetic compounds, the application of external hydrostatic pressure does not destroy the magnetic order, but reinforces it. The pressure dependence of the Curie temperature and the superconducting transition temperature is shown on Fig. 4.1. The Curie temperature increases from 9.5 K at $P = 0$ up to 17 K at $P = 13$ GPa [80, Hardy 2005]. Superconductivity, however, is suppressed with pressure and has been extrapolated to vanish around $P = 3$ GPa. The hydrostatic pressure pushes the system away from the ferromagnetic instability, reducing the magnetic fluctuations and thus the superconducting temperature.

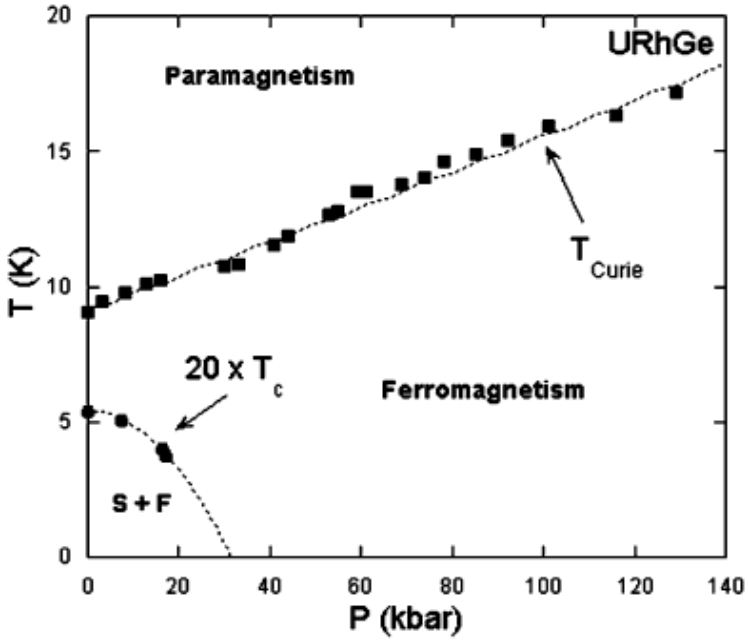

Figure 4.1: Pressure-temperature phase diagram of URhGe, taken from Ref. [80, Hardy 2005].

Like in UCoGe, the superconducting phase diagram of URhGe shows a strong anisotropy. When a magnetic field is applied along the easy magnetization c-axis, the upper critical field has the low value of $H_{C2} \approx 0.6$ T. For a field along the a-axis or the b-axis, the critical field is higher with values of $H_{C2} \approx 2$ T and 1.3 T, respectively [84, 82, Hardy 2005, Aoki 2012]. With a superconducting temperature of $T_{SC} = 0.22$ K, these upper critical field values all exceed the Pauli limitation which would give $H_{C2}^{Pauli}(T = 0) \approx 0.4$ T (see Eq. 3.1). This means that the upper critical field is dominated by the orbital limit. This observation makes triplet spin pairing most favorable for superconductivity.

The extrapolation of the magnetization at zero temperature as a function of magnetic field along all three directions is shown in Fig. 4.2. It shows a clear anisotropy. At zero

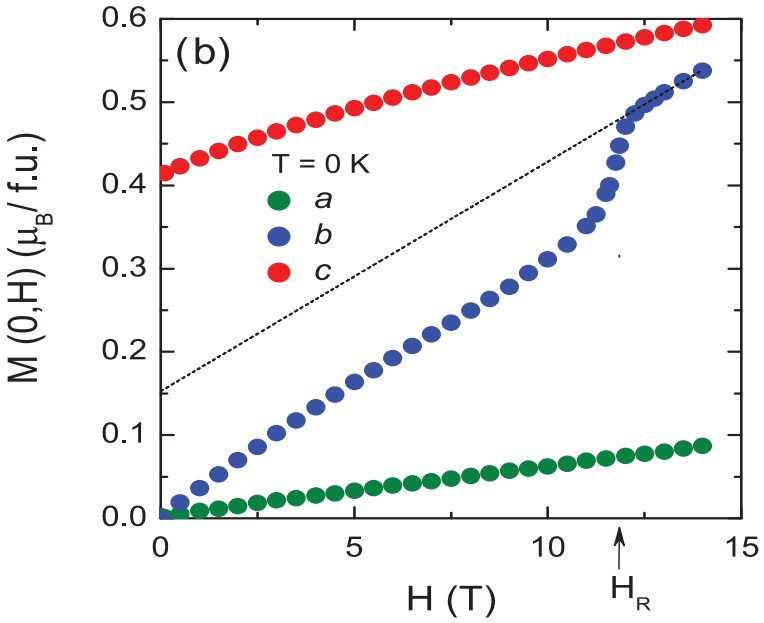

Figure 4.2: Extrapolation of the magnetization at zero temperature for magnetic fields up to 14 T along the three crystallographic axes, taken from Ref. [78, Hardy 2011].

temperature, applying an external field along the a-axis only induces a low magnetization of less than 0.1 μ_B at $H = 14$ T, making this axis the hardest magnetization axis. When the magnetic field is applied along the c-axis, the magnetization increases slowly and non-linearly from the spontaneous value of 0.4 μ_B at zero field to 0.6 μ_B at 14 T. For a field applied along the b-axis, the magnetization increases rapidly and is almost linear up to $H = 11$ T where the magnetization value is about 0.35 μ_B, close to the spontaneous magnetization. Then it jumps suddenly up to almost 0.5 μ_B at $H_R = 11.75$ T and continues to increase with an almost similar slope. It is interesting to note that while the system orders ferromagnetically along the c-axis, the susceptibility inside the ferromagnetic phase is higher along the b-axis. In itself, this result would not be very surprising if the system was close to saturation, but for U^{3+} and U^{4+} the free ion moment value is about 3.2 μ_B. In contrary, the system's spontaneous magnetization along the c-axis is only 0.4 μ_B, which is very far from the saturated value that can be expected [78, Hardy 2011]. This large difference suggests a strong itinerant character of the 5f electrons in this system. The magnetization jump when the magnetic field is applied along the b-axis corresponds to the re-orientation of the moments from the c-axis to the b-axis. This transition also corresponds to the collapse of the ferromagnetic order.

This can be seen on Fig. 4.3, displaying the measured magnetization along the b- and c-axes and the total magnetization as a function of magnetic field applied along the b-axis, by neutron diffraction measurements [85, Lévy 2005]. The magnetization along the c-axis was obtained by substracting the one along the b-axis to the total magnetization, using the formula : $M_c = \sqrt{M_{tot}^2 - M_b^2}$. It shows clearly the jump in magnetization along the b-axis at H_R and remarkably, the magnetization along the c-axis stays constant in the ferromagnetic phase and suddenly drops to zero at H_R. At low temperature, this re-orientation occurs at a field $H_R = 11.75$ T for a perfect alignment along the b-axis. The evolution of the Curie temperature under magnetic field along b-axis connects with

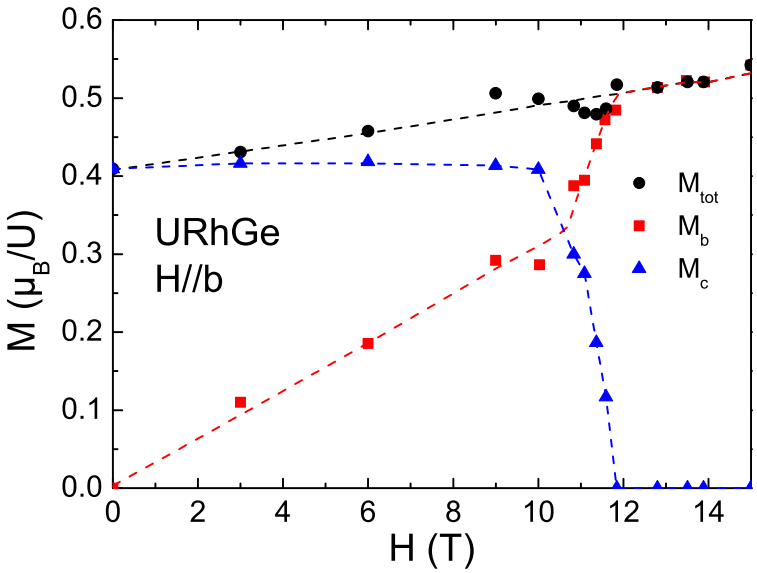

Figure 4.3: Magnetic field dependence of the total magnetization (black circles), magnetization along the b-axis (red squares) by neutron diffraction and along the c-axis (pink triangles) obtained from the other two. Adapted from Ref. [85, Lévy 2005].

the field-induced transition and at low enough temperature, superconductivity reappears in the so-called reentrant superconducting phase [85, Lévy 2005]. Remarkably, the maximum of the superconducting temperature in the reentrant superconducting phase (T_{SC} = 0.45 K), situated at $H = H_R$, is higher than the zero-field one, as can be seen on the temperature-magnetic field phase diagram shown on Fig. 4.4.

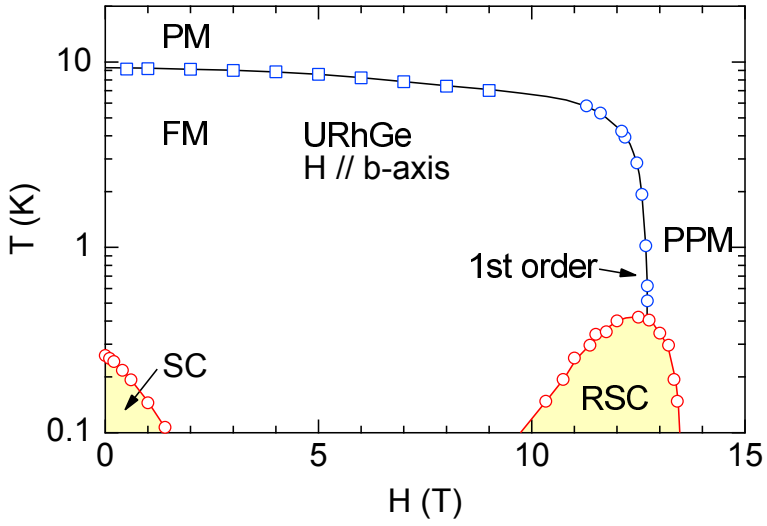

Figure 4.4: Temperature-magnetic field phase diagram of URhGe with in the inset the magnetoresistance curve at low temperature, taken from Ref. [90, Aoki 2014].

The relative field dependence of the Sommerfeld coefficient for field along all three crystallographic directions of the orthorhombic structure of URhGe is shown in the left

panel of Fig. 4.5. Since the experimental measurement of the Sommerfeld coefficient γ as a function of magnetic field is difficult due to hyperfine contribution to the specific heat at low temperature and high magnetic field, this dependence was extracted from the temperature dependence of the magnetization using the Maxwell relation:

$$\left(\frac{\partial \gamma}{\partial H}\right)_T = \left(\frac{\partial^2 M}{\partial T^2}\right)_H \tag{4.1}$$

For a magnetic field applied along the a-axis, γ is almost completely flat, confirming that nothing happens in this direction for this field range. The dependence along the c-axis decreases with magnetic field up to 14 T. This is probably due to the suppression of the magnetic fluctuations along the c-axis when the field is applied in the same direction as the magnetic moments [83, Wu 2016]. When the magnetic field is applied along the b-axis, γ increases with field and has a peak at H_R. The field dependence of the A coefficient of the resistivity of three different samples for H along the b-axis, shown in the right panel of Fig. 4.5, shows similar behavior to γ. Although the A coefficient decreases initially, most likely due to a misalignment of the field along c-axis, there is a sharp peak at H_R which is not sample dependent. Since the Sommerfeld coefficient γ is proportional to the effective mass and the A coefficient is proportional to its square, the aforementioned results indicates that the effective mass and therefore the electronic correlations are enhanced when approaching the transition, possibly explaining the presence of the reentrant superconductivity [86, 78, Miyake 2008, Hardy 2011].

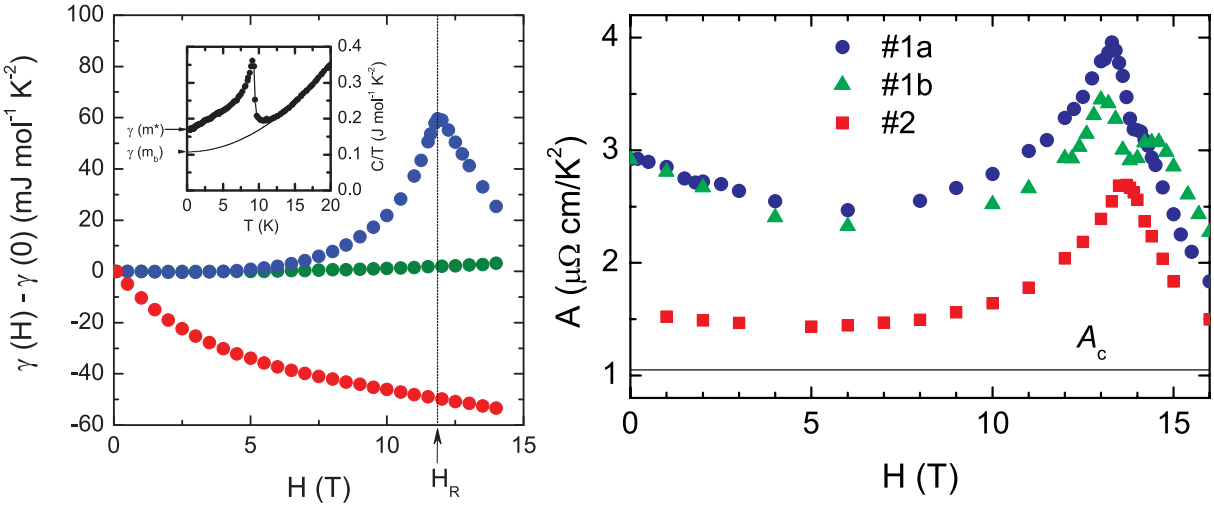

Figure 4.5: Left: Relative field dependence of the Sommerfeld coefficient γ for all three crystallographic directions of the orthorhombic structure, taken from Ref. [78, Hardy 2011]. Right Field dependence of the A coefficient of resistivity for three different samples with $H \parallel b$, taken from Ref. [86, Miyake 2008].

The reentrant superconducting phase extends from 8 to 13 T when the magnetic field is perfectly aligned along the b-axis. If the field is tilted from b- to c-axis, the re-orientation field H_R is shifted to a higher value and the superconducting dome is shifted as well but the maximum temperature and the field ranged are reduced, until it disappears around an angle of 6° [100, Lévy 2009]. The left panel of Fig. 4.6 shows a schematic phase diagram

of URhGe in the T-H_b-H_c space. When the magnetic field is misaligned from b- to c-axis, the transition at H_R, at low temperature, becomes a crossover [88, 93, Huxley 2007, Yelland 2011]. The application of hydrostatic pressure also shifts H_R and the reentrant superconductivity to higher fields and reduces its maximum temperature and field range [81, Miyake 2009]. This can be due to the fact that since the magnetic field is higher, it becomes closer to the orbital limitation field and therefore decreases the maximum temperature at which superconductivity is observed. As can be seen on Fig. 4.6, tilting the field from the b to the a-axis reduces the field range of the reentrant superconductivity slightly, but drives the reentrant superconductivity at least up to 35 T [87, Lévy 2007].

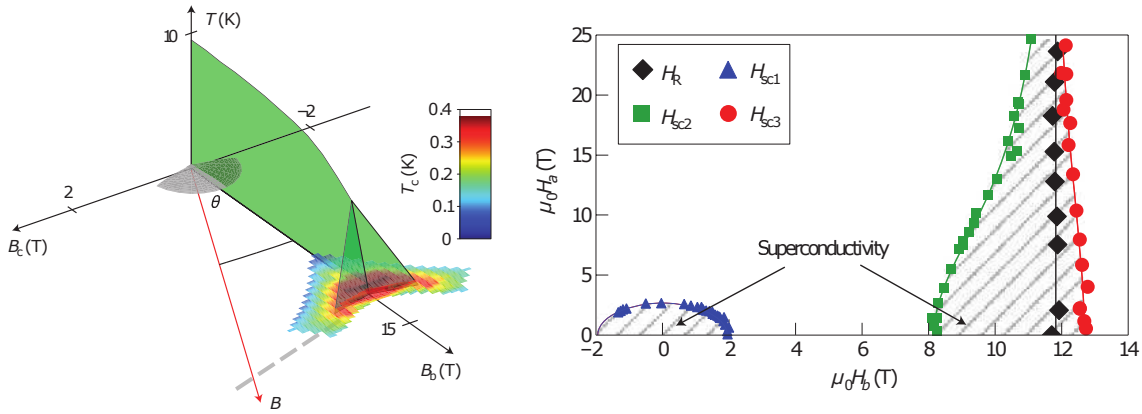

Figure 4.6: Left : Schematic phase diagram of URhGe in the temperature-$H \parallel b$-$H \parallel c$ space, taken from Ref. [93, Yelland 2011]. Superconducting phase diagram of URhGe in the $H \parallel b$-$H \parallel a$ plane, taken from Ref. [87, Lévy 2007].

It has been confirmed that the magnetic transition in URhGe is of first order at low temperature by recent nuclear magnetic resonance [89, Kotegawa 2015] with a change from second to first order at a tricritical point which has been estimated in a rather large temperature and magnetic field window from (7 K, 10 T) to (4 K, 12 T). The Hall effect at T = 800 mK [90, Aoki 2014] as well as the magnetic torque [100, Lévy 2009] show a clear hysteresis, signature of the first order character of the transition. From a theoretical point of view, as was seen in chapter 1.2.2, it is expected that an itinerant ferromagnetic order should be suppressed through a first order transition at zero temperature [26, Belitz 2005] with the application of pressure and therefore no quantum critical point should occur. This raises the questions whether the same behavior should be expected with the application of magnetic field and why superconductivity appears around this transition.

It was discussed theoretically that the collapse of the ferromagnetic order through a first order transition gives rise to an increase of the longitudinal fluctuations that are believed to be responsible for superconductivity in URhGe [91, Mineev 2015]. The asymmetry of the superconducting dome around H_R, with a slow increase in the ferromagnetic phase and a fast decrease in the polarized paramagnetic state may indicate that the quantization axis in this compound has changed at H_R and in the polarized phase the fluctuations are quickly killed by the magnetic field, similar to what happens in URhGe as well as in UCoGe when the field is applied along the easy magnetization c-axis [92, Wu 2016].

Recent NMR measurements on Co doped URhGe shows that there is indeed a increase of the flucutations, both longitudinal and transverse, at the magnetic transition [94, Tokunaga 2015]. Since it would seem that no quantum critical point occurs in this system, they suggested that the fluctuations were coming from the tricritical point. This is supported by recent theoretical works that show that rather strong fluctuations can come from tricritical points [96, 97, Mercaldo 2011, Misawa 2009] when the system is close to a quantum critical point, which may be the case for URhGe. Similar enhancement of the fluctuations was demonstrated when the field is rotated from the b- to the a-axis and it was found that in this case, the only relevant quantity is the magnetic field along the b-axis [95, Tokunaga 2016].

Other explanations have been suggested to explain the presence of superconductivity in this region of the phase diagram. One would be given by the role of the Fermi surface and the presence of a Lifshitz transition at H_R, similar to what was suggested for the S-shape of UCoGe. Quantum oscillations show that when one crosses the transition with a magnetic field tilted by 10° from b- to c-axis there is a modification of the Fermi surface [93, Yelland 2011]. It was observed that a small frequency of 600 T exists inside the ferromagnetic phase but disappears in the polarized paramagnetic one. According to this study, the disappearance of this frequency leads to a lowering of the Fermi velocity and therefore an increase of the orbital limiting field, allowing for the superconductivity to reappear as shown in Fig. 4.7.

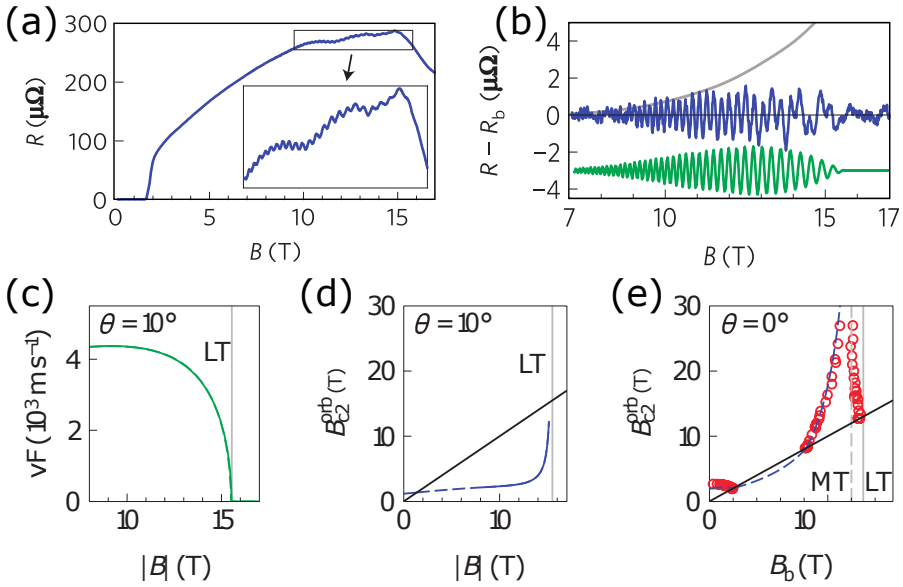

Figure 4.7: (a) Resistivity as a function of magnetic field for a field misaligned by 10° from b to c-axis at $T = 20$ mK. (b) Field dependence of the amplitude of the oscillating signal. (c) Estimated field variation of the Fermi velocity of this branch of the Fermi surface. (d) Resulting field variation of the orbital limiting field if this branch was the only one involved in superconductivity. (e) Extrapolation of the orbital limiting field for a magnetic field perfectly aligned along the b-axis. Taken from Ref. [93, Yelland 2011].

While there is no doubt that the signal from this frequency disappears at what is assumed to be a crossover between the ferromagnetic phase and the polarized one (the

extension of H_R), the interpretation is, in my opinion, not so straightforward. The Fermi velocity taken for the orbital limitation field is an averaged value over the whole Fermi surface. Therefore, the collapse of this pocket of the Fermi surface, which represents only about 1.5 % of the total specific heat, is not likely to be responsible for superconductivity. It would require that the averaged value of the Fermi velocity over the Fermi surface goes to zero as well, which would indicate that the whole Fermi surface is collapsing, and the increase of the Sommerfeld coefficient at the transition indicates, in contrary, that the density of states increases at the transition.

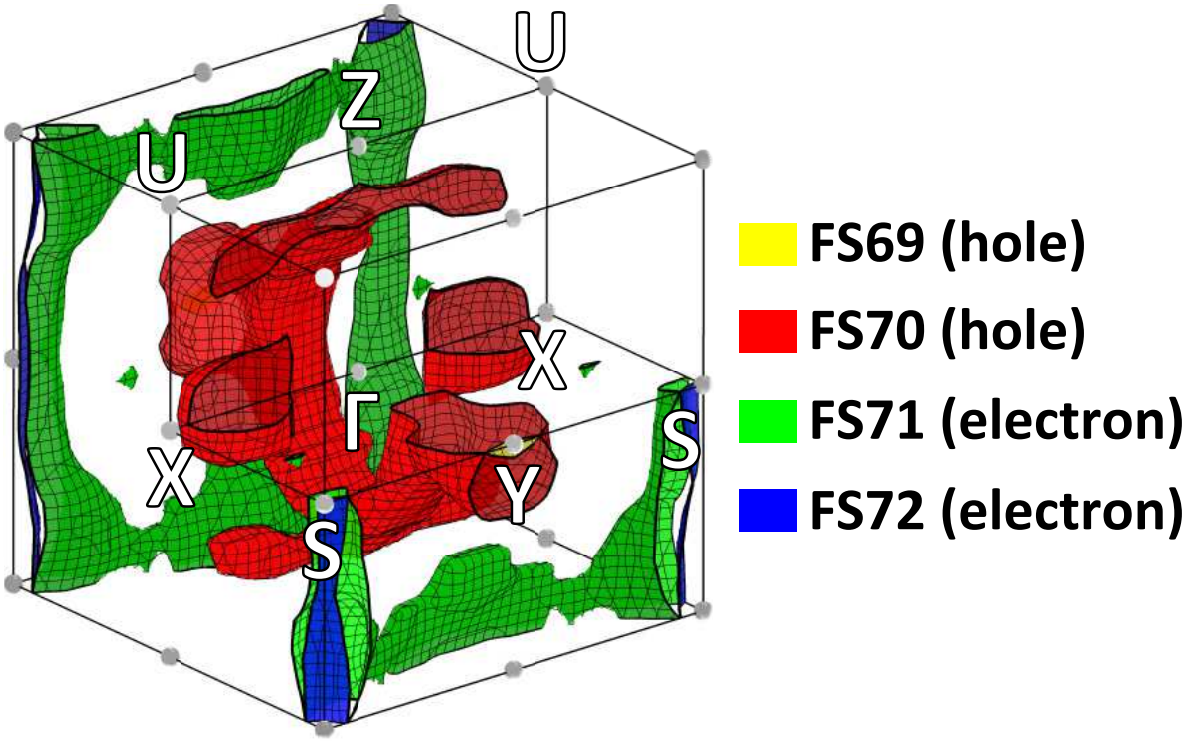

Figure 4.8: Calculated Fermi surface of URhGe, taken from Ref. [98, Fujimori 2014].

The evolution of the Fermi surface across the field induced spin reorientation transition is still unclear. As already mentioned in Ref. [93, Yelland 2011], a small sheet is found to disappear at the crossover field corresponding to the continuation of H_R at 10° from b- to c-axis which the authors put in order to eliminate reentrant superconductivity, making difficult the comparison to the perfectly aligned case where the transition is first order at low temperature. Hall effect measurements may suggest as well that some part of the Fermi surface disappears as it shows a rather sudden increase above H_R [90, Aoki 2014].

Very little is known about the Fermi surface of URhGe. The difficulty to obtain high quality single crystals makes the observation of quantum oscillations very rare and the low symmetry of the unit cell makes band structure calculation hard as well. Angle resolved photoemission spectroscopy measurements on URhGe confirmed that the f-electrons are mostly itinerant and showed a very small difference in the bands below the Fermi energy between the paramagnetic and the ferromagnetic phases [98, Fujimori 2014]. The band structure calculation performed in Ref. [98, Fujimori 2014] seems to match the photoemission spectra and shows rather large electron pockets on the edges of the Brillouin zone

that are connected to the other Brillouin zones in the k_z direction along with an also large hole pocket in the center of the zone that is connected in the k_y direction. The calculated Fermi surface is shown on Fig. 4.8.

Such a topology of the Fermi surface would be consistent with the large anisotropy of the system where the a-axis is the hardest magnetization axis and the relative equivalence between c and b for the easy one. However, the band structure calculation has only been made in the paramagnetic phase and the only measured pocket by Shubnikov-de Haas experiment inside the ferromagnetic phase may be, according to Ref. [93, Yelland 2011], almost spherical when rotating from b- to c-axis, which does not seem to correspond to any of the calculated surfaces.

In order to clarify the nature of the critical point at H_R and a possible reconstruction of the Fermi surface, we decided to perform thermoelectric power experiment as it is a very sensitive probe for Fermi surface changes (see chapter 1.1.1).

4.1.2 Spin reorientation under magnetic field in the longitudinal configuration

Thermoelectric power and resistivity measurements were performed on an URhGe single crystal of good quality (RRR = 36). The main study has been done with the direction of the thermal/electrical current along the b-axis and the magnetic field applied along the same direction. The longitudinal configuration allows, for transport measurements, to be unaffected by any orbital effect, which may make the anomalies in the signal more difficult to observe, as previously mentioned in chapter 3.1.1.3.

The temperature dependence for fields from 0 to 9 T of the Seebeck coefficient is shown on Fig. 4.9. At zero field a rather broad minimum at $T_C = 9.5$ K is seen, where the ferromagnetic anomaly was detected with other probes. At lower temperature, a broad maximum appears at $T^* = 4$ K and another minimum at $T_{coh} = 0.8$ K below which the thermoelectric power becomes almost linear and goes to zero at $T = 0$ K. When increasing the magnetic field, the Curie temperature increases slightly for $H = 5$ T probably due to a small misalignment ($<1^\circ$) to the c-axis and then decreases slightly, the T^* anomaly decreases in temperature until it disappears and T_{coh} increases and becomes a kink. At 9 T, values are $T_C = 8$ K and $T_{coh} = 1$ K. $T^*(\mathrm{H} = 8\ \mathrm{T}) = 3$ K. The anomalies T^* and T_{coh} define new energy scales in the system. As will be seen later, T^* most likely is the manifestation of magnetic excitations. Since below T_{coh} the Seebeck coefficient goes linearly to 0 at $T = 0$ K, it shows the entry of the system into a Fermi liquid state where one band dominates the others and sets the sign and slope of the thermoelectric power at very low temperature.

In Fig. 4.10, on the left panel, the field dependence from 0 to 16 T of the thermoelectric power for various temperatures from 0.25 to 1.75 K is shown. At 1.75 K, the Seebeck coefficient is negative below $H_R = 11.75$ T and becomes positive above, which appears as a sharp minimum. H_R appears at the lowest value reported in literature and this is a good indication that the field component along the c-axis is very small, thus the sample is perfectly aligned. With decreasing temperature, the transition becomes sharper and finally step-like. At temperatures below 0.4 K, the Seebeck coefficient undergoes two step-like transitions where it goes first to 0 in the reentrant superconducting state between 10.5 and 12.5 T at $T = 250$ mK and then goes to a positive value in the high

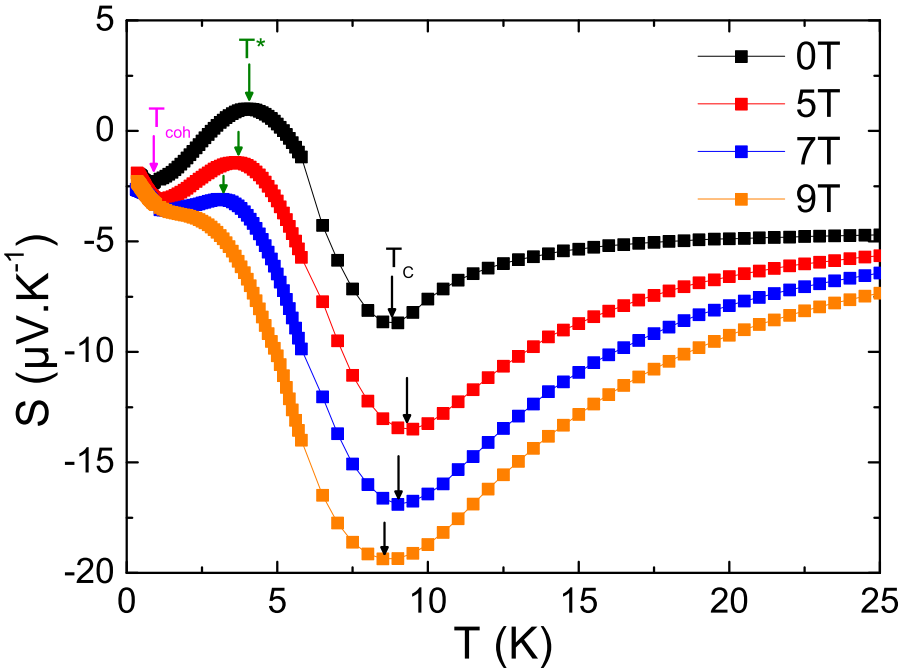

Figure 4.9: Temperature dependence of the Seebeck coefficient for fields up to 9 T. The Curie temperature is detected at 9.5 K at zero field. Two other energy scales T^* and T_{coh} are also seen.

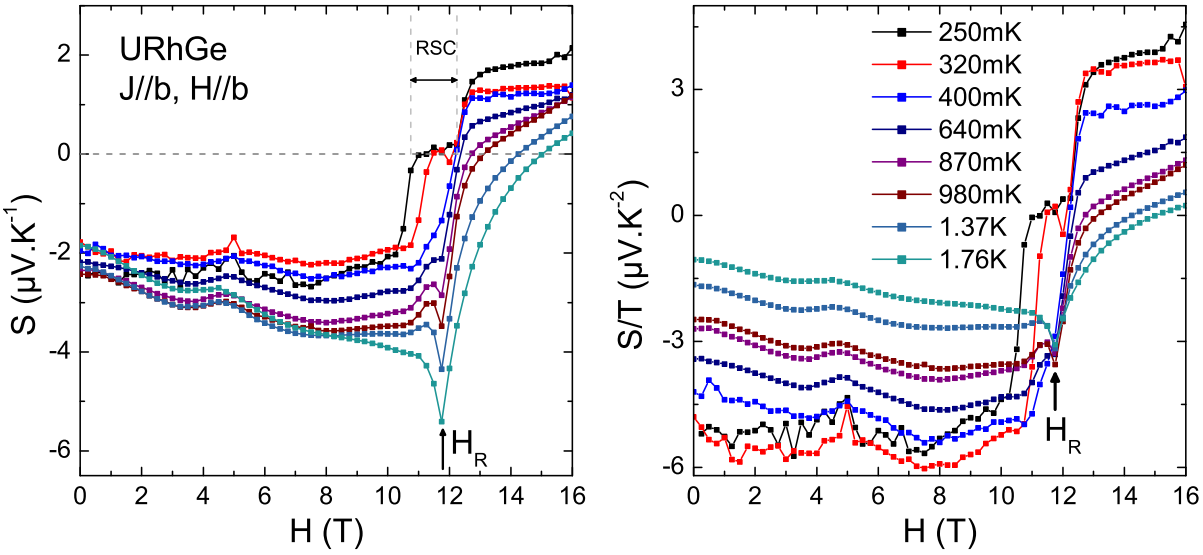

Figure 4.10: Field dependence at low temperature (from 0.25 to 1.75 K) of the thermoelectric power (left) and the Seebeck renormalized by temperature (right). RSC indicates the field range of the reentrant superconductivity.

field polarized paramagnetic phase. As shown before, the sign of the thermoelectric power at very low temperature is set, in a multi-band system, by the carrier type of the band dominating the entropy transport. Namely, the negative value of S in the

ferromagnetic phase ($H < H_R$) indicates that an electron pocket of the Fermi surface is dominating while in the polarized phase ($H > H_R$), it is a hole pocket. While it is not possible to identify the different pockets generating the Seebeck signal, the most natural explanation to this change of sign is that the Fermi surface is reconstructed when the ferromagnetic order is suppressed at H_R. On the right panel of Fig. 4.10, the same field dependence at the same temperatures of the thermoelectric power renormalized by temperature. Interestingly, for temperatures above the reentrant superconductivity, at H_R, the value of S/T is independent of temperature and is equal to -3 μV.K^{-1}. This may indicate that the electronic singularity in the density of states occurs for a given value of the entropy per carrier.

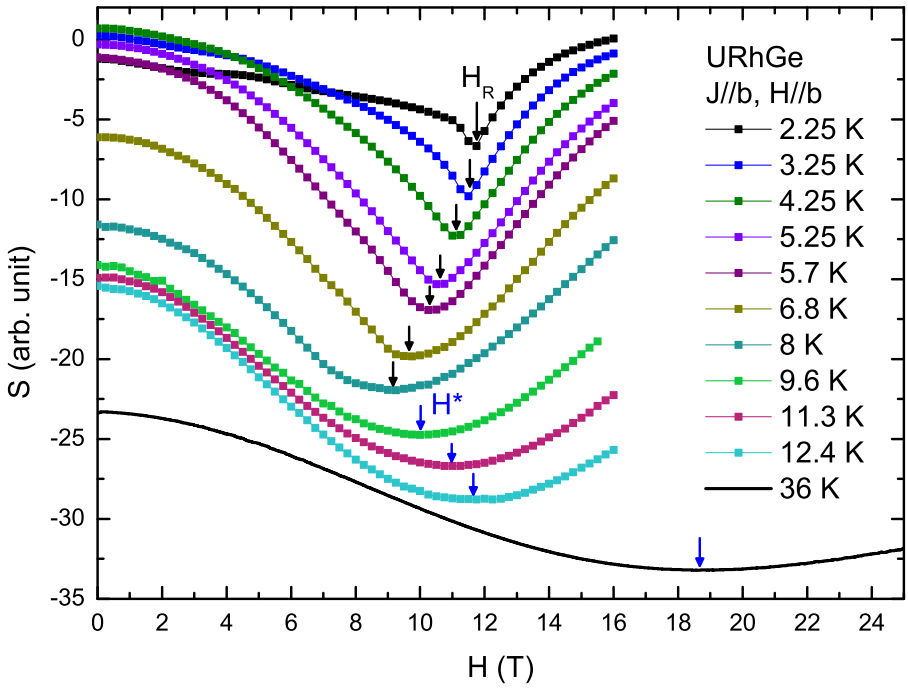

Figure 4.11: Field dependence of the thermoelectric power at high temperature. The anomaly at H_R broadens and move to lower field. Above $T_C = 9.5$ K a broad anomaly can still be seen and it moves to higher field, up to $H = 18.5$ T at $T = 36$ K.

The field dependence of the thermoelectric power for temperatures from $T = 2.25$ K to $T = 36$ K is shown on the left panel of Fig. 4.11. With increasing temperature, the anomaly marking the transition at H_R broadens and is shifted to lower field. Above the Curie temperature, $T_C = 9.5$ K, a broad minimum at H^* can be seen and it moves to higher field with increasing temperature. This minimum is still observable at $T = 36$ K where $H^* = 18.5$ T. It defines a line in the phase diagram that is likely to mark a crossover between the paramagnetic and polarized paramagnetic states.

The temperature-magnetic field phase diagram obtained by reporting all the anomalies is shown in the left panel of Fig. 4.12. The different energy scales seem to converge where the re-orientation transition becomes vertical, so this probably indicates the position of the tricritical point. The horizontal bars on the phase diagram give an indication of the width of the transition. This width was estimated by taking the field range given by the two points ten percent above the minimum that defines the transition, as shown on

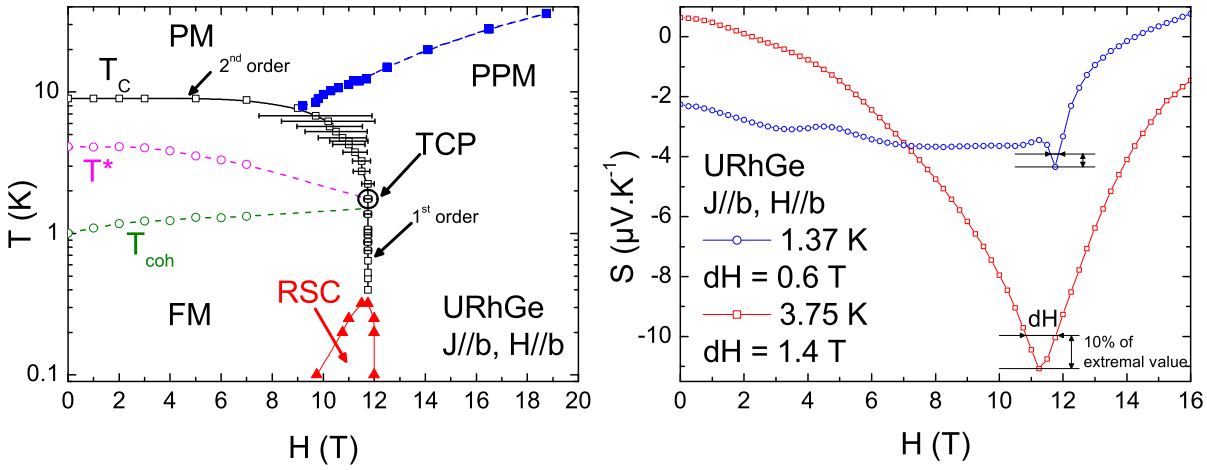

Figure 4.12: Left : Temperature-magnetic field phase diagram of URhGe obtained by thermoelectric power. Right : Analysis of the width of the transition for $T = 1.37$ K and $T = 3.75$ K.

the right panel of Fig. 4.12. At very low temperature, where superconductivity appears, the analysis was not possible because the transition becomes step-like. It is quite clear that while the transition at low temperature is very narrow, it becomes suddenly much broader at higher temperature. This broadening of the transition happens at the same field where H_R starts to move toward lower fields. This is another evidence of the location where the transition shifts from second to first order and so of the tricritical point in this system. The determination of the tricritical point is difficult in URhGe due to the fact that the hysteresis (in Hall effect, for example) at the first order transition is very small and thus difficult to detect. All these observations suggest a position of the tricritical point of $(T, H)_{TCP} \approx (2\text{ K}, 11.5\text{ T})$.

The direct observation of a tricritical point has a major consequence on the criticality of the system: no second order quantum critical point is expected. In order to verify the presence of a quantum critical point in URhGe, we measured the temperature dependence of the resistivity in the vicinity of the transition. As shown in chapter 1.2.3, since URhGe is three dimensional and ferromagnetic, one would expect the resistivity to be non-quadratic with temperature, with $\rho \propto T^{5/3}$ in the quantum critical regime.

The left panel of Fig. 4.13 shows the resistivity obtained at zero field and for magnetic fields below H_R (4, 8 and 10 T) as a function of T^2. In inset is shown the temperature dependence of the resistivity at zero field, where the Curie temperature and the superconducting transition are observed at $T_C = 9.5$ K and $T_{SC} = 0.2$ K, respectively. The resistivity as a function of T^2 for fields above H_R (13, 14, 15 and 16 T) is shown on the right panel of Fig. 4.13. The dashed lines show fits of the resistivity performed in a temperature range from 400 to 800 mK (above the maximum of the reentrant superconductivity) with the law: $\rho = \rho_0 + \text{AT}^n$. The fits were performed by forcing the n-exponent to take the Fermi liquid value : $n = 2$. In the low field region, one can see that the resistivity deviates from the Fermi liquid behavior with a n-exponent greater than 2 and at $H = 10$ T, the T^2 law is satisfied up to $T = 4$ K. In the high field region, however, the deviation from the T^2 law is with a n-exponent lower than 2. Additionally, the temperature T_{FL} where the resistivity deviates from the fit by more than 0.6 $\mu\Omega$.cm (arbitrary chosen) increases

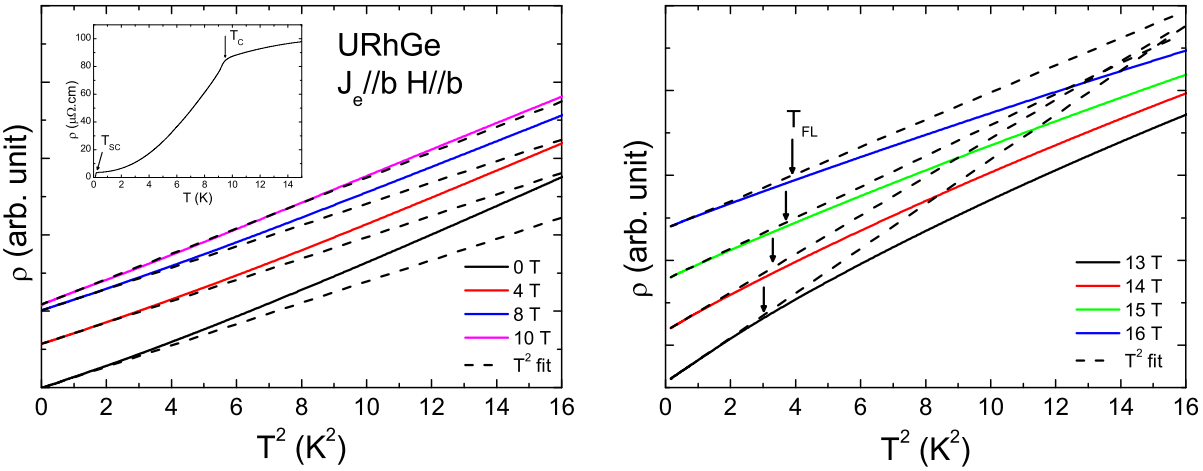

Figure 4.13: Resistivity as a function of T^2 along with T^2 fits performed from $T = 0.4$ K to $T = 0.8$ K for fields $H = 0$, 4, 8 and 10 T below H_R (left) and $H = 13$, 14, 15 and 16 T above H_R (Right). For high fields, the arrow marked as T_{FL} shows the temperature where the resistivity deviates from the T^2 law by more than 0.6 $\mu\Omega$.cm and gets a n-exponent lower than 2.

with magnetic field, indicating that the Fermi liquid gets stabilized as the magnetic field is set further away from H_R.

Fitting in the same temperature range (400 - 800 mK) while leaving the n-exponent as a degree of freedom leads to finding the parameters shown in Fig. 4.14. As previously reported in the literature [86, 78, Miyake 2008, Hardy 2011], the A coefficient displays a peak at H_R, indicating that there is an increase of the effective mass hence the fluctuations at the transition. ρ_0 shows a small increase with field and a small peak at H_R, suggesting that the scattering of electrons with impurities and defects of the crystal does not change much across the transition. However, contrary to what was reported in Ref. [93, Yelland 2011], the exponent was not found to become greater than 2 at low temperature when magnetic field is increased. Instead, the exponent measured in this study is always $n \approx 2$. The origin of this phenomenon could be that in Ref. [93, Yelland 2011], the resistivity was measured in a transverse configuration and on a very high quality sample (RRR $\approx$ 130), allowing for orbital motions of the quasiparticles to have an important effect on the field dependence of the resistivity, thus leading to an apparent change of the n-exponent. In our study, the longitudinal configuration does not allow for any orbital effect to take place, so only the diffusive scattering process is extracted from the temperature dependence of the resistivity, allowing us to directly compare with the Fermi liquid prediction.

As we have seen in chapter 1.2.3, the scattering with ferromagnetic fluctuations close to a quantum critical point is predicted to give a temperature dependence of T^n with $n = 5/3$ for 3 dimensional fluctuations and $n = 4/3$ for 2 dimensional fluctuations. It is then clear that, as was previously suggested, the enhancement of the fluctuations observed by the peak in the A coefficient of resistivity cannot be described by a theory of a second order quantum critical point with quantum spin fluctuations. It is interesting to note that the field at which the A coefficient starts to increase is roughly where the crossover line connects with the ferromagnetic order one at a field $H^* \approx 8.8$ T. H^* also seems to correspond to the field where the magnetization along the c-axis and the Curie

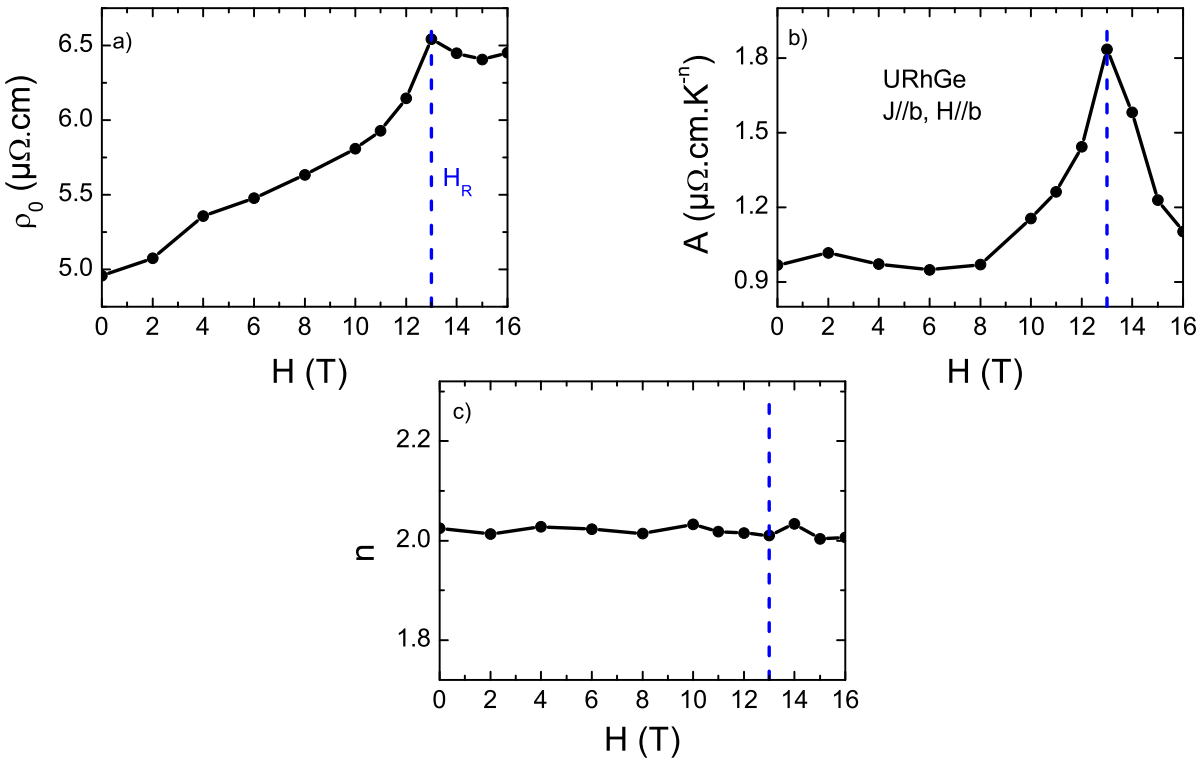

Figure 4.14: Parameters of the $\rho = \rho_0 + AT^n$ fits obtained on the temperature window of 400 - 800 mK with all parameters free to vary as a function of magnetic field. (a) the residual resistivity ρ_0, (b) the A coefficient and (c) the n-exponent of the resistivity.

temperature starts to decrease, suggesting that this point of the phase diagram may be important regarding the increase of the magnetic fluctuations.

In order to see how the n-exponent of resistivity deviates from the T^2 law when the temperature is increased, the resistivity data were fitted by fixing ρ_0 to the value obtained from the fit in the 400-800 mK temperature range and the other two parameters (A and n) were left free. The fitting window was then shifted by 0.1 K steps up to 15 K. This gives the variation of the n-exponent as a function of temperature and magnetic field, shown on Fig. 4.15 as a color scale. It is interesting to note that inside the ferromagnetic phase, the exponent is always greater than 2 and shows a maximum following rather well the T^* anomaly detected in the temperature dependence of the Seebeck coefficient. For fields higher than H_R the exponent is, as stated before, equal to 2 at low temperature and deviates to lower values as the temperature increases. When the magnetic field increases further above H_R, the system is pushed away from the magnetic instability and the deviation temperature increases.

In yellow is a large line representing the region with $n \approx 5/3$, which corresponds, as mentioned in chapter 1.2.3, to what is expected for ferromagnetic quantum fluctuation in 3 dimensional systems [8, Moriya 1985]. In the case of a quantum critical point, this line should go to zero temperature when joining with the transition but in URhGe, the line goes to a finite temperature instead, most likely the tricritical point, indicating that the magnetic fluctuations may originate from this point. Indeed, one would expect the fluctuations to be maximum when the transition switches from second order to first

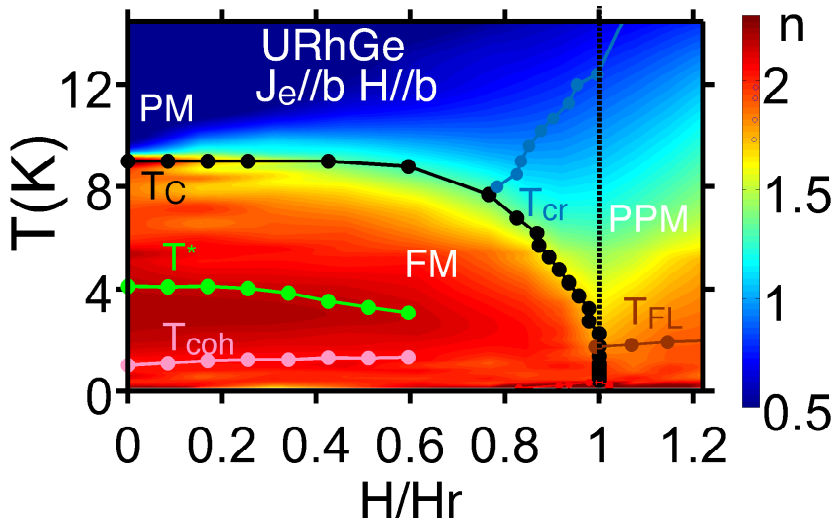

Figure 4.15: Color scale map of the n-exponent of the resistivity as a function of the magnetic field normalized by H_R and the temperature. Superimposed is the phase diagram obtained by thermoelectric power measurements.

order. There is no evidence from the temperature dependence of resistivity that these spin fluctuations extend down to lower temperature than T_{TCP}. The nature of the fluctuations involved in the enhancement of the A and Sommerfeld coefficients and in the superconductivity at low temperature remains unknown.

4.1.3 Results for the transverse configuration $J_Q \parallel c$

The large anisotropy of URhGe makes it interesting to study the transport properties with different current, electrical or thermal, directions with respect to the crystallographic axes. The transverse configurations we measured also allowed to measure Nernst effect (see chapter 1.1.1). Thermoelectric power, Nernst effect and resistivity measurements were performed on URhGe single crystals of good quality with a residual resistivity ratio of 38 for $J_Q \parallel a$ and 23 for $J_Q \parallel c$. The magnetic field is applied along the b-axis.

The thermoelectric power at low temperature as a function of magnetic field for the sample with $J_Q \parallel c$ is shown in Fig. 4.16. It is always negative up to 16 T, and shows small and broad anomalies around $H = 2$ T and $H = 6$ T. At 100 mK, superconductivity is observed from 10.75 T to 12.75 T. The field range of superconductivity is reduced as temperature is increased and is no longer seen at 410 mK, instead showing a rather sharp peak at H_R. As temperature increases further, the transition becomes less clear and is finally smeared out around 4.5 K. For this direction, H_R is located at 12.5 T, indicating a misalignment of approximately 2° from b- to c-axis. While at high field increasing temperature only increases the negative value of the Seebeck coefficient, at low field it stays close to zero and changes sign to become positive around 2 K.

The field dependence of the thermoelectric power in this current direction seems to be largely dominated by scattering effects as the background is large compared to the peak at H_R. The reasons behind this behavior are difficult to determine, but it is possible

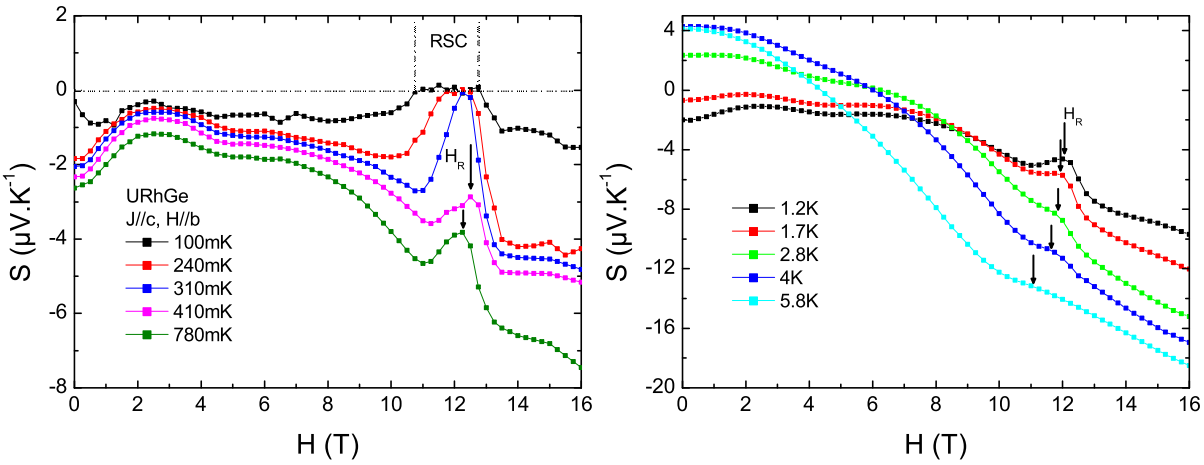

Figure 4.16: Field dependence of the thermoelectric power for a thermal gradient applied along the a-axis and for temperatures from $T = 100$ mK to $T = 780$ mK (left) and from $T = 1.2$ K to $T = 5.8$ K.

to formulate hypothesis about the effects taking place here. The orbital effect which is allowed to take place in this configuration could influence the Seebeck effect and cause such a field dependence. In such an anisotropic system, the pocket of the Fermi surface dominating the thermoelectric power in this direction may not be the same as the one dominating in the longitudinal configuration. As we can identify neither the pockets dominating the Seebeck coefficient nor the ones reconstructed at H_R, it is difficult to draw a definitive conclusion, but it is possible that the part of the Fermi surface responsible for the field dependence of the thermoelectric power at low temperature in this direction remains untouched at H_R. Finally, given the relative Ising character of the magnetic order in URhGe, it is possible that the small misalignment of the magnetic field along the c-axis leads to a thermoelectric response far from the perfectly aligned case. Additionally, in this configuration, the large background contribution makes the analysis of the width of the transition difficult. While it is possible to see that with increasing temperature the transition becomes less marked, locating the position of the tricritical point solely from the field dependence of the thermoelectric power is not possible.

The temperature dependence of the Seebeck coefficient leads to similar results as for $J_Q \parallel b$ and is shown on Fig. 4.17. At zero field the Curie temperature is at 9.5 K and the two anomalies T^* and T_{coh} are also observed at 4 K and 1 K, respectively. Under magnetic field, T_C increases slightly with field because of the misalignment along the c-axis and the temperature dependence of the other anomalies are the same as before. Here the Curie temperature appears as a maximum instead of a minimum, the Seebeck is negative in the high temperature region but changes sign above T_C at $T = 12.5$ K and then becomes negative again at $T = 1.9$ K below T^*. The fact that we find the same anomalies for this current direction strongly suggests that these are intrinsic to the compound and not specific to a given crystallographic direction.

The field dependence of the Nernst effect for temperatures from $T = 1.1$ K to $T = 6.9$ K is shown on Fig. 4.18. At low temperature, the Nernst coefficient shows no field variation and remains zero within the noise limit of the measurement inside the ferromagnetic phase. When crossing the magnetic transition, it suddenly jumps to a rather high value

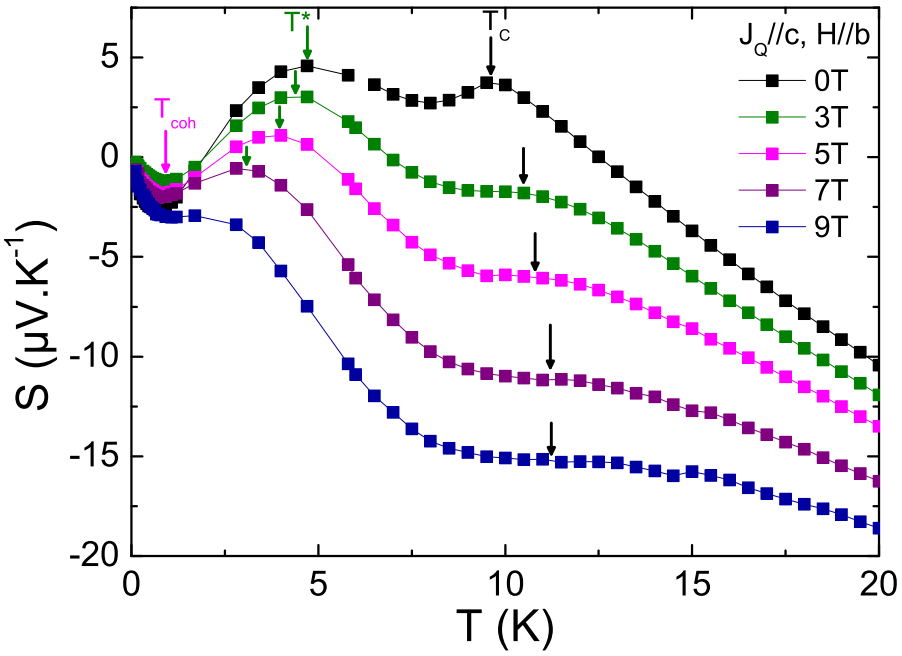

Figure 4.17: Temperature dependence of the thermoelectric power for $J_Q \parallel c$ and magnetic field from 0 to 9 T.

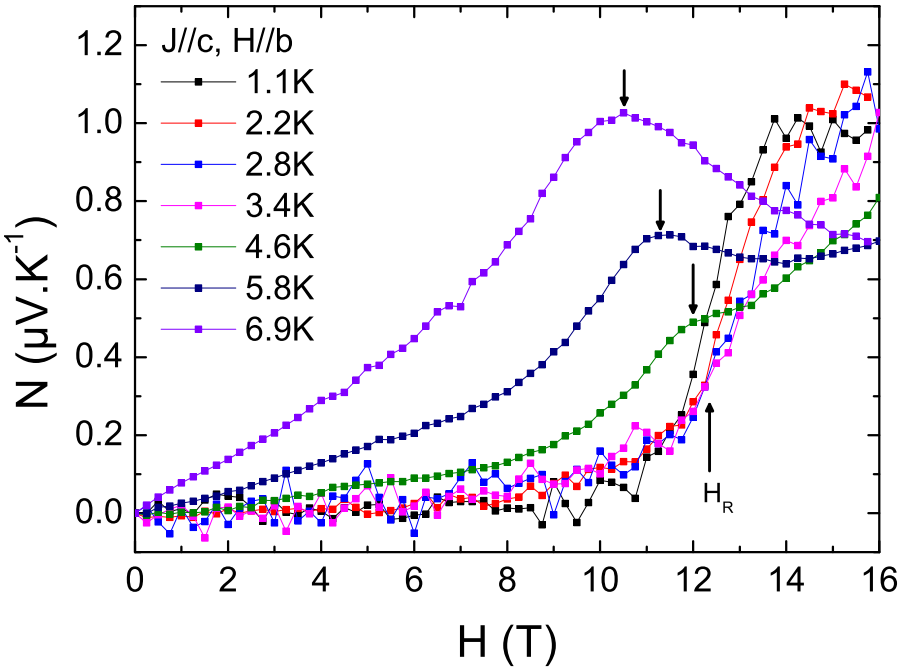

Figure 4.18: Field dependence of the Nernst effect for temperatures from $T = 1.1$ K to $T = 6.9$ K.

of 1 μV.K^{-1}. When temperature increases, the step-like transition turns into some kind of plateau at $T = 4.6$ K and then becomes a broad maximum at higher temperature.

The temperature dependence of the Nernst effect at low fields is shown on the left

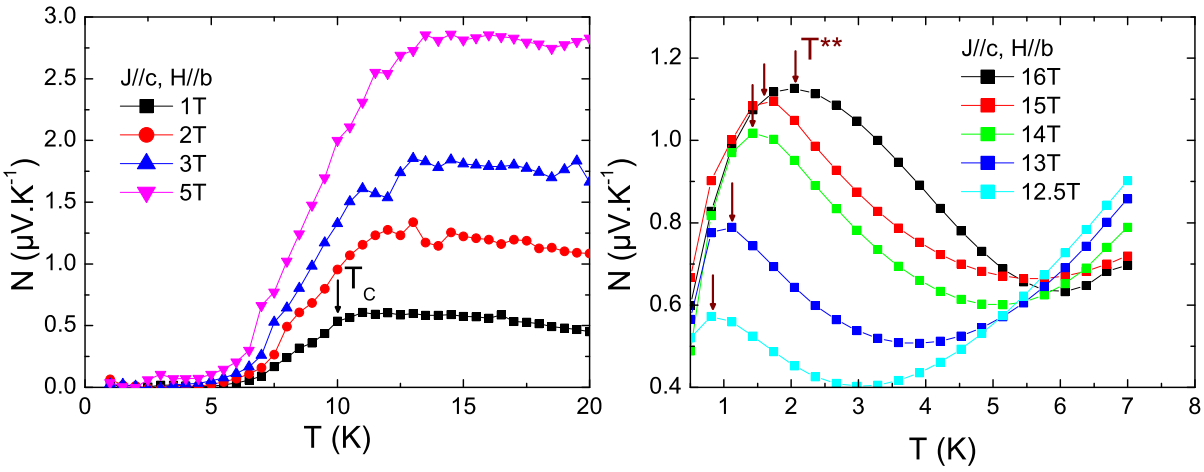

Figure 4.19: Temperature dependence of the Nernst coefficient for magnetic fields from 1 T to 5 T (left) and from 12.5 T to 16 T (right).

panel of Fig. 4.19. It is non-zero above T_C, in the paramagnetic phase, but as soon as the system enters the ferromagnetic state, the value drops rapidly down to zero or at least too low to be measured by our setup. The origin of this behavior remains unclear. Comparison with the Hall effect in Ref. [90, Aoki 2014] shows a similar behavior, with a very low value in the ferromagnetic phase that increases at the magnetic transition, and could be related to the reconstruction of the Fermi surface at H_R, with a disappearance of some of the carriers.

The temperature dependence of the Nernst effect at fields higher than H_R is shown on the right panel of Fig. 4.19. A broad maximum of the Nernst coefficient is detected at $T^{**} \approx 2$ K for $H = 16$ T and moves to lower temperature when the magnetic field is brought closer to $H_R \approx 12.5$ T for this measurement. This anomaly is reminiscent of what was observed in $CeCoIn_5$ where the same T^{**} anomaly in Nernst effect was attributed to a separation between the Fermi liquid regime at low temperature and the non-Fermi liquid one at high temperature [99, Izawa 2007]. In URhGe, the line defined by the Nernst coefficient seems to roughly correspond to the one observed in n-exponent of the resistivity in Fig. 4.15, indicating that this may be the same kind of separation than the one observed in Ref. [99, Izawa 2007].

The different anomalies obtained by Seebeck (open squares) and Nernst effect (open triangles) measurements are reported on the phase diagram on Fig. 4.20. One can notice that the line taken from the Nernst and the point where the magnetic transition becomes vertical would indicate that the tricritical point here is at $T \approx 0.8$ K, much lower than what was found for $J_Q \parallel b$. This is most likely due to the misalignment to the c-axis. Indeed, the tricritical point can be tuned here by the magnetic field applied along the c-axis. As mentioned before, previous resistivity measurements have suggested that there may be a critical end point when the field is rotated from b- to c-axis at an angle $\theta \approx 4.5^\circ$ [100, 93, Lévy 2009, Yelland 2011]. Therefore it suggests that the first order character of the transition should disappear around that point and so the tricritical point should be lower in temperature when the field is misaligned along the c-axis.

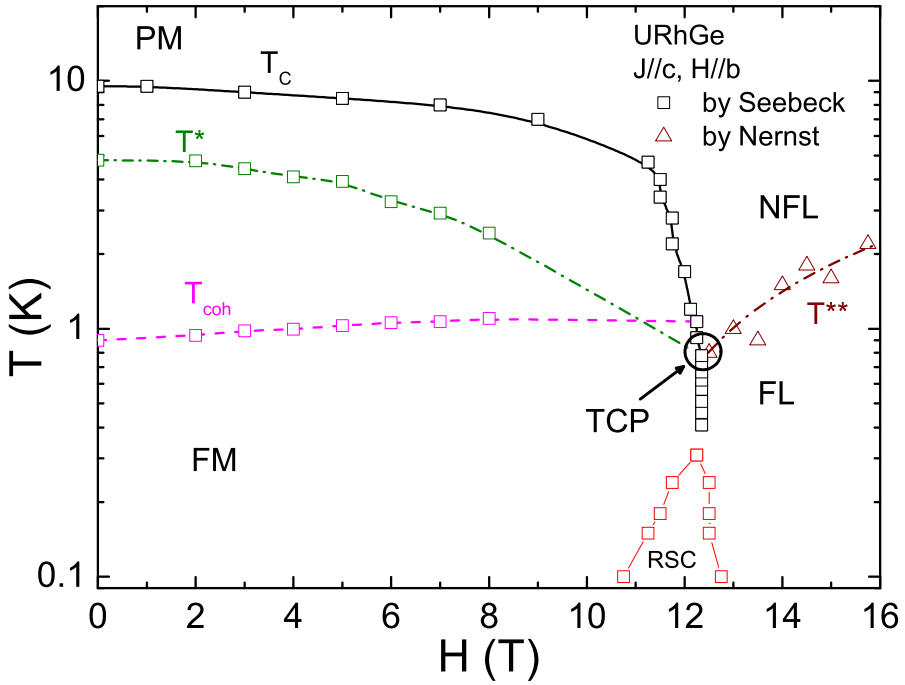

Figure 4.20: Magnetic field-temperature phase diagram of URhGe. Open squares shows the anomalies obtained in thermoelectric power and open triangles the one obtained in Nernst effect.

4.1.4 Transverse configuration with $J_Q \parallel a$

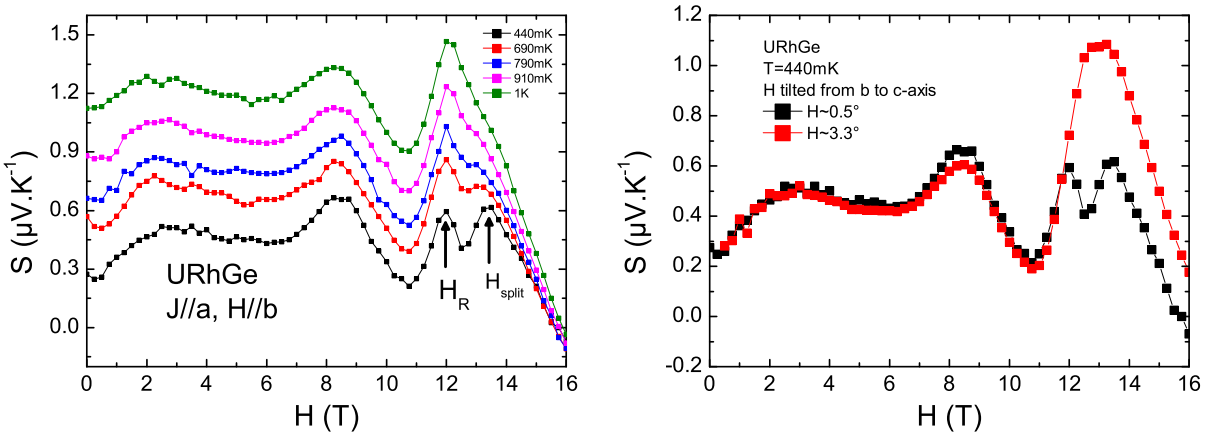

Figure 4.21: Left: Field dependence of Seebeck coefficient for temperatures from $T = 0.44$ K to $T = 1$ K. Right: Comparison between the field dependence of Seebeck with the magnetic field at 0.5° and at 3.3° from the b- to the c-axis.

A good way to observe a modification of the Fermi surface at the transition is by the observation of quantum oscillations and a subsequent change in these oscillations, for which we needed the sample of the best quality and high magnetic fields. The sample in the configuration of $J_Q \parallel a$ and $H \parallel b$ was measured both in a superconducting magnet

up to 16 T and in a resistive magnet in LNCMI Grenoble up to 33 T. The averaged field dependence of the Seebeck coefficient is shown on the left panel of Fig. 4.21 for temperatures from 0.44 K to 1 K. In this sample, probably due to the geometry, it was difficult to apply the thermal gradient without heating the sample a lot, therefore the measurements were not good at lower temperature and superconductivity was not observed. Just like in the other two configurations, the thermoelectric power displays small anomalies around $H = 2$ T, $H = 6$ T and $H = 8$ T. At 1 K, the transition from the ferromagnetic to the polarized paramagnetic state is marked by a large maximum at $H_R = 12$ T followed by a sudden drop to the Seebeck, indicating that the field is misaligned by approximately 0.5° from b- to c-axis. When the temperature gets lower, a shoulder appears around $H_{split} = 13$ T and becomes as large as the main peak at $T = 440$ mK. This behavior is similar to that observed in $CeRu_2Si_2$ where it was suggested that the Fermi surface reconstruction in this system happened like a Lifshitz transition on the different bands of the multiband system [55, 56, Daou 2006, Boukahil 2014]. Contrary to the other two directions, the Seebeck coefficient here is positive and changes sign only above the magnetic transition around $H = 15.5$ T. If the magnetic field is slightly more misaligned to the c-axis up to 3.3°, not only H_R increases to 13 T, but the splitting structure disappears, as shown on the right panel of Fig. 4.21. A possibility could be that the small misalignment moves the peak at H_R faster than the one at H_{split} and at 3.3°, they are almost at the same field and merge to display only one larger peak. However, since no systematic angular dependence of the Seebeck coefficient has been made, it is difficult to determine how this second peak at H_{split} changes when the field is rotated from b- to c-axis. The Lifshitz transition could also be sensitive to the field along the c-axis, meaning that it would be sensitive to the first order nature of the transition.

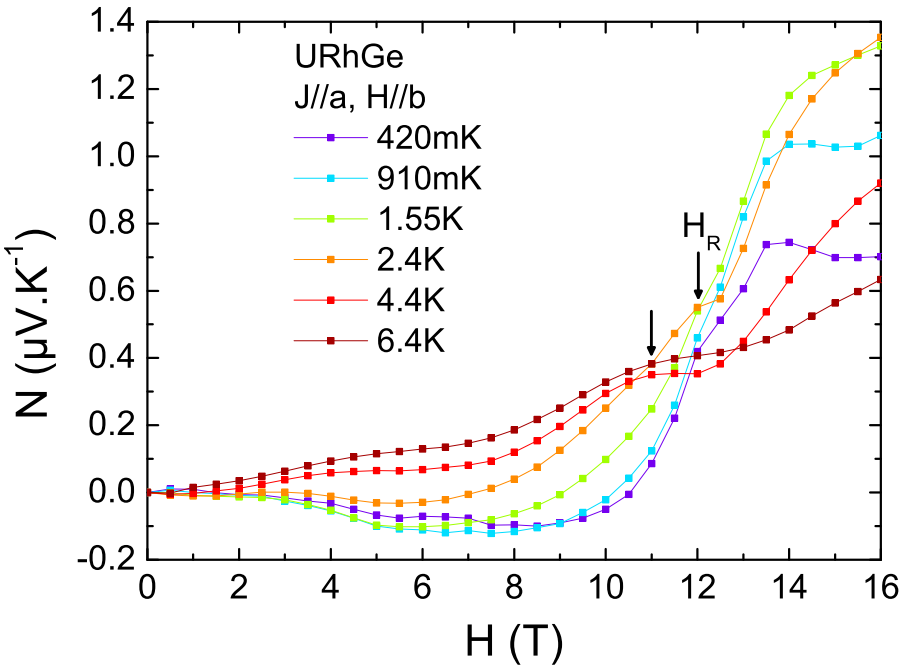

Figure 4.22: Field dependence of the Nernst effect with $J_Q \parallel a$ and $H \parallel b$ for temperatures from $T = 0.42$ K to $T = 6.4$ K.

The Nernst effect in this configuration is shown as a function of magnetic field in Fig. 4.22. The field dependence displays a very similar behavior as the one for $J_Q \parallel c$. At low temperature, the Nernst effect is negative at low field with a low value of the order of 0.1 μV.K^{-1} and then jumps to a positive value one order of magnitude larger at H_R. At higher temperature, above 2 K, the Nernst effect is always positive and shows a plateau at H_R before increasing again.

4.1.5 Comparison of the different current directions

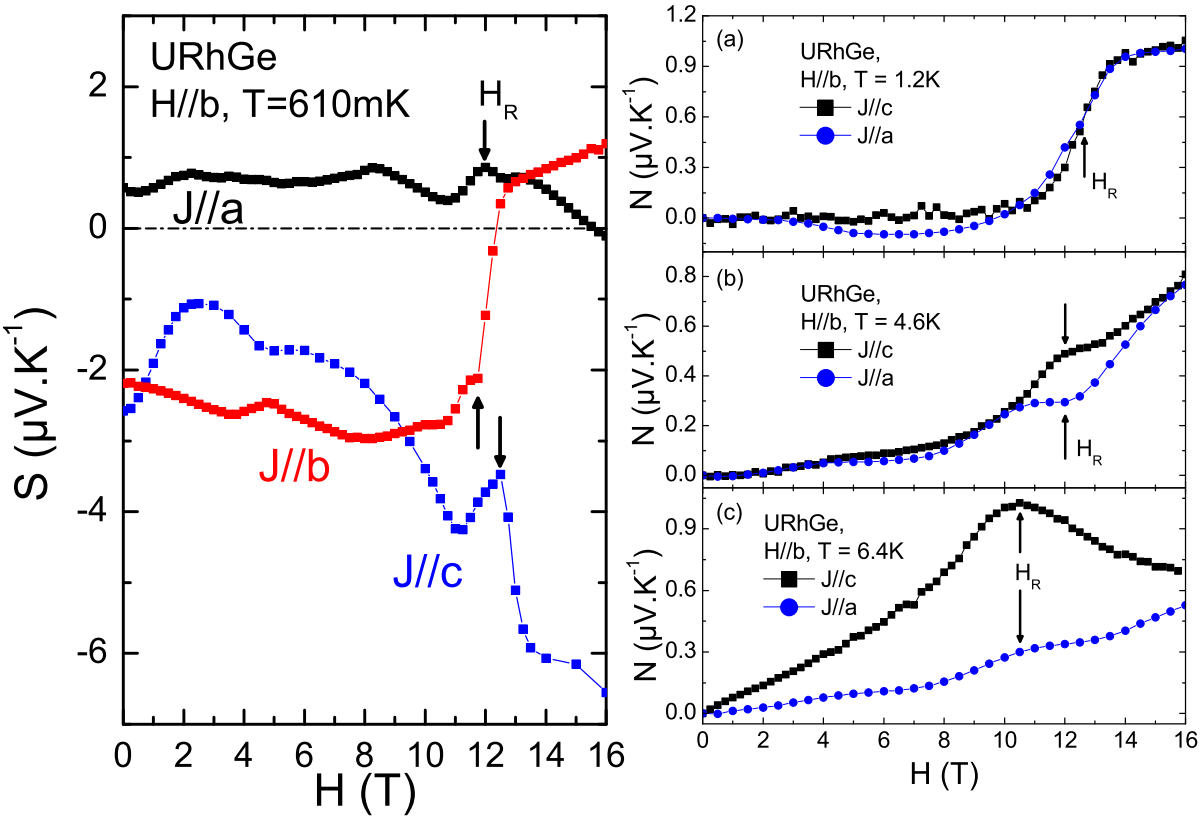

Figure 4.23: Left : Field dependence of the thermoelectric power at $T = 610$ mK for thermal current along the three crystallographic directions. Right : (a) Field dependence of the Nernst effect for thermal current along the a- and c-axis at $T = 1.2$ K, (b) $T = 4.8$ K and (c) $T = 6.4$ K.

The field dependence of the thermoelectric power for thermal current applied along the three crystallographic directions at $T = 610$ mK is shown on the left panel of Fig. 4.23. The general dependence with magnetic field is very different from one current direction to another. However, the small anomalies around $H = 2$ T and $H = 6$ T are always detected regardless of the chosen direction and maybe similar to the ones observed in UCoGe for $H \parallel c$. This suggests that these anomalies are directly related to the magnetic field polarization of the bulk material. The anomaly at $H_{split} \approx 13$ T is only detected in the configuration with $J_Q \parallel a$. $J_Q \parallel b$ is the only direction of heat current in which the

thermoelectric power abruptly changes sign at H_R at low temperature.

The comparison of the field dependence of the Nernst effect at different temperatures for $J_Q \parallel a$ and $J_Q \parallel c$ is shown on the right panel of Fig. 4.23. At $T = 1.2$ K (a), the Nernst effect has a very similar behavior. They are different between $H = 4$ T and $H = 10$ T where it is negative for $J_Q \parallel a$ and zero for $J_Q \parallel c$. They have otherwise the same value. At $T = 4.6$ K (b), the two curves deviates from each other only around the magnetic transition at H_R where the plateau does not occur at the same value of the Nernst effect for the two directions ($N = 0.3$ μV.K^{-1} for $J_Q \parallel a$ and $N = 0.5$ μV.K^{-1} for $J_Q \parallel c$) but they go again to the same value at higher magnetic field. At $T = 6.4$ K, the two curves are much more different. While the Nernst effect for $J_Q \parallel c$ shows a broad but large peak and still have a large value at $H = H_R$, the peak for $J_Q \parallel a$ seems to be dampened and the transition appears more like a plateau than a peak. It is surprising that, while the Seebeck coefficient is very sensitive to the thermal current direction at low temperature, it is not the case for the Nernst effect, at least for $J_Q \parallel a$ and $J_Q \parallel c$, which is only strongly different at much higher temperature. At this time no explanation to this phenomenon was found.

4.1.6 Fermi surface of the polarized paramagnetic state

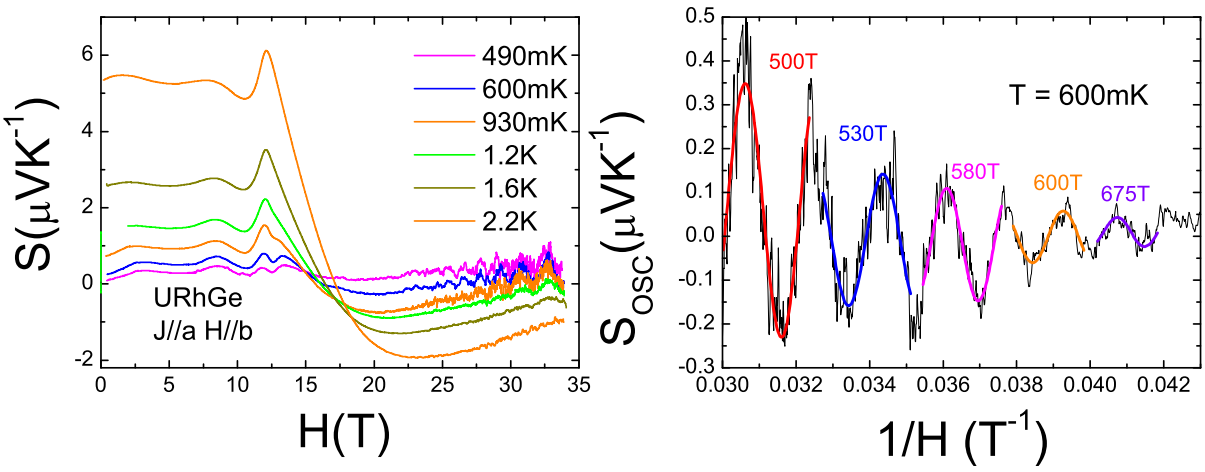

Figure 4.24: Left: Field dependence of the thermoelectric power for $J_Q \parallel a$ up to $H = 34$ T. Right: Oscillating part of the signal as a function of $1/H$ at $T = 600$ mK. Superimposed are sinusoidal fits on different inverse field intervals.

Continuous measurements of the thermoelectric power up to 34 T in a resistive magnet in LNCMI Grenoble is shown in the left panel of Fig. 4.24. The behavior observed for fields below 16 T is the same as what was measured with the superconducting magnet, with the transition peak being split at low temperature. At higher field, the thermoelectric power continues to decrease, becomes negative and then starts increasing again. Additionally, quantum oscillations can be resolved below 1.2 K and at fields higher than 22 T. The Fast Fourier Transform of the signal from 22 to 34 T gives that the oscillations originate from a single pocket with a frequency of 600 T. This frequency is close to the one observed

in Ref. [93, Yelland 2011] which disappears at the critical field corresponding to the continuation of H_R when the field is misaligned by 10° from b- to c-axis. However, there is almost a 10 T gap in the magnetic field windows used for analysis between the two measurements, making comparisons difficult. It is quite possible that it is an entirely different pocket of the Fermi surface. A closer inspection of the oscillating part of the Seebeck at $T = 600$ mK, displayed in Fig. 4.24 as a function of H^{-1}, shows that this frequency is not constant with magnetic field. Sinusoidal fits of the oscillations on different inverse field windows corresponding to one oscillation period were performed for magnetic fields from $H = 24$ T to $H = 32$ T to extract the field dependence of the frequency of the oscillations. The sinusoidal fits were performed at all temperatures on the same field intervals. The amplitude of the fits is then plotted as a function of temperature and fitted with Pantsulaya-Varlamov formula in order to extract the effective mass on each field range. Since the frequency is not constant with respect to magnetic field and the frequency is rather low, this makes Fast Fourier Transform analysis difficult to perform on small intervals and sinusoidal fits are more precise. The frequency and effective mass

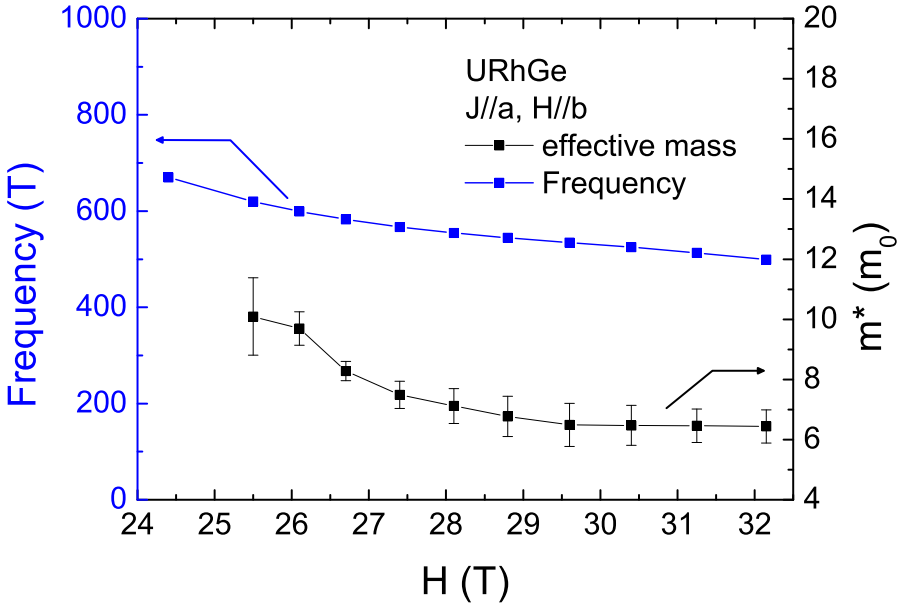

Figure 4.25: Field dependence of the frequency of the measured branch (left ordinate) and of its effective mass (right ordinate).

dependence with magnetic field are shown on Fig. 4.25. The effective mass decreases with increasing field with $m^* \approx 10\ m_0$ at 25.5 T to $m^* \approx 6\ m_0$ at 32 T. The frequency of the oscillation is also decreasing as the field is increased and goes from $F \approx 675$ T at $H = 24.5$ T to $F \approx 500$ T at $H = 32$ T. The decrease of the frequency with field suggests that there is a non-linear Zeeman effect and thus a non-linear magnetization at high field. No magnetization data exists above 16 T, and a crude linear extrapolation to the curve in Ref. [78, Hardy 2011] would give a magnetization of $M \approx 1.2\ \mu_B$/U at 34 T, which is still quite far from the expected saturation value of free uranium ion which would be closer to 3.2 μ_B. However, the reduction of the uranium moment due to crystal field effect is unknown, so no definitive conclusion can be drawn. The same frequency was also observed by Shubnikov-de Haas oscillations in magnetoresistance [104,

G. Bastien, unpublished], with a similar field dependence. The effective mass, however, shows an important discrepancy between the two measurements. While the highest mass measured in the Seebeck coefficient is of 10 m_0, the value found in Shubnikov-de Haas is 17 m_0. It is rather surprising given that the same comparison in UCoGe did not show such discrepancy on the effective mass. In both thermoelectric power and resistivity measurements, the signal to noise level was not good, so the uncertainty on the effective mass may be rather large.

4.1.7 Conclusion

In this study, we performed systematic thermoelectric power measurements with a thermal gradient applied along all three crystallographic directions and a magnetic field along the b-axis in the ferromagnetic superconductor URhGe. Additionally, we measured the temperature dependence of resistivity at various magnetic field in order to extract the n-exponent of resistivity as a function of temperature and magnetic field and measured the Nernst effect for $J_Q \parallel a$ and c.

The longitudinal configuration showed a sharp negative peak along with a change of sign in the thermoelectric power at the spin reorientation transition at $H = H_R$ at low temperature. This change of sign indicates that the Fermi surface is modified at H_R and the dominant carrier type goes from electrons ($S < 0$) in the ferromagnetic phase to holes ($S > 0$) in the polarized paramagnetic phase. However, no change of sign was detected in the two transverse configurations. At higher temperature, the transition broadens and the analysis of the width of this transition allowed us to locate the tricritical point close to $(T, H)_{TCP} = (2\text{ K}, 11.5\text{ T})$, where the transition switches from second to first order. This tricritical point is roughly located where the ferromagnetic transition field does not depend on temperature anymore.

The first order nature of the transition was further confirmed by the temperature dependence of the resistivity for magnetic fields close to H_R. For all fields, at low temperature, the system behaves like it is expected in a Fermi liquid regime, with a quadratic temperature dependence for the resistivity: $n = 2$. However, above H_R, we found that when the temperature is increased, the Fermi liquid state is broken and the n-exponent becomes less than 2. By looking for the region where $n = 5/3$, the expected temperature dependence for quantum spin fluctuations associated with a second order ferromagnetic quantum critical point, we found that this defines an energy scale, confirmed by Nernst effect measurements, that connects to H_R where the transition becomes independent of temperature. This may indicate that the observed fluctuations are coming from the tricritical point in this system. However, the resistivity shows no evidence of the presence of these fluctuations at low temperature. The magnetic fluctuations responsible for the reentrant superconductivity must therefore be of different nature, and maybe of different origin.

4.1.8 Discussion on URhGe

While a lot of interest has been dedicated to the reentrant superconductivity in URhGe, the microscopic origin of the spin reorientation at H_R, despite the very prob-

able link between the two, has still not been clarified and deserves further investigations. It has been proposed [88, Huxley 2007] that the phase diagram of URhGe should be similar to the one of UGe_2, with the presence of tricritical wings and quantum critical end points. However, the comparison with the phase diagram of UGe_2 and the theoretical phase diagram given in Ref. [26, Belitz 2005] may not be relevant because the tuning parameter is not the same. In the case of UGe_2, the ferromagnetism is suppressed by the application of hydrostatic pressure and it pushes the system toward a disordered, paramagnetic phase. In URhGe, the tuning parameter is a magnetic field applied along a hard magnetization axis, and there is no evidence that the high field, spin reoriented phase behaves like a paramagnet.

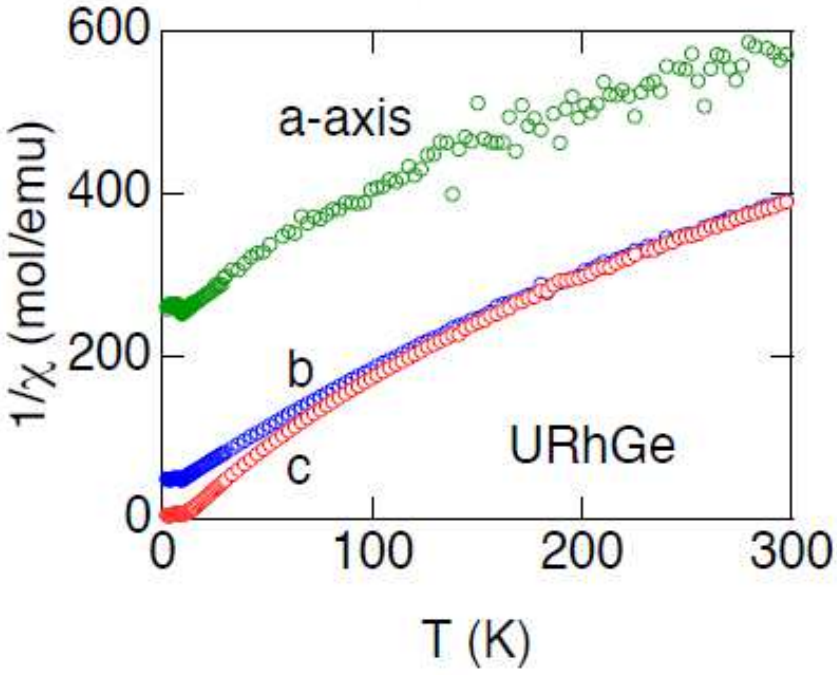

Figure 4.26: Temperature dependence of the inverse susceptibility for a magnetic field H = 1 T applied along all three crystallographic directions.

A question that was never addressed is why is there a first order spin reorientation transition when a magnetic field is applied along the b-axis and especially at a field as low as H_R = 11.75 T? Band calculations predict a weak anisotropy between the b- and c-axis and a strong one between the a- and c-axis [101, 102, Diviš 2002, Shick 2002] Precise susceptibility measurements where performed recently. The temperature dependence of the inverse of magnetic susceptibility at a field H = 1 T applied along all three crystallographic directions is shown on Fig. 4.26. The susceptibility does not follow the Curie-Weiss law in the paramagnetic state for any of the crystallographic axes. For temperatures above T = 100 K and up to room temperature, the susceptibility along the b- and c-axes have the exact same value but the one along the a-axis is much lower. This is maybe due to the crystal field effect that is established at high temperature and influences the magnetic anisotropy so that the a-axis becomes a hard magnetization axis. However, it does not seem to break appart the isotropy between the b- and c-axes.

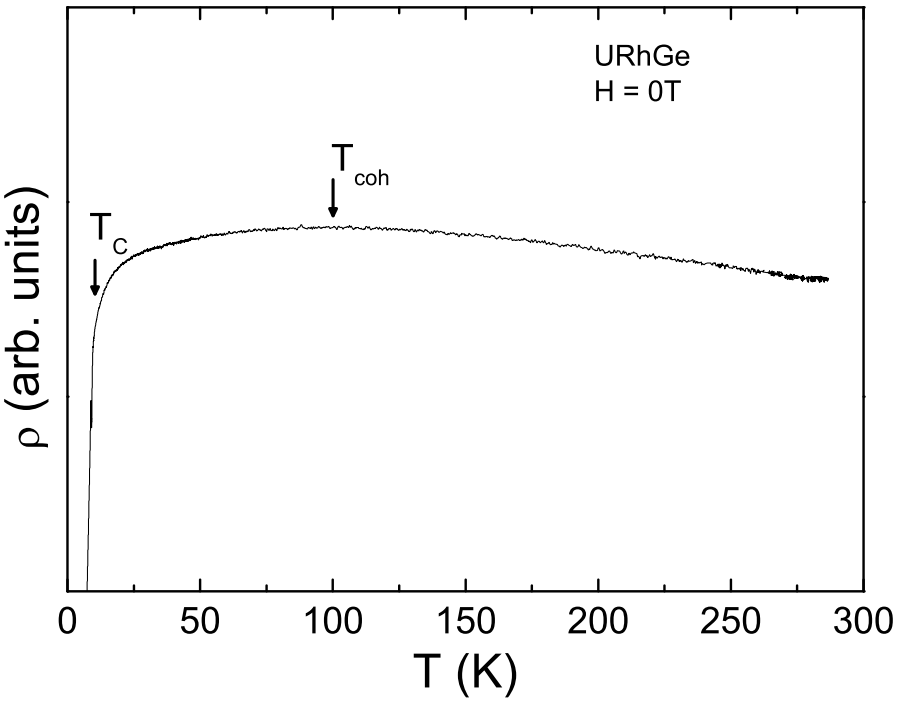

Figure 4.27: Temperature dependence of the electrical resistivity with no magnetic field applied.

The electrical resistivity as a function of temperature is shown on Fig. 4.27. A broad maximum which may correspond to the coherence temperature, where the Fermi surface starts to be established, is observed at $T_{coh} \approx 100$ K. Since in URhGe the ferromagnetism is itinerant, the anisotropy of the exchange interaction will be directly linked to the anisotropy of the Fermi surface, and it is possible that the separation between the susceptibility between the b- and c-axes below $T = 100$ K comes from this exchange interaction. It is notable that the anisotropy induced by the Fermi surface is rather weak compared to the one induced by crystal field effect since even at $T \gtrsim T_C$, the difference in susceptibility between the b- and c-axes is small and with the a-axis it is very large. We have seen that, in URhGe, the Fermi surface is rather unstable with the application of magnetic field. This means that the anisotropy of the exchange interaction can be easily changed between the b- and c-axes with a rather low magnetic field, in this case for $H_R = 11.75$ T, switching the easy magnetization axis. A change in the topology of the Fermi surface before or at the transition could explain a sudden change in the magnetic anisotropy, inducing the metamagnetic-like transition in URhGe.

An interesting measure that could be done would be the temperature dependence of the magnetic susceptibility along the b- and c-axes with a magnetic field $H > H_R$ applied along the b-axis to observe how the two compare at high temperature. It would also be interesting to force the crystal field effect to "choose" between the b- and c-axes by the application of uniaxial pressure, for example. One can imagine that if the crystal field effect can be modified enough to favor the b-axis, given the weak anisotropy induced by the Fermi surface, it may be possible to change the ground state at low temperature, or at least reduce H_R. This may also increase the reentrant superconductiviting maximum temperature, since the magnetic field needed to induce it would be lower. Although it

would most probably be difficult to perform, the growth of URhGe in the form of thin films may be interesting. Indeed, the reduction of dimensionality adds another anisotropy in the system, called "shape anisotropy", which can favor one axis with respect to the others.

4.2 UPd_2Al_3

In this section, we have studied the magnetic polarization in the antiferromagnetic superconductor UPd_2Al_3 by means of thermoelectric power and de Haas-van Alphen measurements for a magnetic field applied in the basal plane. We report the presence and the angular dependence of a new branch in the antiferromagnetic state, as well as the observation in the thermoelectric power of a Fermi surface reconstruction at the metamagnetic transition through the observation of quantum oscillations in the polarized paramagnetic state. The Fermi surface of UPd_2Al_3 being better known, both theoretically and experimentally, the study of the metamagnetic transition may help understand how the magnetic polarization of the Fermi surface induced by magnetic field interplays with the antiferromagnetic properties of the system and maybe generalize to ferromagnetic systems, such as URhGe.

4.2.1 State of the art

Discovered in 1991, UPd_2Al_3 shows coexistence of antiferromagnetism and superconductivity [105, Geibel 1991]. At that time it had attracted attention because of his high superconducting temperature of 2 K, one of the highest in heavy fermion superconductors. The antiferromagnetic order develops below a Néel temperature $T_N = 14$ K. Its Sommerfeld coefficient, extrapolated at $T = 0$ K, $\gamma = 150$ mJ.mol^{-1}.K^{-2} indicates that it belongs to the heavy fermion family with moderately enhanced effective masses. It crystallizes in the hexagonal $PrNi_2Al_3$ strucure (space group P6/mmm) as shown on Fig. 4.28. The magnetic moments are ordered ferromagnetically in the plane orthogonal to the c-axis with a sublattice magnetization of $M_0 = 0.85\ \mu_B$/U [106, 107, Krimmel 1992, Geibel 1991] and the antiferromagnetic ordering is along the c-axis with a vector k = [0,0,1/2].

In this compound, neutron experiments [108, Blackburn 2006] and angle resolved photoemission spectroscopy [109, Fujimori 2010] showed that the magnetism is mostly of itinerant nature, indicating that the Fermi surface and its topology should play an important role in the magnetic properties. The antiferromagnetic order can be suppressed by applying magnetic field in the basal plane (orthogonal to the c-axis) through a metamagnetic transition. Resistivity [110, 111, de Visser 1993, 1994] and magnetization [112, de Visser 1992] both show evidence of a metamagnetic transition at 17.8 T and 18.4 T for field along the b- and a-axes, respectively. Magnetization at very low temperature shows a clear hysteresis at H_M for $H \parallel b$, confirming that the magnetic transition is of first order [113, 114, Sakon 2001, 2002]. When the field is rotated in the ac plane, the magnetic transition is shifted to higher field with a $1/\cos(\theta)$ law. With the magnetic field along the c-axis, no magnetic transition is observed up to 50 T [115, Oda 1994]. The

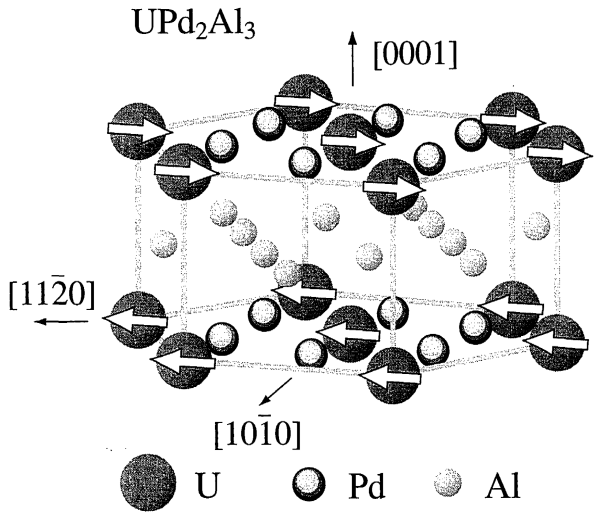

Figure 4.28: Crystal structure of UPd_2Al_3.

magnetic field-temperature phase diagram shown on Fig. 4.29, taken from Ref. [114, Sakon 2002], displays the evolution of the antiferromagnetic order and the superconductivity for a magnetic field applied along the a-axis, drawn by resistivity and magnetization measurements. It shows that the transition at the Néel temperature is second order up to $H = 17$ T at the point labeled A in the phase diagram. At higher field, the transition becomes first order and the Néel temperature quickly drops to $T = 0$ K. It also shows a crossover at temperatures above T_N between the paramagnetic and the polarized phase.

Since the magnetism in this compound is at least partially itinerant, the knowledge of the topology of the Fermi surface is very important to understand the magnetic properties of UPd_2Al_3. Many studies of quantum oscillations have been performed over the years, almost all of them in the antiferromagnetic phase, each adding new branches and their angular dependence to the known Fermi surface. It is well summarized in Ref. [116, Inada 1999]. Many band calculations have been performed in the paramagnetic and antiferromagnetic phase and account remarkably well for the frequencies observed in de Haas-van Alphen experiments [118, 116, 117, 119, 120, Knöpfle 1996, Inada 1999, Sandratskii 1994, Zwicknagl 2003]. In UPd_2Al_3, the band calculations are much easier compared to UCoGe or URhGe, due to the fact that the uranium sites are all equivalent and the hexagonal structure is highly symmetric, contrary to URhGe or UCoGe which have two non-equivalent uranium sites and orthorhombic structure.

The measured branches from Ref. [116, Inada 1999] as well as the calculated frequencies and their angular dependence is shown in the left panel of fig 4.30. Although the values of the frequencies show some discrepancies between the measurements and the calculations, the angular dependences are in good agreement. The shape of the calculated Fermi surface inside the Brillouin zone in the same reference is shown on the right panel of Fig. 4.30. It mainly consists of one cylinder along the c-axis centered at the Γ-point, as well as a "party hat" shape, also connected along the c-axis but situated on the border of the Brillouin zone. Other smaller pockets exist, ellipsoids elongated along the c-axis and centered at H-point and an egg-like surface according to Ref. [118, Knöpfle 1996], almost spherical in Ref. [116, Inada 1999] at the Γ point or elipsoidal in Ref. [119, Zwicknagl

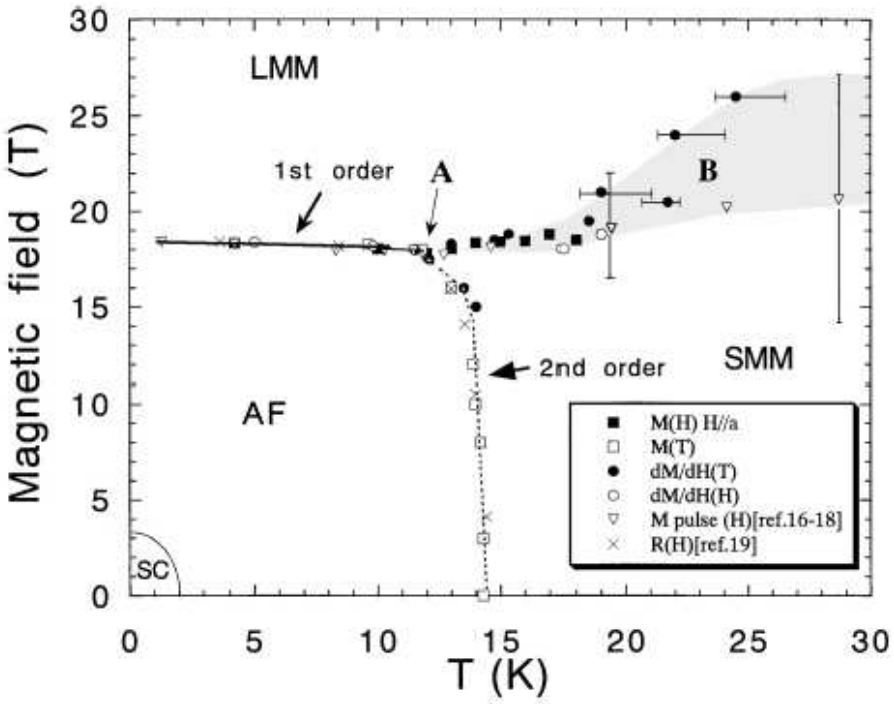

Figure 4.29: Temperature-magnetic field phase diagram of UPd_2Al_3 for a field applied in the basal plane, taken from Ref. [114, Sakon 2002].

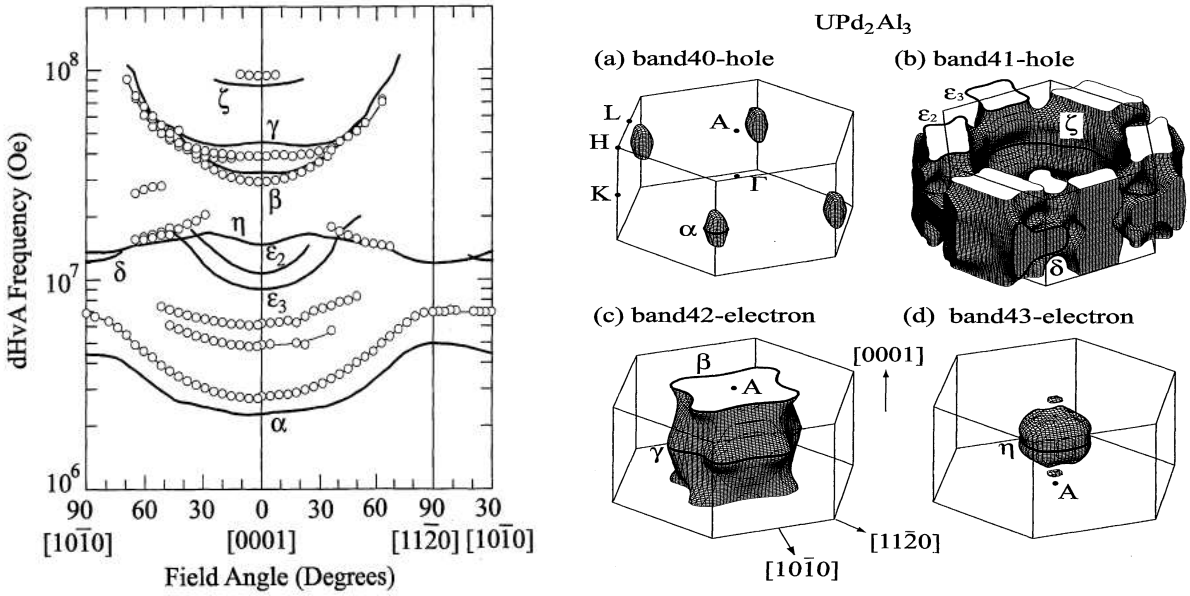

Figure 4.30: Left: angular dependence of the measured (open circles) and calculated (solid lines) de Haas-van Alphen frequencies. Right: Representation of the Fermi surface inside the first Brillouin zone. Taken from Ref. [116, Inada 1999].

2003] at the H-point. In Ref. [118, Knöpfle 1996], the cylinder, party hat and egg-like surfaces have been found to have the most 5f character. The ellipsoids a the H-point, on the other hand, are highly hybridized. The hybridized pockets are usually the most difficult to calculate properly and their shape depends strongly on the calculation method used, as well as small variations in the calculation parameters. It is then interesting to note that the main difference between the different calcutations comes from the closed surface at the Γ point. In Ref. [120, Zwicknagl 2003], calculation was performed in the antiferromagnetic phase. The antiferromagnetic wave vector k = [0,0,1/2] reduces the symmetry of the crystal structure and the unit cell is doubled along the c-axis. This causes a folding of the Brillouin zone, which is halved in the same c direction. Due to this, the "party hat" has become a large ring on the edges of the Brillouin zones, connected to the other zones, although a small variation in the Fermi energy can change its shape greatly going from the open ring to a closed ellipsoidal surface with a change of only 3 meV (40 K). It is not so surprising since the ζ branch attributed to this orbit was found to have a very large effective mass of $m^* = 65\ m_0$.

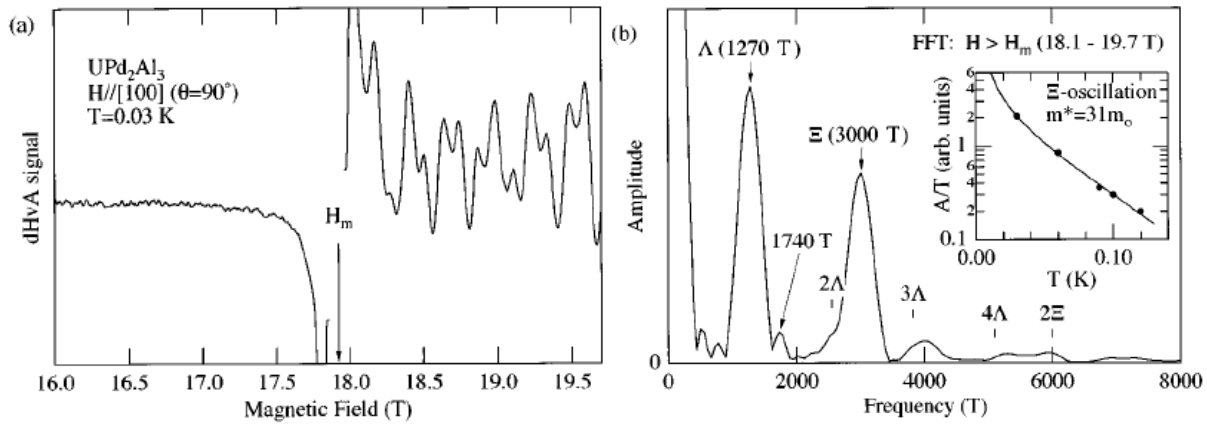

Figure 4.31: (a) Magnetic field dependence of the de Haas-van Alphen signal for a field along the a-axis. (b) Fast Fourier Transform spectrum of the oscillating signal for $H > H_M$ (18.1 T - 19.7 T). Taken from Ref. [122, Terashima 1997].

Only one quantum oscillations measurement was performed through and above H_M = 18 T with the magnetic field along the a-axis [122, Terashima 1997]. The de Haas-van Alphen signal at T = 30 mK as a function of magnetic field applied along the a-axis is shown on Fig. 4.31 (a). It shows a sharp anomaly at H_M and large quantum oscillations are detected above. The Fast Fourier Transform of the oscillating signal for magnetic field from H = 18.1 T to H = 19.7 T is shown on Fig. 4.31 (b). It shows two frequencies, one called Λ at 1270 T and another called Ξ at 3000 T. The amplitude of the Ξ branch is plotted as a function of temperature in inset along with a Lifshitz-Kosevich fit, which gives a high effective mass of 31 m_0. The effective mass of the Λ branch is 5.4 m_0. The

presence of this second branch above H_M indicates that the heavy fermion state still exists after the metamagnetic transition, when the antiferromagnetic order is suppressed. The angular dependence of these two branches when the field is rotated toward the c-axis shows that the Λ branch's frequency only increases slowly with angle, indicating that it may be almost spherical or an ellipsoid slightly elongated along the a-axis. On the other hand, the Ξ branch shows a rather strong angular dependence and increases quickly as the field is rotated to the c-axis, this indicates that this branch of the Fermi surface is probably an ellipsoid largely elongated along the a-axis. It is interesting to note that while the Fermi surface of the paramagnetic and the antiferromagnetic states is strongly anisotropic and oriented along the c-axis with cylinders and ellipsoids, it would seem that above H_M, the anisotropy of the Fermi surface is different, with at least two branches that are more oriented along the a-axis. However, a more complete angular dependence in the a-c plane for fields above H_M would be required to see if the Fermi sheets connected along the c-axis such as the β and γ branches detected in Ref. [116, Inada 1999] still exist in the polarized phase or not.

This raises up the question of the relation between the Fermi surface topology and the magnetism in UPd_2Al_3. It is still not clear whether the Fermi surface topology changes as a result of the collapse of the antiferromagnetic order or if a topology modification is at the origin of this collapse. Therefore, we wanted to observe quantum oscillations through H_M by means of thermoelectric power measurements. Additionally, we performed de Haas-van Alphen measurements inside the antiferromagnetic state with a magnetic field applied in the basal plane where only one branch has been detected and, as we will see later, we failed to observe quantum oscillations in the thermoelectric power in this phase.

4.2.2 Results in the antiferromagnetic phase

de Haas-van Alphen experiment was done on a high quality single crystal of UPd_2Al_3 (RRR $>$ 100) down to 30 mK and up to 15 T. This study was performed with the magnetic field rotated from the a-axis to [110] which will be referred later with the Bravais-Miller indices as $[10\bar{1}0]$ and $[11\bar{2}0]$, respectively. Since for these magnetic field directions the metamagnetic transition occurs at least at 17.8 T, this measurement was done only in the antiferromagnetic phase of UPd_2Al_3. The second harmonic of the susceptibility was measured using the setup depicted in chapter 2.4.

The field dependence of the second harmonic of susceptibility at $T = 30$ mK and from $H = 2$ to 15 T is shown in the left panel of Fig. 4.32 for magnetic field along $[11\bar{2}0]$. Superconductivity disappears at $H_{C_2} = 3.4$ T, which is taken to be where the curve deviates from the straight line at high field. Quantum oscillations can be resolved between 5 and 12 T as shown on the right panel of Fig. 4.32, which is a zoom on this part of the curve. Above 12 T, the oscillations cannot be observed anymore. This is due to the modulation method we used to measure the second harmonic of the signal, which is described in chapter 2.4.

The Fast Fourier Transform of the signal for magnetic field along $[11\bar{2}0]$ shown in the left panel of Fig. 4.33 (a) shows a sharp peak at 690 T. This frequency corresponds to that of the α branch of Ref. [116, Inada 1999]. As previously reported, the frequency does not change when the field is rotated up to $\theta = 30^\circ$ which corresponds to the $[10\bar{1}0]$ axis. Rotating the field gives rise to the possibility of observing another pocket of the Fermi

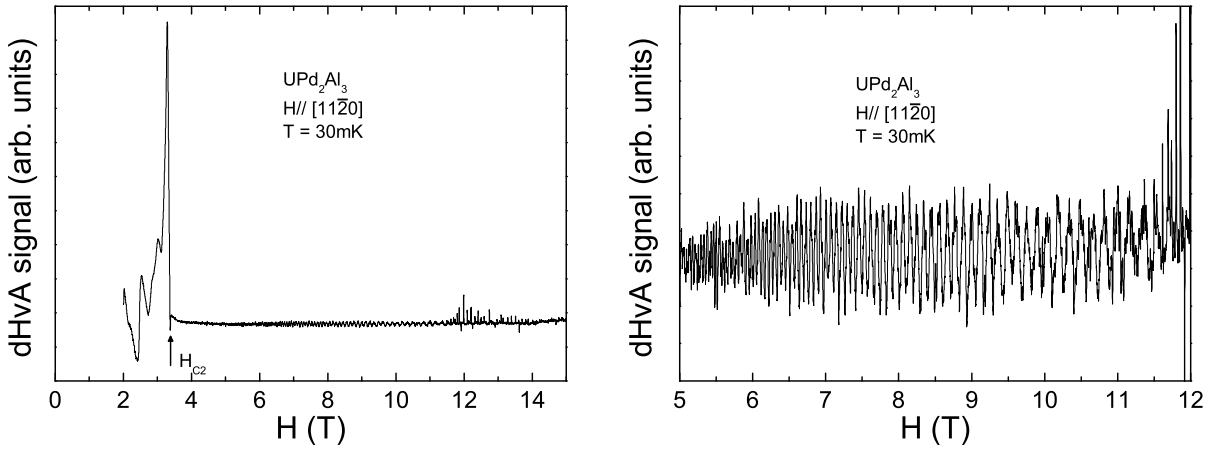

Figure 4.32: Left: Field dependence of the second harmonic of the susceptibility, measured by the modulation method for H from 2 T to 15 T at $T = 30$ mK. Right: Oscillating part of the signal from 5 T to 12 T.

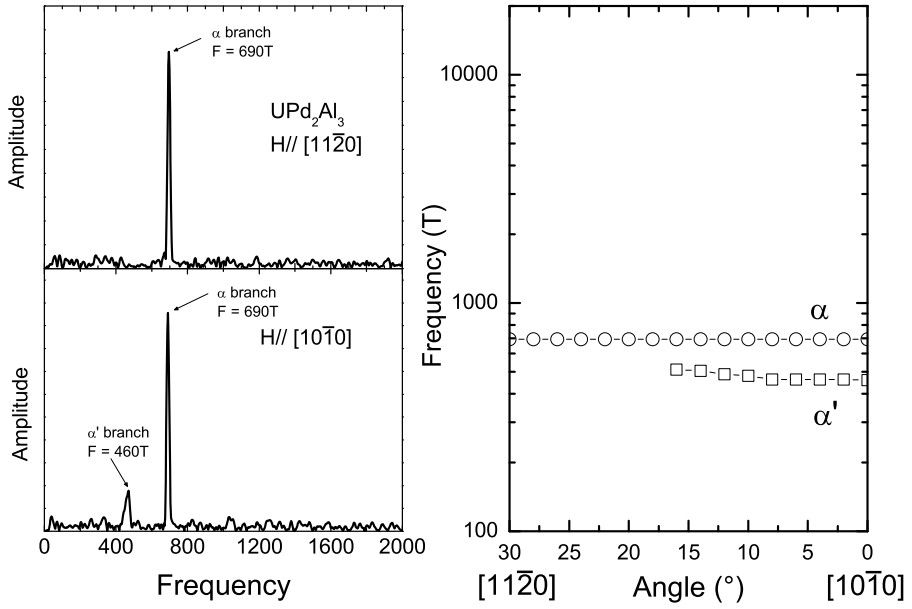

Figure 4.33: Left: Fast Fourier Transform of the oscillating signal of a magnetic field along (a) [11$\bar{2}$0] and (b) [10$\bar{1}$0]. Right: Angular dependence of the two observed branches α (open circles) and α' (open squares) in the basal plane.

surface, as shown on the left panel of Fig. 4.33 (b), with a frequency of 460 T, labeled α' for the magnetic field along the [10$\bar{1}$0] direction. The angular dependence in the basal plane of these two branches is shown on the right panel of Fig. 4.33. The α' branch appears at an angle of $\theta = 14^{\circ}$ with a frequency of 510 T which is decreasing slightly as the field is rotated, reaching 460 T for the field along [10$\bar{1}$0].

The effective masses were extracted for both frequencies, using Lifshitz-Kosevitch fitting, for field along [10$\bar{1}$0] and at 10° from [10$\bar{1}$0] to [11$\bar{2}$0]. The effective mass of the α branch at [11$\bar{2}$0] was previously reported to be of 13 m_0 [121, Haga 2000]. The tempera-

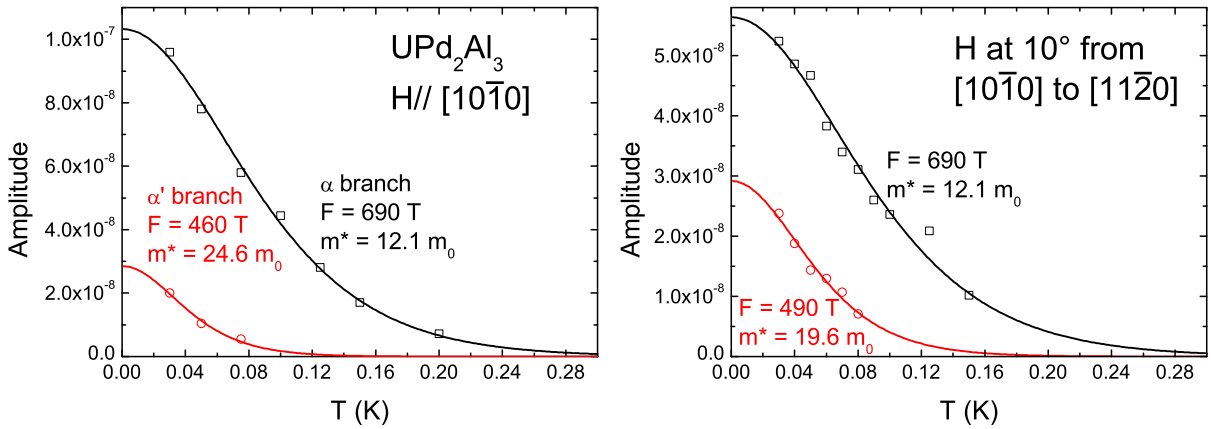

Figure 4.34: Lifshitz-Kosevich fits and effective mass of the α and α' branches for $H \parallel [10\bar{1}0]$ (left) and H at 10° from $[10\bar{1}0]$ to $[11\bar{2}0]$ (right).

ture dependence of the amplitudes of both frequencies as well as the fits are shown on the left panel for $H \parallel [10\bar{1}0]$ and on the right panel for H at 10° from $[10\bar{1}0]$ of Fig. 4.34. For the α branch, just like the frequency, the effective mass doesn't vary much with angle, being of 12.1 m_0 at $[10\bar{1}0]$ and 11.8 m_0 at 10°. This is in accordance with the value found in Ref. [121, Haga 2000]. The α' branch, on the other hand, has a very angle dependent effective mass. It decreases from 24.6 m_0 $[10\bar{1}0]$ to 19.6 m_0 at 10°.

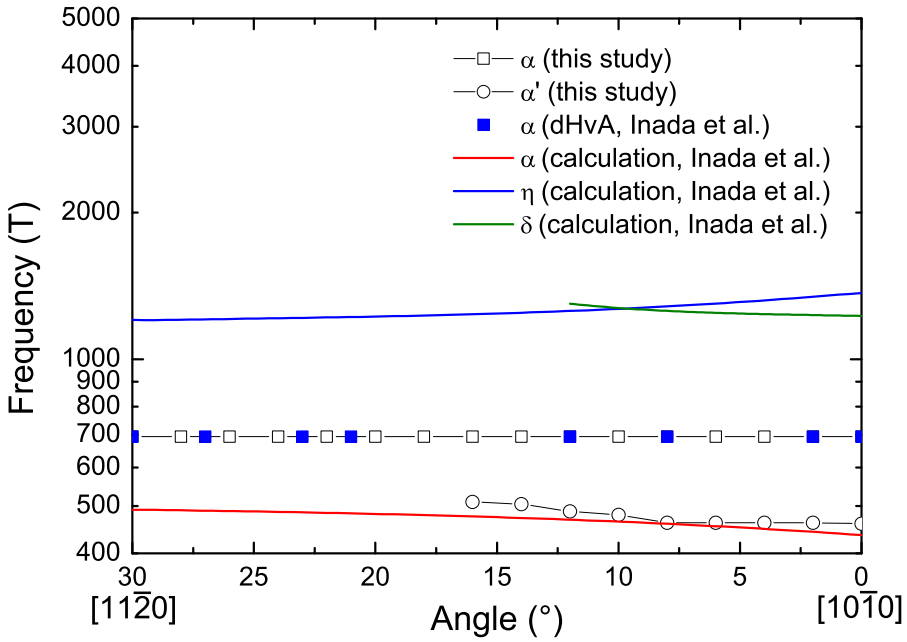

Figure 4.35: Angular dependence of the frequency of the α (black open squares) and α' (black open circles) branches. Superimposed is the dHvA results of α (blue full squares) and the calculated α (solid red line), η (solid pink line) and δ (solid green line) branches, taken from Ref. [116, Inada 1999].

A comparison between the results of this study and the de Haas-van Alphen experiment

and calculations of Ref. [116, Inada 1999] in the same angular dependence is shown on Fig. 4.35. While the experimental α branches of the two studies match perfectly, it is interesting to note that the α' branch matches almost perfectly the calculated α branch. The angular dependence could also correspond to the calculated δ branch and it would explain why it disappears in angle before reaching [11$\bar{2}$0]. However the predicted frequency is much higher than the one observed, making the match unlikely. The η branch is also supposed to exist in this direction but the frequency and angular dependence do not match what is observed in this study. However, in Ref. [118, Knöpfle 1996], the η branch in the [10$\bar{1}$0] direction is situated at a frequency just below the one of the α branch, and may correspond to what is observed. Unfortunately, the calculation does not agree with the observed angular dependence from [10$\bar{1}$0] to [11$\bar{2}$0], and in this study the magnetic field was not rotated toward the c-axis, [0001], so the angular dependence of the α' frequency in this direction remains unknown. It is then hard to draw definitive conclusions.

4.2.3 Metamagnetic transition and Fermi surface of the polarized paramagnetic state

The thermoelectric power was measured on a high quality single crystal of UPd_2Al_3 (RRR $>$ 100) taken from the same batch as the one used in the de Haas-van Alphen experiment. Thermal current was applied along the [11$\bar{2}$0] direction and the magnetic field along the [10$\bar{1}$0] direction. The measurements were carried out down to a temperature of 400 mK and magnetic field up to 29 T.

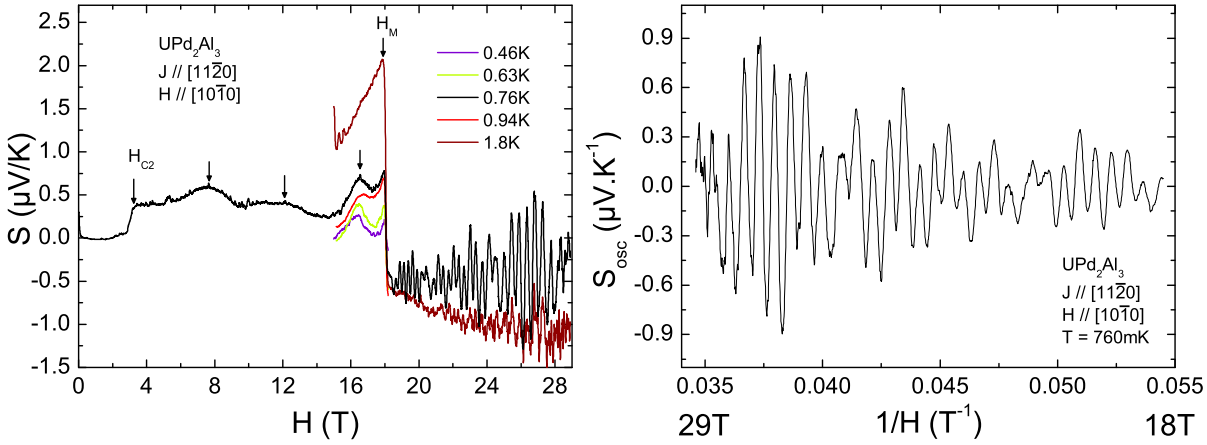

Figure 4.36: Left : Field dependence of the thermoelectric power up to $H = 29$ T along the [11$\bar{2}$0] direction and temperatures from $T = 0.46$ K to $T = 1.6$ K. Thermal current is applied along [10$\bar{1}$0]. Right : Oscillating part of the signal at $T = 760$ mK as a function of inverse magnetic field from $H = 18$ T to $H = 29$ T.

The field dependence for temperatures from 0.46 to 1.8 K is shown on the left panel of Fig. 4.36. At $T = 760$ mK, the Seebeck coefficient in the superconducting phase is zero up to $H_{C_2} = 3.2$ T where it jumps to a low positive value of 0.4 μV.K^{-1}. It then shows several small anomalies around $H = 7.6$, 12 and 16.5 T. At $H_M = 17.9$ T, it displays a very sharp drop to a negative value consistent with the first order metamagnetic phase

transition. Large quantum oscillations appear just above the metamagnetic transition and are visible up to 29 T. The oscillations are still observable at $T = 1.8$ K. Like in URhGe for $J_Q \parallel a$ and $H \parallel b$, the magnetic transition appears as one large peak at high temperature which then splits into two smaller peaks at low temperature, suggesting that the Fermi surface may be modified before H_M. The sharp change of sign of the Seebeck coefficient at the transition suggests that the Fermi surface is modified through the transition. In antiferromagnetic materials, one has to take into account the folding of the Fermi surface. If the antiferromagnetic wave vector is smaller in the k-space than the first Brillouin zone, then the symmetry of the unit cell will be reduced accordingly. In that regards, UPd_2Al_3 constitutes a rather simple example. The antiferromagnetic wave vector is $k = [0,0,1/2]$, meaning that the unit cell of the paramagnetic state is no longer the smallest representation containing all the symmetries of the structure, and one has to double the unit cell of the paramagnetic state in order to get the one of the antiferromagnetic state. Since the unit cell has been doubled in the real space along the c-axis, therefore the first Brillouin zone will be halved along the k_z direction. This effect, called Fermi surface folding, can cause drastic change on the Fermi surface going from the paramagnetic to the antiferromagnetic state. Therefore, in UPd_2Al_3, it would not be unexpected that the Fermi surface changes at the metamagnetic transition. However, it was shown that this folding affects only the "party hat" surface that could be restored at H_M [120, Zwicknagl 2003]. No oscillations were observed in the thermoelectric power below H_M. The oscillating part of the Seebeck at $T = 760$ mK for field from above H_M is shown on Fig. 4.36 (b). It is clear from the shape of the signal that more than one frequency is detected. Since the oscillations appear only above H_M and given their large amplitude already at $H = 18$ T, it is possible that these do not exist in the antiferromagnetic phase. The Fast

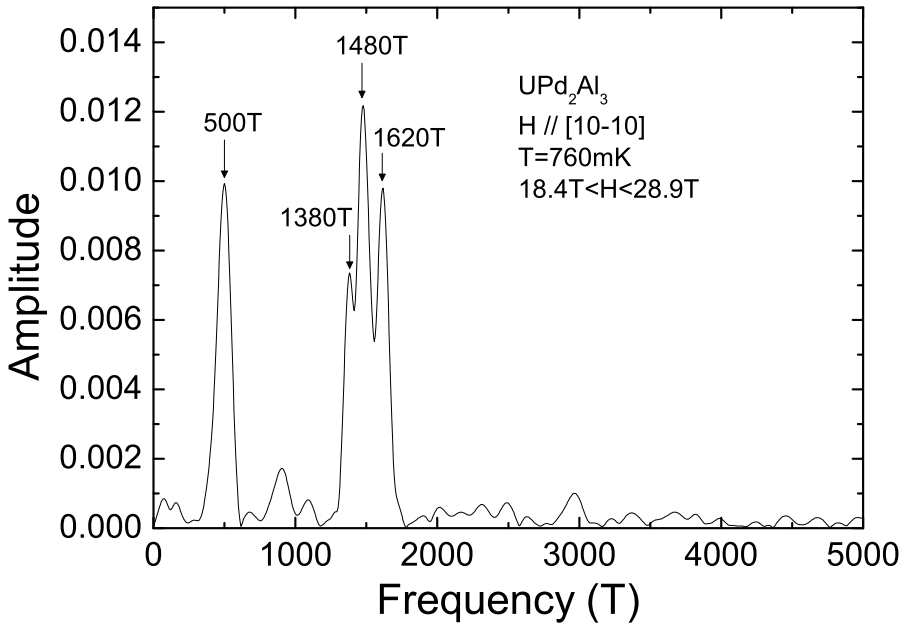

Figure 4.37: Fast Fourier Transform spectrum of the oscillating signal at $T = 760$ mK.

Fourier Transform of the oscillating signal at $T = 760$ mK on the field range [18-29T] is shown in Fig. 4.37. Several frequencies are observed. One around 500 T and three

being very close to each other at 1380, 1480 and 1620 T which will be labeled as μ, ν, π and ω, respectively. Neither the Ξ nor the Λ branches of Ref. [122, Terashima 1997] are detected here. The effective masses of the ν, π and ω branches observed were extracted by fitting the amplitude of the Fast Fourier Transform peaks with the Pantsulaya-Varlamov formula and the fits are shown on the left panel of Fig. 4.38 (a), (b) and (c), respectively. All of these pockets of the Fermi surface have low effective masses : $m^*(\nu) = 4.6\ m_0$, $m^*(\pi) = 4.7\ m_0$ and $m^*(\omega) = 4.7\ m_0$. Considering that previously reported de Haas-van Alphen measurements as well as the ones shown in the previous section detected effective masses higher than 10 m_0, it is unlikely that these branches would have been missed in the antiferromagnetic phase. It is a possibility that these branches have much higher effective mass below H_M, making their detection difficult and would explain why they were never detected. Also their frequencies would maybe fit those predicted for the δ and η branches in Ref. [116, Inada 1999] although there would still be one frequency whose presence could not be explained. It is however not obvious why their effective mass would suddenly drop at the transition, seeing that de Haas-van Alphen oscillations in Ref. [122, Terashima 1997] detect a branch with a large effective mass of 31 m_0, thus ruling out the suppression of the heavy fermion state at the transition. Another explanation would be that these pockets of the Fermi surface appear only when the antiferromagnetic order is suppressed, where the Fermi surface would be reconstructed.

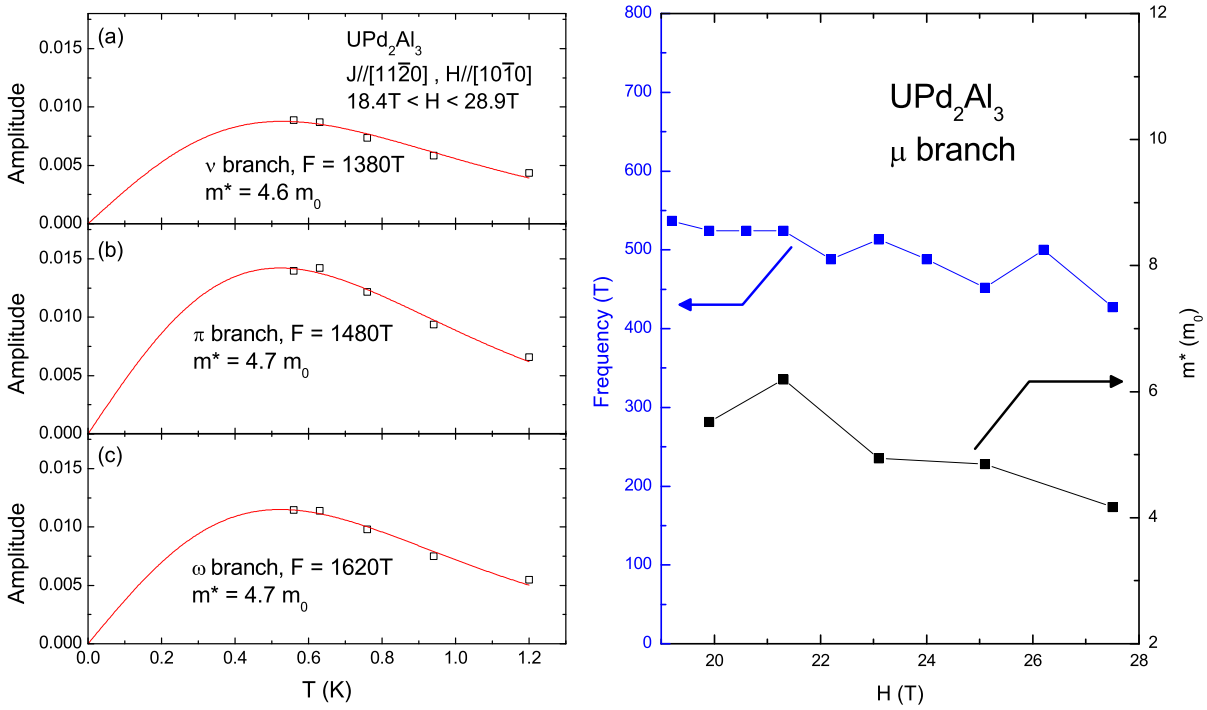

Figure 4.38: Left : Pantsulaya-Varlamov fits of the temperature dependence of the amplitude of the oscillations for the ν (a), π (b) and ω (c) branches. Right : Field dependence of the frequency (left ordinate) and the effective mass (right ordinate) of the μ branch.

The three branches ν, π and ω are very close to each other in frequency and even in the largest magnetic field window we can take their peak are not well separated in the Fast Fourier Transform. This makes it impossible to establish a field dependence of

their frequency or their effective mass. However, since the peak of the μ branch is well separated to the other, we could study the field dependence of the frequency as well as the effective mass, which is shown in the right panel of Fig. 4.38. It was done by performing Fast Fourier Transforms analysis on field ranges of 0.007 T^{-1} from 18 to 29 T shows that the frequency is not constant with magnetic field, going from $F = 540$ T at $H = 19.2$ T to $F = 430$ T at $H = 27.5$ T. If we assume that this pocket is of down-spin, this field dependence indicates the Zeeman effect, is saturating, making the observed frequency decrease compared to the true frequency or that the pocket itself is growing, giving the same result for the observed frequency if the Zeeman effect is assumed to be linear. The former possibility is however unlikely, given that no saturation in the magnetization was found up to 50 T according to Ref. [115, Oda 1994]. The effective mass is also decreasing with field, going from $m^* \approx 6\ m_0$ at $H = 19.2$ T to $m^* \approx 4.5\ m_0$ at $H = 27.5$ T. It is possible that this branch is related to either the α or α' branches that exists in the antiferromagnetic state. However the effective masses are much higher below H_M than above, making the connection difficult.

This study was done with the same magnetic field orientation as in Ref. [122, Terashima 1997]. However, as mentioned before, in this study, neither the Λ nor the Ξ branches were observed above H_M. Additionally, none of the four branches that were observed in thermoelectric power were observed in Ref. [122, Terashima 1997], which is unexpected considering that the effective masses of these branches are quite low, compared to the Ξ branch. The discrepancy between the observed frequencies above the metamagnetic transition cannot be explained. Measurements of the full angle dependence above H_M would be needed.

4.2.4 Conclusion

We have performed de Haas-van Alphen measurements in the antiferromagnetic phase, rotating the magnetic field in the basal plane from $[10\bar{1}0]$ to $[11\bar{2}0]$ and measured the thermoelectric power across the metamagnetic transition with the magnetic field applied along the $[10\bar{1}0]$ direction. In the antiferromagnetic state, quantum oscillations were detected in the de Haas-van Alphen experiment. The previously reported α branch was observed, as well as another one, labeled α', with a lower frequency but a higher effective mass. The thermoelectric power did not show any quantum oscillations in the antiferromagnetic state, most probably due to the fact that in this phase the measured effective masses are high and the lowest temperature we can achieve with the setup we used ($T \approx 500$ mK) was too high. However, the metamagnetic transition at $H_M = 18$ T was observed, as well as quantum oscillations in the polarized paramagnetic state. The single peak at H_M at high temperature splits into two peaks at low temperature like for URhGe with $J_Q \parallel a$, indicating that the Fermi surface may undergo a modification before the transition and there is a sharp change of sign at H_M, like that observed in URhGe with $J_Q \parallel b$. Additionally, the quantum oscillations observed in the polarized paramagnetic state show the presence of four branches (μ, ν, π and ω) that are not observed below H_M, in the antiferromagnetic phase. All these branches have low effective masses $m^* \leq 5\ m_0$. Therefore it is unlikely that they exist below H_M as they were not observed in de Haas-van Alphen experiments.

These results point to a Fermi surface reconstruction at H_M. Whether it is a result of

the unfolding of Fermi surface due to the increase of the Brillouin zone or a more profound modification of the topology of the Fermi surface is not clear. A more complete angular dependence than the one in Ref. [122, Terashima 1997] would be interesting, in order to investigate the topology of the Fermi surface in the polarized paramagnetic state and compare it with the one of the antiferromagnetic state as well as the one from the zero field paramagnetic state. Field dependent band calculations below and above H_M would also shed some light on the role of the Fermi surface in the metamagnetic transition and allow for comparison with experiments and maybe distinguish if a modification of the Fermi surface occurs before the metamagnetic transition. Specific heat measurements around H_M suggest that the Sommerfeld coefficient may be enhanced around this field [123, Kim 2001], like it is the case in URhGe. However, it would be necessary to measure down to lower temperature in order to properly extrapolate the Sommerfeld coefficient and observe to what extent it is enhanced at this transition.

Conclusion

In this thesis, several heavy fermion systems have been studied by transport measurements (Seebeck and Nernst effects, resistivity) and by thermodynamic measurements (de Haas-van Alphen effect). These studies were carried out in low temperature ($T < 100$ mK) and high magnetic field ($H > 30$ T).

In UCoGe, anomalies are observed in the field dependence of thermoelectric power, resistivity and Hall effect when the magnetic field is applied along the easy magnetization c-axis, and quantum oscillations are resolved. The analysis of the field evolution of these branches of the Fermi surface reveals that they appear and disappear at the same fields where the anomalies are detected. This is evidence that the magnetic field can modify the topology of the Fermi surface and that at least some of these anomalies are of Lifshitz nature. The measurement of the field dependence of specific heat in this direction would be interesting to observe its behavior at these Lifshitz transitions.

Two anomalies are detected in the thermoelectric power at $H_{M_1} = 28$ T and $H_{M_2} = 32$ T in $CeIrIn_5$ when the magnetic field is applied along the c-axis. While no quantum oscillations can be seen in the Seebeck coefficient, the torque magnetometry detects the presence of some branches of the Fermi surface and the analysis of the Fast Fourier Transforms of the signal performed below and above H_M shows that a branch has appeared and another one has disappeared at H_M, indicating that this is, like in UCoGe, a Lifshitz transition. The comparison with the calculated Fermi surface leads to a probable neck breaking in one of the Fermi sheets.

The study of URhGe shows that the thermoelectric power can easily detect the spin-reorientation transition at $H_R = 11.75$ T when the magnetic field is applied along the b-axis. The longitudinal configuration shows that the Fermi surface is reconstructed at this transition and the location of the tricritical point, separating the second order from the first order transition line, can be extracted. Resistivity measurements show that the temperature dependence follows the Fermi liquid law at all fields at low temperature. This confirms that the transition is first order at low temperature and that there is no quantum critical point occurring at the transition. The measurements in the two transverse configurations show an anomaly at H_R. Interestingly, the thermoelectric power for $J_Q \parallel a$ shows a splitting of the transition peak at low temperature, similar to what is observed in $CeRu_2Si_2$ [56], most likely linked to a Lifshitz transition. Quantum oscillations can be observed for $H > 22$ T, far above H_R but this branch represents only a small portion of the Fermi surface. The complete understanding of URhGe and especially the behavior with magnetic field applied along the b-axis would require a better knowledge of the topology of the Fermi surface, both from an experimental and a theoretical point of view. Interesting perspectives would be the application of uniaxial stress to reduce the magnetic anisotropy between the b- and the c-axis or follow H_R inside the reentrant

superconducting state with the measurement of magnetostriction, for example.

The knowledge of the Fermi surface of UPd_2Al_3 is already far more advanced than in URhGe. Most of the antiferromagnetic state has been measured and calculated with a fairly good agreement, especially with the magnetic field along the c-axis. However, in this study, a magnetic field applied in the basal plane and rotated from $[10\bar{1}0]$ to $[11\bar{2}0]$ reveals the presence of a new branch that wasn't observed before in the de Haas-van Alphen effect. It is not clear to which part of the calculated Fermi surfaces this branch could correspond. Like in URhGe, the thermoelectric power can easily probe the metamagnetic transition at $H_M = 18$ T for a magnetic field applied along the $[10\bar{1}0]$ direction, and again the transition appears like a single peak at high temperature and splits into two peaks at low temperature. Above the metamagnetic transition, large quantum oscillations are observed and do not correspond to any of the calculated branches in the paramagnetic and antiferromagnetic states. This suggests that the Fermi surface is reconstructed at the metamagnetic transition in this system. However, the understanding of the polarized paramagnetic state in this compound is far from complete. More detailed angular dependence of quantum oscillation measurements as well as band calculations taking into account the magnetic polarization would be needed.

While it is not a trivial task, the study of the Fermi surface in compounds such as itinerant ferromagnetic superconductors can give determinant informations on the reasons behind the presence of superconductivity. For instance, in URhGe, the reentrant superconducting phase is closely linked to the spin-reorientation transition, and the understanding of such a transition could give valuable insight on the superconductivity and its mechanism. Additionally, many compounds, such as iron pnictides or high-T_C cuprates, show superconductivity on the border of phase instabilities, magnetic or not, and it appears that the role of the Fermi surface has not been properly investigated.

Appendix

Résumé

Dans cette thèse, j'ai étudié l'évolution de la surface de Fermi sous l'influence d'un champ magnétique dans des systèmes massifs facilement polarisables à basse température. La première partie est dévouée aux cas du supraconducteur ferromagnétique UCoGe et du supraconducteur paramagnétique $CeIrIn_5$, où la surface de Fermi peut être modifiée sans transition magnétique. Dans UCoGe, plusieurs anomalies successives ont été détectées dans l'effet Seebeck, la résistivité et l'effet Hall, sans transition nette dans l'aimantation. L'observation d'oscillations quantiques montre que ces anomalies sont reliées à des changements de topologie de la surface de Fermi, aussi appelés transitions de Lifshitz. Dans $CeIrIn_5$, une anomalie est détectée dans l'effet Seebeck à $H_M = 28$ T et les oscillations quantiques observées en magnétométrie torque montrent qu'une transition de Lifshitz à lieu à ce champ.

Dans la deuxième partie, j'ai étudié comment varie la surface de Fermi à travers une transition magnétique du premier ordre induite par le champ magnétique dans le supraconducteur ferromagnétique URhGe avec le champ selon l'axe de difficile aimantation b et dans le supraconducteur antiferromagnétique UPd_2Al_3 avec le champ dans le plan basal. Dans URhGe, l'effet Seebeck permet d'observer un changement de la surface de Fermi à la transition de réorientation des spins à $H_R = 11.75$ T et avec la resistivité confirme le caractère premier ordre de la transition en plus de fournir la localisation dans le diagramme de phase du point tricritique. Dans UPd_2Al_3, une nouvelle branche de la surface de Fermi est observée dans les oscillations quantiques de de Haas-van Alphen dans l'état antiferromagnétique et l'effet Seebeck montre que la surface de Fermi change à la transition metamagnétique à $H_M = 18$ T. En outre, quatre nouvelles branches sont observées dans la phase polarisée au delà de H_M et qui ne peuvent être associées à celles calculées dans les états paramagnétique et antiferromagnétique.

Introduction en Français

Il y a un peu plus de cent ans, Kamerlingh Onnes mesurait une résistance nulle à basse température dans le mercure, découvrant ainsi la supraconductivité. Une explication théorique à ce phénomène fit son apparition plusieurs décénies plus tard, avec la théorie BCS. Depuis lors et jusqu'à nos jours, un très grand nombre de supraconducteurs ont été découverts, tels que les cuprates à haute température critique ou encore

les pnictures de fer, qui ne peuvent être décris par cette théorie et ont alors été nommés "non-conventionnels".

Parmis les supraconducteurs non-conventionnels, certains font aussi partie de la famille des composés dits "à fermions lourds", où les corrélations électroniques engendrent des masses effectives pouvant être de plusieurs ordres de grandeurs supérieures à la masse de l'électron libre et qui ont tendance à s'ordonner magnétiquement. Certains d'entre eux présentent même une coexistence entre la supraconductivité et un ordre magnétique à longue portée, réalisant ce qui était auparavant perçu comme impossible. Dans ce contexte, la découverte dans UGe_2 de la coexistence entre ferromagnétisme et supraconductivité a engendré un grand intérêt au sein de la communauté scientifique [32, Saxena 2000]. URhGe appartient à cette petite famille de supraconducteurs ferromagnétiques et bien que sa découverte date de 15 ans [33, Aoki 2001], un grand nombre de questions restent ouvertes. La relation entre le ferromagnétisme itinérant et la supraconductivité, les différences qui existent entre les diagrammes de phase des supraconducteurs ferromagnétiques, le lien entre la phase de supraconductivité réentrante [85, Lévy 2005] and la transition de premier ordre de réorientation des spins lorsqu'un champ magnétique est appliqué selon l'axe de difficile aimantation b, sont parmis elles.

Les réponses à ces questions pourraient se trouver dans l'étude de la surface de Fermi. Même dans les cas simples, le lien exacte entre la surface de Fermi et les propriétés d'un métal à très basse temperature reste mystérieux. L'étude des différentes bandes participant aux propriétés de transport et thermodynamiques ainsi que la topologie de la surface de Fermi peut donner des informations capitales sur les propriétés de l'état fondamental des systèmes étudiés. Les mesures de la surface de Fermi, particulièrement dans les composés à fermions lourds représente un challenge, tant expérimental que théorique, dû à la forte renormalisation des masses effectives et aux conditions extrêmes requises (très basses températures, hauts champs magnétiques). Du point de vue théorique, la présence d'électrons f et leur hybridation avec les électrons de conduction rendent les calculs de bande difficiles.

Dans la plupart des métaux, la structure de bande et la surface de Fermi sont relativement robustes vis à vis d'un paramètre extérieur. Dans les fermions lourds, la pression, la composition chimique ou encore le champ magnétique peut facilement modifier la structure de bande ou l'énergie de Fermi, et donc la surface de Fermi. Un changement de surface de Fermi peut survenir de manière soudaine, avec une reconstruction à une transition qui modifie l'état fondamental du système, ou continument, par ce qu'on appelle communément une transition de Lifshitz, où la topologie de la surface de Fermi change sans qu'une signature thermodynamique soit détectée. La possibilité d'un changement de topologie de la surface de Fermi sous l'influence d'un paramètre extérieur a été étudiée théoriquement il y a plus de 50 ans par I. M. Lifshitz [25, Lifshitz 1960]. Bien que quelques travaux expérimentaux sur le sujets aient été faits dans les années 80, ce n'est que récemment que le sujet a regagné de l'attention avec des études expérimentales et théoriques montrant la présence de ces transitions de Lifshitz, par example dans $YbRh_2Si_2$ [72, Pfau 2013] ou encore $CeRu_2Si_2$ [55, 56, Daou 2006, Boukahil 2014], induites sous champ magnétique.

Dans cette thèse, le principal objectif est d'étudier l'évolution de la surface de Fermi proche de la phase de supraconductivité réentrante dans URhGe et à travers la transition magnétique à H_R. Je me suis concentré sur l'étude de l'effet Seebeck et plus particulièrement sa dépendance en champs magnétique, qui est connu pour être une sonde très sensible aux changements de surface de Fermi, pour tenter de comprendre le lien qui unit

le magnétisme, la supraconductivité et la surface de Fermi. La présence d'anomalies dans la magnétorésistivité mesurée dans le composé parent UCoGe et l'absence de signature de transitions thermodynamiques nous ont poussé à utiliser l'effet Seebeck pour comprendre comment le champ magnétique peut modifier la surface de Fermi dans ce composé. Étant donné que URhGe et UCoGe sont tous les deux ferromagnétiques, nous avons décidé d'étendre notre étude à d'autre composés possédant un état fondamental différent: $CeIrIn_5$ qui est un supraconducteur paramagnétique montrant une anomalie similaire à celles observées dans UCoGe, et UPd_2Al_3, où un ordre antiferromagnétique coexiste avec la supraconductivité et qui montre une transition métamagnétique où la surface de Fermi pourrait être reconstruite.

Cette thèse est donc divisée en quatre parties. La premiére donne un aperçu de l'approche théorique et expérimentale des ordres magnétiques dans la matière condensée, de la surface de Fermi, de sa mesure ainsi que des transitions de Lifshitz. La seconde partie détaille les méthodes expérimentales utilisées pour la croissance et la caractérisation des échantillons ainsi que la mesure de l'effet Seebeck, de la résistivité et des oscillations de de Haas-van Alphen. La troisème partie présente les résultats expérimentaux sur les transitions induites sous champ magnétique sans signature dans l'aimantation obtenus grâce à l'effet Seebeck. Dans le supraconducteur ferromagnétique UCoGe, nos mesures ont complété une étude de résistivité et d'effet Hall, où nous avons examiné l'effet de la polarisation magnétique sur la surface de Fermi, révélant la présence de transitions de Lifshitz successives par l'effet Seebeck et les oscillations quantiques mesurées par cette sonde et en résistivité. Dans le supraconducteur paramagnétique $CeIrIn_5$, l'effet Seebeck ainsi que les oscillations quantiques observées dans la magnétométrie torque ont aussi démontré la présence d'une transition de Lifshitz. Dans la quatriéme et derniére partie, nous avons étudié la suppression d'ordres magnétiques par le champ magnétique avec pour objectif de comprendre quel est le rôle de la surface de Fermi dans ces transitions. La réorientation des spins dans le supraconducteur ferromagnétique URhGe à H_R, lorsque le champ magnétique est appliqué selon l'axe de difficile aimantation b, a été étudiée avec des mesures systématiques d'effet Seebeck ainsi que de résistivité qui ont montré que cette transition était accompagnée d'une reconstruction de la surface de Fermi, et a été confirmée comme étant de premier ordre à basse température. La position du point tricritique a été estimée et un état de non liquide de Fermi a été découvert comme s'étendant depuis ce point. Dans UPd_2Al_3, nous avons étudié la surface de Fermi à travers la transition métamagnétique avec le champ magnétique appliqué dans le plan basal à l'aide de l'effet Seebeck et des oscillations de de Haas-van Alphen. Ces mesures nous ont permis d'observer une reconstruction de la surface de Fermi à la transition métamagnétique dans ce systéme.

Résumé des chapitres en français

Chapitre 1

Le premier chapitre donne un aperçu du traitement des électrons ainsi que de leurs intérations en matiére condensée et plus spécialement dans les composés à fermions lourds. Les bases de la thermoélectricité ainsi que la théorie de Landau des liquides de Fermi sont

abordées. Sont ensuite décrits les ordres magnétiques étudiés dans cette thèse ainsi que l'effet d'un paramètre extérieur avec parfois l'émergence d'un point critique quantique et de la supraconductivité non conventionnelle. Notre étude de ces systèmes a été réalisée par le biais de la surface de Fermi, dont l'origine et la mesure sont décrites. Sont aussi mentionnées les deux théories permettant de traiter les oscillations quantiques observées dans l'aimantation (Lifshitz-Kosevich) et dans l'effet Seebeck (Pantsulaya-Varlamov). Sont enfin abordés les changements de topologie que l'on peut induire dans la surface de Fermi d'un metal, appelés communément "transitions de Lifshitz" et les répercussions d'une telle transition sur les propriétés du système et plus particulièrement l'effet Seebeck.

Chapitre 2

Le second chapitre décrit les méthodes expérimentales mises en œuvre afin de réaliser les mesures nécessaires à cette étude. Les mono cristaux dans cette thèse ont été fabriqués par la méthode de Czochralski dans un four tetra-arc, orientés avec des photographies Laue. Les points suivant détaillent les mesures d'effet Seebeck, qui est la principale sonde utilisée dans cette thèse, la résistivité et les oscillations de l'aimantation par la méthode de modulation du champ. Ces mesures ont été réalisées a très basse température et haut champ magnétique.

Chapitre 3

Le troisième chapitre de cette thèse présente létude de modifications de surface de Fermi en l'absence de transitions magnétiques dans le supraconducteur ferromagnétique UCoGe et le supraconducteur paramagnétique $CeIrIn_5$. La première partie de ce chapitre présente UCoGe, l'état de l'art sur le composé puis les résultats expérimentaux obtenus. L'effet Seebeck, ainsi que la résistivité et l'effet Hall démontrent la présence d'anomalies induites par le champ magnétique, là où des mesures d'aimantation ne montrent aucune transition. Les oscillations quantiques observées permettent de montrer que ces anomalies sont reliées à des modifications de la surface de Fermi et plus précisement celles à $H_4 = 16$ T et $H_5 = 21$ T montrent la disparition de branches de la surface de Fermi, démontrant que ces anomalies sont en fait des transitions de Lifshitz.

La seconde partie présente le cas de $CeIrIn_5$, son état de l'art, puis les résultats obtenus avec l'effet Seebeck ainsi que des oscillations quantiques observées dans le torque magnétique. Alors que l'effet Seebeck indique la présence d'une transition à $H_M = 28$ T, les oscillations quantiques de part et d'autre de la transition montrent qu'une branche de la surface de Fermi y disparait alors qu'une autre apparait. À l'instar d'UCoGe, $CeIrIn_5$ montre la présence d'une transition de Lifshitz induite par le champ magnétique.

Chapitre 4

Le quatrième et dernier chapitre montre des instabilités de surface de Fermi associées à des transitions magnétiques dans le supraconducteur ferromagnétique URhGe et le supraconducteur antiferromagnétique UPd_2Al_3. La premiére partie présente URhGe,

où une transition correspondant à la reorientation des moments magnétiques de l'axe c vers l'axe b au champ magnétique $H_R = 11.75$ T existe lorsqu'un champ magnétique est appliqué selon l'axe b, autour de laquelle la supraconductivité dite "réentrante" apparait. L'effet Seebeck à basse température dans la configuration longitudinale montre un brutal changement de signe à la transition, indiquant un changement de surface de Fermi entre les deux phases. L'étude de la dépendance en température de la résistivité montre qu'à suffisamment basse temperature, le régime de liquide de Fermi est conservé à travers la transition magnétique, confirmant son caractère premier ordre. La largeur de la transition en effet Seebeck ainsi que les nouvelles échelles d'énergie observées donnent une localisation relativement précise du point tricritique, où la transition passe de second à premier ordre. L'étude des configurations transverses avec le courant de chaleur selon les axes a et c montrent que, bien que le composé présente une forte anisotropie, les effets observés sont bien intrinsèques à URhGe.

Dans la deuxième partie, le composé UPd_2Al_3 est présenté. Lorsqu'un champ magnétique est appliqué dans le plan basal, qui est un plan de facile aimantation, l'ordre antiferromagnétique est détruit et le système traverse une transition métamagnétique à H_M. La surface de Fermi de l'état antiferromagnétique a déjà été mesurée dans de nombreuses études expérimentales et théoriques. Dans cette thèse, la mesure d'oscillations quantiques dans la susceptibilité magnétique montre l'existence d'une nouvelle branche de la surface de Fermi lorsque le champ est appliqué dans le plan basal. L'effet Seebeck, à la transition métamagnétique à H_M, change brutalement de signe et montre également des oscillations quantiques d'une grande amplitude. Les branches observées dans cet état polarisé n'ont jamais été détectées dans la phase antiferromagnétique et leur faible masse effective suggère qu'elles apparaissent à la transition. Ceci prouve que la surface de Fermi est reconstruite à la transition métamagnétique.

Conclusion en Français

Dans cette thèse, plusieurs composés à fermions lourds ont été étudiés à l'aide de mesures thermoélectriques, de résistivité et d'effet de Haas-van Alphen. Ces mesures ont été réalisées à basse température ($T \approx 100$ mK) et hauts champs magnétiques ($H > 30$ T).

Dans UCoGe, des anomalies ont été observées dans la dépendance en champ de l'effet Seebeck, de la résistivité et de l'effet Hall pour un champ magnétique appliqué selon l'axe de facile aimantation c. Des oscillations quantiques ont également été observées. L'analyse de l'évolution en champ magnétique de ces branches de la surface de Fermi a révélé qu'elles apparaissent et disparaissent aux même champs où les anomalies ont été détectées. Cela prouve que le champ magnétique peut modifier la topologie de la surface de Fermi et que certaines des anomalies observées sont des transitions de Lifshitz. La mesure de la dépendance en champ de la chaleur spécifique serait intéressante pour observér son comportement à ces transitions de Lifshitz.

Une anomalie du même type a été détectée dans l'effet Seebeck à $H_M = 28$ T dans le composé $CeIrIn_5$ avec un champ magnétique appliqué selon l'axe a. Bien qu'aucune oscillation quantique n'ait pu être observée dans l'effet Seebeck, il en est autrement de la magnétométrie torque qui détecte la présence de branches de la surface de Fermi.

L'analyse de la transformée de Fourier du signal en dessous et au dessus de H_M montre qu'une branche apparait et une autre disparait à H_M, démontrant la présence d'une transition de Lifshitz.

L'étude d'URhGe montre que l'effet Seebeck peut facilement détecter la transition de réorientation des spins à H_R lorsqu'un champ magnétique est appliqué selon l'axe de difficile aimantation b. La configuration longitudinale montre que la surface de Fermi est reconstruite à la transition et la position du point tricritique qui sépare la ligne de transition entre second ordre et premier ordre peut être extraite. Les mesures de résistivité montrent que la dépendance en température suit la loi des liquides de Fermi à tous les champs à suffisamment basse température. Cela confirme le caractère premier ordre de la transition à basse température et qu'aucun point critique quantique n'est présent à cette transition. Les mesures dans les deux configurations transverses montrent une anomalie moins prononcée à H_R. L'effet Seebeck, pour $J_Q \parallel a$, montre une séparation du pic en deux à la transition, similaire à ce qui a été observé dans $CeRu_2Si_2$ [55, 56, Daou 2006, Boukahil 2014]. Des oscillations quantiques peuvent être observées à $H > 22$ T, loin au delà de H_R, mais cette branche ne représente qu'une faible portion de la surface de Fermi. Pour comprendre les phénomènes présents dans URhGe et particulièrement le comportement lorsque le champ est appliqué selon l'axe b, il faudrait connaitre mieux la topologie de la surface de Fermi, tant expérimentalement que théoriquement. Des perspectives intéressantes seraient l'application d'une pression uniaxe afin de modifier l'anisotropie du composé ainsi que d'étudier ce qu'il advient de la transition à l'intérieur du dôme de supraconductivité réentrante, par des mesures de magnétostriction, par exemple.

La connaissance de la surface de Fermi d'UPd_2Al_3 est beaucoup plus avancée que dans URhGe. La plupart des poches de l'état antiferromagnétique a été mesuré et calculé avec un bon accord entre les différentes études. Cependant, dans cette étude, un champ magnétique appliqué dans le plan basal et tourné depuis l'axe $[10\bar{1}0]$ vers $[11\bar{2}0]$ révèle la présence d'une nouvelle branche qui n'avait pas été observée auparavant. La partie de la surface de Fermi calculée à laquelle cette branche correspond n'est, à ce jour, pas claire. Comme dans URhGe, l'effet Seebeck détecte facilement la transition métamagnétique pour un champ selon l'axe $[10\bar{1}0]$ et montre un brutal changement de signe, en plus d'avoir la même séparation du pic en deux à basse température. Au delà de la transition métamagnétique, des oscillations quantiques avec une grande amplitude apparaissent et ne correspondent à aucune des branches calculées dans les états paramagnétiques et antiferromagnétiques ou observées dans l'état antiferromagnétique. Cela suggère que la surface de Fermi est reconstruite à la transition métamagnétique dans ce système. Cependant, la compréhension de l'état polarisé paramagnétique est loin d'être complète et des mesures plus détaillées d'oscillations quantiques (telle qu'une dépendance angulaire) ainsi que des calculs de bandes prenant en compte la polarisation magnétique sont nécessaires.

Bien que la tâche soit loin d'être triviale, l'étude de la surface de Fermi dans des composés tels que ceux montrant la coexistence de la supraconductivité et du ferromagnétisme itinérant peut donner des informations cruciales sur les raisons se trouvant derrière l'apparition de la supraconductivité dans ces systèmes. Par exemple, dans URhGe, le lien entre la supraconductivité réntrante et la transition de réorientation des spins est fort, et la compréhension d'une telle transition pourrait donner des informations importantes quant à la supraconductivité et son mécanisme. En outre, de nombreux composés, tels les pnictures de fer ou encore les cuprates à haute température critique, montrent l'apparition de la supraconductivité proche d'instabilités, magnétiques ou non, et le rôle de la surface

de Fermi n'a été que peu exploré.

Bibliography

[1] L. D. Landau, Soviet Physics Jetp-ussr 3 920-925, 1957.

[2] A. J. Leggett, Rev. Mod. Phys. 47 331, 1975.

[3] N. F. Mott and H. Jones, *The Theory of the Properties of Metals and Alloys*, Clarendon Press, Oxford (1936).

[4] K. Miyake and H. Kohno, J. Phys. Soc. Jpn. 74, 254-258 (2005).

[5] J. Kondo, Prog. Theor. Phys. 32, 37 (1964).

[6] M. A. Ruderman and C. Kittel, Phys. Rev. 96, 99 (1954).

[7] S. Doniach, Physica B+C 91, 231-234 (1977).

[8] T. Moriya, *Spin Fluctuations in Itinerant Electron Magnetism*, Springer Series in Solid-State Sciences Volume 56 (1985).

[9] G. Knebel, D. Braithwaite, P. C. Canfield, G. Lapertot and J. Flouquet, Phys. Rev. B 65, 024425 (2001).

[10] N. D. Mathur, F. M. Grosche, S. R. Julian, I. R. Walker, D. M. Freye, R. K. W. Haselwimmer and G. G. Lonzarich, Nature 394, 39-43 (1998).

[11] F. Steglich, H. Pfau, S. Lausberg, S. Hamann, P. Sun, U. Stockert, M. Brando, S. Friedemann, C. Krellner, C. Geibel, S. Wirth, S. Kirchner, E. Abrahams and Q. Si, J. Phys. Soc. Jpn. 83, 061001 (2014).

[12] H. v. Löhneysen, A. Rosch, M. Vojta and P. Wölfle, Rev. Mod. Phys. 79, 1015 (2007).

[13] J. A. Hertz, Phys. Rev. B 14, 1165 (1976).

[14] A. J. Millis, Phys. Rev. B 48, 7183 (1993).

[15] H. Abe, H. Kitazawa, H. Suzuki, G. Kido and T. Matsumoto, Physica B 246-247, 141-143 (1998).

[16] V. Taufour, D. Aoki, G. Knebel and J. Flouquet, Phys. Rev. Lett. 105, 217201 (2010).

[17] M.I. Bartashevich, T. Goto, M. Yamaguchi, I. Yamamoto and R. J. Radwanski, Solid State Comm. 87, 1093-1095 (1993).

[18] P. Bonville, P. Bellot, J.A. Hodges, P. Imbert, G. Jéhanno, G. Le Bras, J. Hammann, L. Leylekian, G. Chevrier, P. Thuéry, L. D'Onofrio, A. Hamzic and A. Barthélémy, Physica B 182, 105-117 (1992).

[19] I. M. Lifshitz and A. M. Kosevich, Sov. Phys.-JETP 2 636, 1956

[20] R. B. Dingle, Proc. Roy. Soc. A 211 517, 1952.

[21] R. C. Young, J. Phys. F: Met. Phys. 3, 721 (1973).

[22] R. Fletcher, J. Phys. F: Met. Phys. 11, 1093 (1981).

[23] R. Fletcher, Phys. Rev. B 28, 6670 (1983).

[24] A. Palacio Morales, A. Pourret, G. Knebel, G. Bastien, V. Taufour, D. Aoki, H. Yamagami and J. Flouquet, Phys. Rev. B 93, 155120 (2016).

[25] I. M. Lifshitz, Zh. Eksp. Teor. Fiz. 38, 1569 (1960); [Sov. Phys. JETP 11, 1130 (1960)].

[26] D. Belitz, T. R. Kirkpatrick, and Jörg Rollbühler, Phys. Rev. Lett. 94, 247205 (2005).

[27] A. A. Varlamov and A. V. Pantsulaya, Solid State Comm. 56, 787-790 (1985).

[28] F. Völklein and E. Kessler, Thin Solid Films 155, 197-208 (1987).

[29] C. Enss and S. Hunklinger, *Low Temperature Physics*, Springer Verlag, Heidelberg (2005).

[30] A. V. Pantsulaya and A. A. Varlamov, Phys. Lett. A 136, 317-320 (1989).

[31] N. T. Huy, A. Gasparini, D. E. de Nijs, Y. Huang, J. C. P. Klaasse, T. Gortenmulder, A. de Visser, A. Hamann, T. Görlach, and H. v. Löhneysen, Phys. Rev. Lett. 99, 067006 (2007).

[32] S. S. Saxena, P. Agarwal, K. Ahilan, F. M. Grosche, R. K. W. Haselwimmer, M. J. Steiner, E. Pugh, I. R. Walker, S. R. Julian, P. Monthoux, G. G. Lonzarich, A. Huxley, I. Sheikin, D. Braithwaite and J. Flouquet, Nature 406, 587-592 (2000).

[33] D. Aoki, A. Huxley, E. Ressouche, D. Braithwaite, J. Flouquet, J.-P. Brison, E. Lhotel and C. Paulsen, Nature 413, 613-616 (2001).

[34] T. Akazawa, H. Hidaka, T. Fujiwara, T. C. Kobayashi, E. Yamamoto, Y. Haga, R. Settai and Y. Ōnuki, J. Phys.: Condens. Matter 16 29-32 (2004).

[35] W. A. Fertig, D. C. Johnston, L. E. DeLong, R. W. McCallum, M. B. Maple, and B. T. Matthias ,Phys. Rev. Lett. 38, 987 (1977).

[36] M. Ishikawa and Ø. Fischer, Solid State Commun., 23 37-39 (1977).

[37] K. H. J. Buschow, E. Brück, R. G. van Wierst, F. R. de Boer, L. Havela, V. Sechovsky, P. Nozar, E. Sugiura, M. Ono, M. Date, and A. Yamagishi, Journal of Applied Physics 67, 5215 (1990).

[38] T. Ohta, Y. Nakai, Y. Ihara, K. Ishida, K. Deguchi, N. K. Sato, and I. Satoh, J. Phys. Soc. Jpn. 77, 023707 (2008).

[39] T. Ohta, T. Hattori, K. Ishida, Y. Nakai, E. Osaki, K. Deguchi, N. K. Sato and I. Satoh, J. Phys. Soc. Jpn. 79, 023707 (2010).

[40] A. de Visser, N. T. Huy, A. Gasparini, D. E. Nijs, D. Andreica, C. Baines and A. Amato, Phys. Rev. Lett. 102, 167003 (2009).

[41] G. Bastien, D. Braithwaite, D. Aoki, G. Knebel and J. Flouquet, Phys. Rev. B 94, 125110 (2016).

[42] E. Hassinger, D. Aoki, G. Knebel, and J. Flouquet, J. Phys. Soc. Jpn. 77 (7), 073703 (2008).

[43] N. T. Huy, D. E. de Nijs, Y. K. Huang, and A. de Visser, Phys. Rev. Lett. 100, 077002 (2008).

[44] R. A. Klemm and K. Scharnberg, Physica B & C 135, 53-56 (1985).

[45] D. Aoki, T. D. Matsuda, V. Taufour, E. Hassinger, G. Knebel, and J. Flouquet, . Phys. Soc. Jpn. 78 (11), 113709 (2009).

[46] L. Malone, L. Howald, A. Pourret, D. Aoki, V. Taufour, G. Knebel, and J. Flouquet, Phys. Rev. B 85, 024526 (2012).

[47] I. Paul and G. Kotliar, Phys. Rev. B 64, 184414 (2001).

[48] W. Knafo, T. D. Matsuda, D. Aoki, F. Hardy, G. W. Scheerer, G. Ballon, M. Nardone, A. Zitouni, C. Meingast and J. Flouquet, Phys. Rev. B 86, 184416 (2012)

[49] D. Aoki, I. Sheikin, T. D. Matsuda, V. Taufour, G. Knebel, and J. Flouquet, J. Phys. Soc. Jpn. 80, 013705 (2011).

[50] D. Aoki, A. Gourgout, A. Pourret, G. Bastien, G. Knebel, and J. Flouquet, C. R. Phys. 15, 630 (2014).

[51] S.-i. Fujimori, T. Ohkochi, I. Kawasaki, A. Yasui, Y. Takeda, T. Okane, Y. Saitoh, A. Fujimori, H. Yamagami, Y. Haga, E. Yamamoto, and Y. Ōnuki

[52] P. Monthoux and G. G. Lonzarich, Phys. Rev. B 63, 054529 (2001).

[53] M. Samsel-Czekała, S. Elgazzar, P. M. Oppeneer, E. Talik, W. Walerczyk and R Troć, J. Phys.: Condens. Matter 22 015503 (2010).

[54] A. Pourret, A. Palacio-Morales, S. Krämer, L. Malone, M. Nardone, D. Aoki, G. Knebel and J. Flouquet, J. Phys. Soc. Jpn. 82, 034706 (2013).

[55] R. Daou, C. Bergemann and S. R. Julian, Phys. Rev. Lett 96, 026401 (2006).

[56] M. Boukahil, A. Pourret, G. Knebel, D. Aoki, Y. Ōnuki and J. Flouquet, Phys. Rev. B 90, 075127 (2014).

[57] K. Behnia, D. Jaccard and J. Flouquet, J. Phys.: Condens. Matter 16 5187 (2004)

[58] R. Bel, H. Jin, K. Behnia, J. Flouquet and P. Lejay, Phys. Rev. B 70, 220501 (2004).

[59] G. Bastien, A. Gourgout, D. Aoki, A. Pourret, I. Sheikin, G. Seyfarth, J. Flouquet and G. Knebel., Phys. Rev. Lett. 117, 206401 (2016).

[60] I. Sheikin, Habilitation à Diriger des Recherches, 2014.

[61] H. Hegger, C. Petrovic, E. G. Moshopoulou, M. F. Hundley, J. L. Sarrao, Z. Fisk and J. D. Thompson: Phys. Rev. Lett. 84 4986 (2000).

[62] T. Shang, R. E. Baumbach, K. Gofryk, F. Ronning, Z. F. Weng, J. L. Zhang, X. Lu, E. D. Bauer, J. D. Thompson and H. Q. Yuan, Phys. Rev. B 89, 041101 (2014).

[63] C. Petrovic, R. Movshovich, M. Jaime, P. G. Pagliuso, M. F. Hundley, J. L. Sarrao, Z. Fisk and J. D. Thompson, Europhys. Lett., 53 (3), 354-359 (2001).

[64] R. Movshovich, M. Jaime, J. D. Thompson, C. Petrovic, Z. Fisk, P. G. Pagliuso, and J. L. Sarrao, Phys. Rev. Lett. 86, 5152 (2001).

[65] Y. Haga, Y. Inada, H. Harima, K. Oikawa, M. Murakawa, H. Nakawaki, Y. Tokiwa, D. Aoki, H. Shishido, S. Ikeda, N. Watanabe, and Y. Ōnuki, Phys. Rev. B 63, 060503 (2001).

[66] T. Takeuchi, T. Inoue, K. Sugiyama, D. Aoki, Y. Tokiwa, Y. Haga, K. Kindo and Y. Ōnuki, J. Phys. Soc. Japan, 70, 877 (2001).

[67] E. C. Palm, T. P. Murphy, D. Hall, S. W. Tozer, R. G. Goodrich and J. L. Sarrao, Physica B 329-333, 587 (2003).

[68] J. S. Kim, J. Alwood, P. Kumar, and G. R. Stewart, Phys. Rev. B 65, 174520 (2002).

[69] Y. Haga, Y. Inada, H. Harima, K. Oikawa, M. Murakawa, H. Nakawaki, Y. Tokiwa, D. Aoki, H. Shishido, S. Ikeda, N. Watanabe and Y. Ōnuki, Phys. Rev. B 63, 060503 (2001).

[70] S. Elgazzar, I. Opahle, R. Hayn and P. M. Oppeneer, Phys. Rev. B 69, 214510 (2004).

[71] A. Pourret, G. Knebel, T. D. Matsuda, G. Lapertot and J. Flouquet, J. Phys. Soc. Jpn. 82, 053704 (2013).

[72] H. Pfau, R. Daou, S. Lausberg, H. R. Naren, M. Brando, S. Friedemann, S. Wirth, T. Westerkamp, U. Stockert, P. Gegenwart, C. Krellner, C. Geibel, G. Zwicknagl, and F. Steglich, Phys. Rev. Lett. 110, 256403 (2013).

[73] H. Harima, private communication.

[74] D. Aoki, G. Seyfarth, A. Pourret, A. Gourgout, A. McCollam, J. A. N. Bruin, Y. Krupko, and I. Sheikin, Phys. Rev. Lett. 116, 037202 (2016).

[75] K. Prokes, T. Tahara, Y. Echizen, T. Takabatake, T. Fujita, I. H. Hagmusa, J. C. P. Klaasse, E. Brück, F. R. De Boer, M. Divis and V. Sechovsky, Physica B 311, 220-232 (2002).

[76] R. Troc and V. H. Tran, J. Magn. Magn. Mater. 73, 389-397 (1988).

[77] B. Chevalier, E. Hickey, J. R. Etourneau, J. Magn. Magn. Mater. 90/91, 499-500 (1990).

[78] F. Hardy, D. Aoki, C. Meingast, P. Schweiss, P. Burger, H. v. Löhneysen, and J. Flouquet, Phys. Rev. B 83, 195107 (2011)

[79] N. Tateiwa, Y. Haga, T. D. Matsuda, E. Yamamoto, and Z. Fisk, Phys. Rev. B 89, 064420 (2014).

[80] F. Hardy, A. Huxley, J. Flouquet, B. Salce, G. Knebel, D. Braithwaite, D. Aoki, M. Uhlarz and C. Pfleiderer, Physica B 359-361, 1111-1113 (2005).

[81] A. Miyake, D. Aoki and J. Flouquet, J. Phys. Soc. Jpn. 78, 063703 (2009).

[82] D. Aoki, M. Taupin, C. Paulsen, F. Hardy, V. Taufour, H. Kotegawa, E. Hassinger, L. Malone, T. D. Matsuda, A. Miyake, I. Sheikin, W. Knafo, G. Knebel, L. Howald, J.-P. Brison, and J. Flouquet, J. Phys. Soc. Jpn. 81, SB002 (2012).

[83] B. Wu, to be published.

[84] F. Hardy and A. D. Huxley, Phys. Rev. Lett. 94, 247006 (2005).

[85] F. Lévy, I. Sheikin, B. Grenier and A. Huxley, Science 309, 1343-1346 (2005).

[86] A. Miyake, D. Aoki and J. Flouquet, J. Phys. Soc. Jpn. 77, 094709 (2008).

[87] F. Lévy, I. Sheikin and A. Huxley, Nat. Phys. 3, 460-463 (2007).

[88] A. D. Huxley, S. J. C. Yates, F. Lévy and I. Sheikin, J. Phys. Soc. Jpn. 76, 051011 (2007).

[89] H. Kotegawa, K. Fukumoto, T. Toyama, H. Tou, H. Harima, A. Harada, Y. Kitaoka, Y. Haga, E. Yamamoto, Y. Ōnuki, K. M. Itoh and E. E. Haller, J. Phys. Soc. Jpn. 84, 054710 (2015).

[90] D. Aoki, G. Knebel and J. Flouquet, J. Phys. Soc. Jpn. 83, 094719 (2014).

[91] V. P. Mineev, Phys. Rev. B 91, 014506 (2015).

[92] B. Wu, accepted in Nat. Comm.

[93] E. A. Yelland, J. M. Barraclough, W.Wang, K. V. Kamenev and A. D. Huxley, Nat. Phys. 7, 890-894 (2011).

[94] Y. Tokunaga, D. Aoki, H. Mayaffre, S. Krämer, M.-H. Julien, C. Berthier, M. Horvatić, H. Sakai, S. Kambe and S. Araki, Phys. Rev. Lett. 114, 216401 (2015).

[95] Y. Tokunaga, D. Aoki, H. Mayaffre, S. Krämer, M.-H. Julien, C. Berthier, M. Horvatić, H. Sakai, T. Hattori, S. Kambe and S. Araki, Phys. Rev. B 93, 201112 (2016)

[96] M. T. Mercaldo, I. Rabuffo, A. Naddeo, A. Caramico D'Auria and L. De Cesare, Eur. Phys. J. B 84, 371-379 (2011).

[97] T. Misawa, Y. Yamaji and M. Imada, J. Phys. Soc. Jpn 78, 084707 (2009).

[98] S.-i. Fujimori, I. Kawasaki, A. Yasui, Y. Takeda, T. Okane, Y. Saitoh, A. Fujimori, H. Yamagami, Y. Haga, E. Yamamoto and Y. Ōnuki, Phys. Rev. B 89, 104518 (2014).

[99] K. Izawa, K. Behnia, Y. Matsuda, H. Shishido, R. Settai, Y. Ōnuki and J. Flouquet, Phys. Rev. Lett. 99, 147005 (2007)

[100] F. Lévy, I. Sheikin, B. Grenier, C. Marcenat and A. Huxley, J. Phys.: Condens. Matter 21 164211 (2009).

[101] M. Diviš, L.M. Sandratskii, M. Richter, P. Mohnd and P. Novák, J. Alloys Compd. 337, 48 (2002).

[102] A. B. Shick, Phys. Rev. B 65, 180509 (2002).

[103] A. Gourgout, A. Pourret, G. Knebel, D. Aoki, G. Seyfarth and J. Flouquet, Phys. Rev. Lett 117, 046401 (2016).

[104] G. Bastien, unpublished.

[105] C. Geibel, C. Schank, S. Thies, H. Kitazawa, C.D. Bredl, A. Böhm, M. Rau, A. Grauel, R. Caspary, R. Helfrich, U. Ahlheim, G. Weber and F. Steglich, Z. Phys. B - Condensed Matter 84, 1 (1991).

[106] A. Krimmel, P. Fischer, B. Roessli, H. Maletta, C. Geibel, C. Schank, A. Grauel, A. Loidl, and F. Steglich, Z. Phys. B - Condensed Matter 86, 161-162 (1992).

[107] C. Geibel, U. Ahlheim, C. D. Bredl, J. Diehl, A. Grauel, R. Helfrich, H. Kitazawa, R. Köhler, R. Modler, M. Lang, C. Schank, S. Thies, F. Steglich, N. Sato and T. Komatsubara, Physica C 185-189, 2651-2652 (1991).

[108] E. Blackburn, A. Hiess, N. Bernhoeft, M. C. Rheinstädter, W. Häuler and G. H. Lander, Phys. Rev. Lett. 97 057002 (2006).

[109] S.-i Fujimori, T. Ohkochi, T. Okane, Y. Saitoh, A. Fujimori, H. Yamagami, Y. Haga, E. Yamamoto and Y. Ōnuki, IOP Conf. Ser.: Mater. Sci. Eng. 9, 012045 (2010).

[110] A. de Visser, K. Bakker, L. T. Tai, A. A. Menovsky, S. A. M. Mentink, G.J. Nieuwenhuys and J. A. Mydosh, Physica B 186-188, 291-293 (1993).

[111] A. de Visser, H. P. van der Meulen, L. T. Tai and A. A. Menovsky, Physica B 199-200, 100-102 (1994).

[112] A. de Visser, H. Nakotte, L. T. Tai, A. A. Menovsky, S. A. M. Mentink, G. J. Nieuwenhuys and J. A. Mydosh, Physisca B 179, 84-88 (1992).

[113] T. Sakon, T. Namiki and M. Motokawa, J. Phys. Soc. Jpn 70, 3046-3051 (2001).

[114] T. Sakon, N. K. Sato, Y. Nakanishi, T. Komatsubara and M. Motokawa, Jpn. J. Appl. Phys. 41, 3673-3677 (2002).

[115] K. Oda, T. Kumada, K. Sugiyama, N. Sato, T. Komatsubara and M. Date, J. Phys. Soc. Jpn. 63, 3115-3121 (1994)

[116] Y. Inada, H Yamagami, Y. Haga, K. Sakurai, Y. Tokiwa, T. Honma, E. Yamamoto, Y. Ōnuki, T. Yanagisawa, J. Phys. Soc. Jpn. 68, 3643-3654 (1999).

[117] L. M. Sandratskii, J. Kübler, P. Zahn and I. Mertig, Phys. Rev. B 50, 15834-15842 (1994).

[118] K. Knöpfle, A Mavromaras, L. M. Sandratskii and J. Kübler, J. Phys. Condens. Matter 8, 901-909 (1996).

[119] G. Zwicknagl and P. Fulde, J. Phys. Condens. Matter 15, 1911-1916 (2003).

[120] G. Zwicknagl, A. Yaresko and P. Fulde, Phys. Rev. B 68, 052508 (2003).

[121] Y. Haga, Y. Inada, H. Yamagami, K. Sakurai, Y. Tokiwa, E. Yamamoto, T. Honma and Y. Ōnuki, Physica B 281-282, 780-781 (2000).

[122] T. Terashima, C. Haworth, M. Takashita, H. Aoki, N. Sato and T Komatsubara, Phys. Rev. B 55, 13369-13372 (1997).

[123] J. S. Kim, N. K. Sato and G. R. Stewart, Journal of Low Temperature Physics 124, 527-535 (2001).

[124] D. Shoenberg, *Magnetic Oscillations in metals*, Cambridge University Press, New York (1984).